2010

DEVELOPMENT OF A NOVEL Z-AXIS PRECISION POSITIONING STAGE WITH MILLIMETER TRAVEL RANGE BASED ON A LINEAR PIEZOELECTRIC MOTOR

Tarek Mohammad

DEVELOPMENT OF A NOVEL Z-AXIS PRECISION POSITIONING STAGE WITH MILLIMETER TRAVEL RANGE BASED ON A LINEAR PIEZOELECTRIC MOTOR

(Spine title: A Novel Z-Axis Piezoworm Nanopositioner)

(Thesis format: Monograph)

by

Tarek Mohammad

Graduate Program in Mechanical and Materials Engineering

A thesis submitted in partial fulfillment
of the requirements for the degree of
Master of Engineering Science

The School of Graduate and Postdoctoral Studies
The University of Western Ontario
London, Ontario, Canada

THE UNIVERSITY OF WESTERN ONTARIO
School of Graduate and Postdoctoral Studies

CERTIFICATE OF EXAMINATION

Supervisor	Examiners
Dr. Shaun P. Salisbury	Dr. Ralph O. Buchal
Supervisory Committee	Dr. O. Remus Tutunea-Fatan
Dr. Michael D. Naish	Dr. James C. Lacefield

The thesis by

Tarek Mohammad

entitled:

Development of a Novel Z-Axis Precision Positioning Stage with Millimeter Travel Range based on a Linear Piezoelectric Motor

is accepted in partial fulfillment of the
requirements for the degree of
Master of Engineering Science

Date: _____

_____
Chair of the Thesis Examination Board

Development of a Novel Z-Axis Precision Positioning Stage with Millimeter Travel Range based on a Linear Piezoelectric Motor

Tarek Mohammad

Master of Engineering Science
Department of Mechanical and Materials Engineering
The University of Western Ontario
2010

Abstract

Piezoelectric-based positioners are incorporated into stereotaxic devices for microsurgery, scanning tunneling microscopes for the manipulation of atomic and molecular-scale structures, nanomanipulator systems for cell microinjection and machine tools for semiconductor-based manufacturing. Although several precision positioning systems have been developed for planar motion, most are not suitable to provide long travel range with large load capacity in vertical axis because of their weights, size, design and embedded actuators. This thesis develops a novel positioner which is being developed specifically for vertical axis motion based on a piezoworm arrangement in flexure frames. An improved estimation of the stiffness for Normally Clamped (NC) clamp is presented. Analytical calculations and finite element analysis are used to optimize the design of the lifting platform as well as the piezoworm actuator to provide maximum thrust force while maintaining a compact size. To make a stage frame more compact, the actuator is integrated into the stage body. The complementary clamps and the amplified piezoelectric actuators based extenders are designed such that no power is needed to maintain a fixed vertical position, holding the payload against the force of gravity. The design is extended to a piezoworm stage prototype and validated through

several tests. Experiments on the prototype stage show that it is capable of a speed of 5.4 mm/s, a force capacity of 8 N and can travel over 16 mm.

Keywords: Precision Positioning, Compact Vertical Stage, Piezoworm Motor, Complementary Clamp, Amplified Piezoelectric Actuator.

Acknowledgements

First of all, I praise God the almighty for providing me this opportunity and granting me the capability to proceed successfully. This thesis appears in its current form due to the assistance and guidance of several people.

It is hard to overstate my gratitude to my supervisor Dr. Shaun P. Salisbury for his enthusiasm, his inspiration, and his great efforts to explain things clearly and simply, he helped to make this research really enjoyable to me. Throughout my work, he provided encouragement, sound advice, good teaching, and effective technical guidance. The research would not have been possible without his financial support.

I am indebted to the great people who have taught me this subject matter: my undergraduate teachers and graduate teachers. I am also grateful to Chris Vandelaar and Dave Lunn for their good work on helping me building prototype and maintaining the experimental equipment. I would like to thank to my lab colleagues and many student colleagues for providing a stimulating and fun environment in which to learn and grow. I would like to acknowledge the secretaries in the Mechanical and Materials Engineering department of UWO, for assisting me in many different ways.

Lastly, and most importantly, I wish to thank my parents, Alhaj Mohammad Sikander and Nurun Nahar Begum, for their love, understanding, patience, endless support, and never failing trust in me. I would also like to thank my entire extended family for their understanding of my study abroad. My brother, my sisters, my brothers-in-law, and some uncles were particularly supportive.

Table of Contents

List of Tables

List of Figures

Chapter 1

1 Introduction

1.1 Background

Precision linear stages have become essential devices in bio instrument systems, optics, semiconductor-based manufacturing and machining industries because of their salient features such as high positioning resolution, high stiffness, force capacity, speed, and adequate dynamic range [1] - [4]. As an actuator for the precision stage, a piezoelectric actuator is preferred to a conventional electro-magnetic actuator because it provides better linear displacement-voltage characteristic, higher precision, faster response time, and more compactness. Piezoelectric based positioners are widely used for characterization of the surface properties of all types of materials, microsurgery equipment and for the manipulation of atomic and molecular-scale structures including biomolecules such as proteins and DNA where precise and rapid positioning is required. Generally, most of the current positioning stages designed for above mentioned

applications are X positioners or XY positioners performed at the nanometre scale. Therefore, the recent technological advances in precision engineering and the concurrent developments of advanced manufacturing techniques and bio instruments have given rise to an urgent requirement for the development of precision positioning systems capable of executing large displacements in vertical direction with nanoscale resolution and high load capacity or simply Z nanopositioner. Although several means of precision positioning exist in literature, most of them are neither suitable nor readily lend themselves to provide long travel vertical motion. Typically, the motion in this axis is achieved by mounting a stage on an L-bracket which often has low force capacity and lacks compactness. The actuator must have to provide enough output force to lift a mass mounted on it along with positioner weight against the effect of gravity.

While a number of researches have been conducted in piezoelectric actuator designs, such improvements have generally focused on the mechanics and control systems to provide high resolution, better stiffness, increased output force and reduced drift. Despite these improvements it is often desirable during an experimental or manufacturing procedure to execute long range approach of a probe/tool with respect to the target sample. Although current linear positioners can achieve nanometer resolution, they have a very limited travel range (only a few hundred μm). This limitation has been addressed by designing hybrid system or dual stage, where either the piezoelectric actuator driven positioner with nanometer resolution is mounted piggy-back style on top of a coarser micropositioners or the moving platform is decoupled from a brushless linear motor, a lead screw or a ball screw of the positioner by frictionless flexure and piezo actuators in order to provide the extended travel range. The performance of such

systems, in terms of design accuracy, resolution, travel range and drift, are obviously determined by the coarser mechanical component. Therefore, such systems do not provide reliable performance below the micron level. Some linear positioners employ traditional rotary motors such as DC or stepper motors to achieve extended travel range. These rely on transmission devices such as lead screw or ball screw and nut, rack and pinion, or conveyer belt to convert rotational motions into linear motions. Such motors are incapable of very high resolution movement due to some degrees of nonlinearity and errors like friction or backlash, making them inadequate for nanopositioning applications. Another common method to multiply the travel range is lever mechanism. Lever mechanisms could amplify overall travel ranges from a dozens to a few thousand μm at the cost of lower stiffness and speed. And this range is still too small to span the area of interest in many applications.

In this research we pursued a new class of compact Z nanopositioning systems that addressed the drawbacks of the traditional technologies and at the same time found increasing usage in biomedical research and other applications requiring long range vertical motion nanopositioning.

1.2 Literature Review

Nanopositioners are mechatronic systems designed to move objects over a working range with high resolution, accuracy and fast response time. Such a system is basically comprised of four elements: at least one actuator or a number of actuators that provide motion, a mechanical translation mechanism or stage where the actuator is typically integrated, a position sensor to measure the displacement, and control electronics to maintain the desired position. The accuracy, speed, output force and

stroke are important performance factors of a precision stage. In general, a mechanical stage consists of a moveable component with a rigid structure. The moveable and static portions are machined from a metal block or bar and, sometimes, connected by flexure hinges. The moveable component can move in any or all of three translational axes as well as in angular axes such as rotation or tilt, depending on the design.

Piezoelectric actuators are promising because of their attractive features such as high positioning resolution, high stiffness, high output force and high speed. Among other advantages are no magnetic fields, vacuum and clean room compatible. The limitations are very small range and significant hysteresis which is a function of frequency, voltage and load [5]. This very limited displacement severely restricts its immediate implementation for long-range precise positioning. This can be addressed by an inchworm® or piezoworm motor consisted of three or more piezoelectric actuators which can produce precisely controlled unlimited travel and is extraordinarily fast.

Applications in a variety of fields require novel positioners to provide faster throughputs and high output force across longer travels with increasing dynamic and static accuracy. In many applications, compactness is desired, yet long travel ranges are demanded. Such novel nanopositioning tools have high demands in biomedical applications, such as stem cell manipulation [6], in-vitro fertilization [7] and electrophysiology [8]. The details on the application of the nanopositioners are presented in the following sub-section.

1.2.1 Examples of Z-axis Nanopositioning Applications

In this section, some of detailed applications in established technologies are discussed herewith for a review of emerging issues in nanopositioning systems that

provide vertical motion over extended ranges. This section also outlines the design challenges associated with Z precision positioning stages.

1.2.1.1 Stereotaxic devices

Stereotaxic devices play important roles in breast skin calcifications [9] and in minimally invasive surgical intervention in tumor surgery [10], and neurosurgery [11]. The stereotaxic instruments incorporate motorized stages and/or encoders mounted on to linear stages which enable a probe/tool to be positioned with respect to the target area prior to surgery. Recently, Discovery Technology International has developed a novel robotic system for stereotaxic surgery (Fig. 1.1). This new system combines two main systems: the RoboMate system and a nanopositioning XYZ system that can provide 100 mm of travel range in each direction. The whole system has total height of 600mm. The Z axis motion is achieved by a positioner attached to an L-bracket mounted on the top of XY positioner.

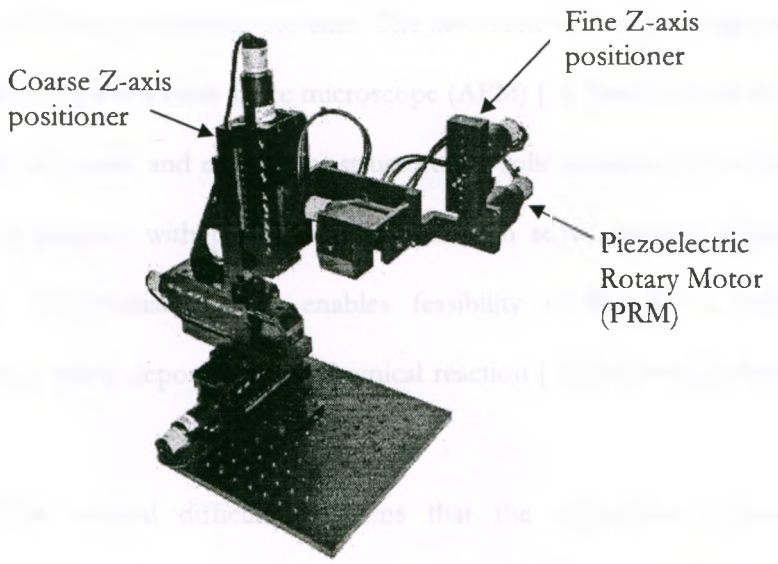

Fig. 1. 1. DTI's NanoRobot-6AX for stereotaxic applications [12].

The RoboMate incorporates two piezoelectric rotary motors and a vertical stage which enable it to provide both the angular approach and the linear movement of the probe/tool at the same time. As a result, the first rotary motor of RoboMate is mounted via a secure bracket to the Z-axis of the nanopositioning system. This is actually the limitation of a positioning stage designed for the motions in horizontal axis when used for the purpose of achieving motions in vertical axis. Such configurations often have low force capacity. Instead of mounting the motor directly on the positioner, secure and rigid brackets are always needed. This is particularly inconvenient in biomedical applications where long range to cover the entirety of the target body is required and miniaturization of the system is also desirable. This wide range of applications with operation under such critical conditions poses new challenges for Z-axis nanopositioning devices.

1.2.1.2 Scanning Probe Microscopes

Successful manipulation and interrogation at the atomic scale depends heavily on the performance of Nanopositioning systems. The invention of the scanning tunneling microscope (STM) [13] and atomic force microscope (AFM) [14] have opened the doors of rigorous study of atomic and electronics structures of solid surfaces [15] which is an important part of physics, with particular applications in semiconductor physics and microelectronics. In chemistry, STM enables feasibility studies for a variety of applications such as metal deposition and chemical reaction [16] on semiconductor and metal surfaces.

One of the several difficult problems that the researchers creating and developing STM faced was the precise positioning of the tip's location and movement. The distance between the tip and the surface must be within a few nanometers. By

appropriately controlling the piezoelectric based positioner, an STM achieves precise control over the tip's location over the sample. The movement in the Z direction directly affects the scanning precision, while the X and Y directions define the area scanned at the surface. The configuration shown in Fig. 1.2 places the STM tip on a fine Z-positioner which is placed on combined XYZ coarse positioners and the sample is placed on a combined XY fine positioner.

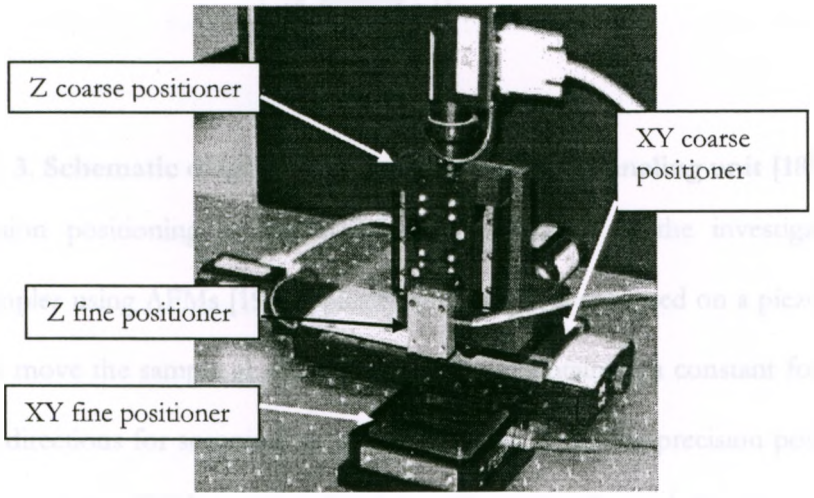

Fig. 1. 2. Experimental setup of the STM module positioner [17].

An ultrahigh vacuum STM with a piezoworm for coarse positioning is designed in [18]. The piezoworm is composed of five piezoelectric stacks where three of them are used as clamps and the remaining two as extender between the clamps. STM has contributed to the innovations of various related probe-type measuring techniques like the near-field scanning optical microscope (NSOM) and the magnetic force microscope (MFM) [5].

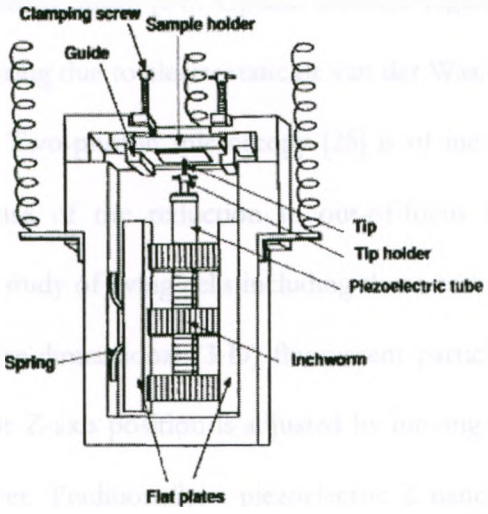

Fig. 1. 3. Schematic diagram of piezoworm driven tunneling unit [18].

Precision positioning of the AFM-probe is critical to the investigation of biological samples using AFMs [19]. Typically, the sample is mounted on a piezoelectric tube that can move the sample in the Z direction for maintaining a constant force, and the X and Y directions for scanning the sample (see Fig. 1.3). The precision positioning in Z axis between the AFM probe and the sample surface is needed to maintain the probe-sample force at no more than $1nN$ [20, 21] for preventing the damage and distortion of soft biological cells [22, 23]. In addition, high speed AFM probe positioning is essential for imaging the movements of a living cell or the formation of surface features during materials processing..

The near-field scanning optical microscope (NSOM) can generate images with a resolution of about 15 nm if the probe-sample distance is within about 5 nm [24]. Here, Z nanopositioning is critical for a distortion-free and high-resolution image. A signal generated by the probe scanning position (X-Y) and distance from the surface (Z) is used to display an image of the topography in the same way that an electron beam paints

a television or computer screen image [24]. Optical distance regulation is a promising solution to the problems arising due to electrostatic or van der Waals attraction between the probe tip and a liquid. Two-photon microscopy [25] is of increasing utility to the field of cell biology because of the reduction in out-of-focus photobleaching and photodamage, allowing the study of living cells including those cases where UV imaging is not possible. During three-dimensional (3-D) fluorescent particle tracking [26] in a two-photon microscope, the Z-axis position is adjusted by moving the objective with a piezoelectric based positioner. Traditionally, a piezoelectric Z nanopositioner equipped with a linear variable differential transformer (LVDT) sensor and operated in closed-loop configuration is placed below the objective. The function of the Z nanopositioner on the objective is to change the laser focus at two planes. The difference of the fluorescence intensity in the two planes is used to calculate the Z-axis position of the fluorescent particle. Therefore, exploiting the full potential of these microscopes relies heavily upon the development of high precision Z nanopositioning stages. Speidel et al. [26] presents a method for 3-D tracking with a different basis that uses standard epifluorescence video imaging in off-focus mode and allows the tracking of particles with 100-ms temporal resolution. However, it is limited to particles moving less than 3 μm in the Z direction. Therefore, improved microscopy techniques are demanded by several fields, such as basic materials science, nanotechnology and life science. The solution lies on long range high precision positioning systems with large load capacity. In sum, long range Z axis nanopositioning is an emerging field in high-speed fluorescence and confocal microscopy applications.

1.2.1.3 Nanomanipulator Systems

Nanomanipulator systems are used for micro and nano particle handling, micro and nanoscale production processes such as MEMS assembly and nano welding. A typical nanomanipulation tool used for these purposes accommodates piezo-motor actuated nanopositioners in order to achieve several degrees of freedom - one in each orthogonal axis (X, Y, and Z) and, in some cases, a fourth for tilting capability. Actuators for micro and nanomanipulation must exhibit high resolution, large travel ranges, robustness against external influences [28] and high bandwidth.

Cell microinjection procedure can be tedious for large numbers of cells and the procedure frequently damages and kills the cells, even conducted by the highly skilled operators [29]. One of the reasons to cell death is that most microinjection instruments do not have very fine positioning and its precise control over needle movement during injection. This can be addressed by designing proper microneedle [29] or microgripper [30, 31] connected to an end-effector and a nanopositioner enables precise X, Y and Z manipulation of the end-effector.

Precise high velocity in the Z direction is needed in the typical cell manipulation such as clean penetration without dimpling, especially for tough cell membrane. Probing of individual cells of primary plant tissues uses two techniques [32]:

1. Measurement of the static pressure on the vacuole of a cell by a fine tube. Here the insertion of the extremely fine tube through the cell membrane is performed by micromanipulation device. For better performance, nanomanipulation devices with Z-axis nanopositioners are required.

2. Application of a very fine glass probe and a highly sensitive load cell. In some cases, it is necessary to achieve a load resolution of ±15 μN for a load from 0 to 0.06N [33]. The load cell has to be driven vertically downward into the test material. The improvement of the results can be achieved by a Z-axis positioner that provides travel upto several millimeters with positional resolution in nanometer scale.

1.2.1.4 Optics

Nanopositioning mechanism could provide the level of precision motion required by optical alignment systems [34], [35], astronomical telescopes [36] or optical fabrication. Future interstellar explorer missions will require a high-bandwidth communications, preferably optical communications, link with a terrestrial monitoring station [4]. One major difficulty in operating an optical communication system over such great lengths is that the beam steering mechanism must have extended travel ranges with very positioning accuracy. A nano-radian scale error in the beam placement when transmitting data to a planet far away from Earth could result in kilometre scale error when the beam reaches the planet or vise versa [4].

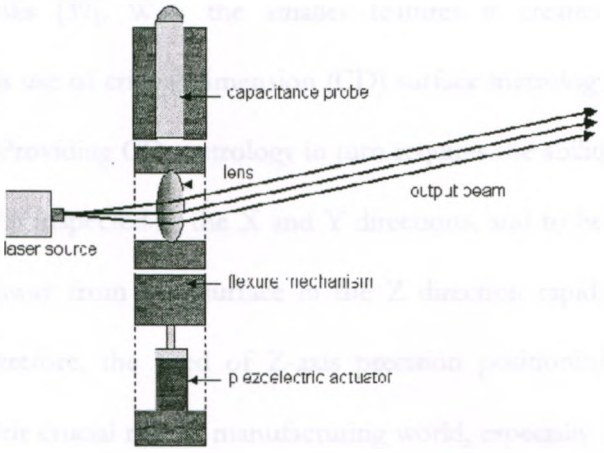

Fig. 1. 4. A nanopositioner used in Beam steering applications [4].

1.2.1.5 Manufacturing

Most of the current positioning devices are used in biomedical applications and research labs since they have their limitations in responding to manufacturing requirements. High precision positioning over long range is becoming increasingly demanding to bridge the gap between micro and nano fabrication when linking compound geometric patterns containing nanostructures with their much larger I/O connections [37]. Today manufacturing techniques such as casting, grinding, milling and even lithography are to continue the miniaturization trends. At the same time electronic devices continue to grow more powerful and versatile while they continue to become physically smaller. Semiconductor manufacturers now routinely use μm scale design rules. Smaller feature sizes are providing the driving force for the development of next generation lithography techniques such as electron-beam lithography and ultraviolet photolithography [38].

With these changes comes a pressing need to inspect the wafers produced rigorously, and even to inspect some of the tools used to produce the wafers such as advanced photomasks [39]. With the smaller features it creates, next generation lithography demands use of critical dimension (CD) surface metrology [40] that is faster and more accurate. Providing CD metrology in turn requires the ability to move a probe across a surface to be inspected in the X and Y directions, and to be able to move the probe toward and away from that surface in the Z direction rapidly, repeatedly, and accurately [40]. Therefore, the need of Z-axis precision positioning stages increased drastically due to their crucial role in manufacturing world, especially for the fabrication and assembly of micro and nano-sized objects. A magnetically levitated multi-axis

nanopositioner for precision manufacturing applications has been designed in [41]. The stage is capable of generating translation of 300 μm in Z axis and it can carry and precisely position a payload as heavy as 0.4 kg with the pull-out force of 8.08 N in the vertical direction.

In recent years, several Z axis precision positioning stages have been designed by Physik Instrumente [42]. However, the vertical travel ranges of these stages are limited to micrometre range only and the output forces provided by these are also low. These limited travel ranges are impractical considering the own heights of the stages. Although Physik Instrumente has very recently developed a linear stage for vertical motion termed as M-714 that has long travel range and high load capacity, it relies on hybrid drive technology that uses both piezoelectric actuators and DC servo motor. It requires backlash and stick/slip compensations and simultaneous control of both drives.

1.2.2 Actuators for Nanopositioning

DC motors are used in positioning stages for general applications where high output force and high speed are required. If an application requires linear motions, lead screw or ball screw are used to provide rotator-to-linear motion. The lead screws have the capacities of high stiffness, thrust, and speed, but suffer from backlash and stick slip. The tradeoff between backlash and stick slip does not help in achieving high positioning resolution and load capacity simultaneously. Ball screw actuators are capable of providing even more thrust and longer range at higher speed. However, these motors are bulky and this is particularly inconvenient in case of Z-axis stage positioners since the effect of gravity has to be considered. On the other hand, voice coil motors are very accurate but lack stiffness and sometimes generate significant electrical disturbances.

Therefore, it can be concluded that the traditional motors are not suitable for nanopositioning.

In this section, we discussed about five types of actuators suitable for precision positioning. They are piezoelectric actuators, magnetic actuators, electrostatic actuators, shape memory alloy actuators, and thermal actuators. Selection of actuators depends on application requirements such as structural size, force, displacement, response speed, power consumption, complexity of control and costs.

1.2.2.1 Piezoelectric Actuators

A piezoelectric ceramic is a mass of perovskite crystals, in which each crystal is composed of a small, tetravalent metal ion placed inside a lattice of larger divalent metal ions and O_2 [43]. Common types of ceramic are $BaTiO_3$, PZT or $(Pb(ZrTi)O_3)$, ZnO. Although the piezoelectric effect was first used by Pierre Curie in 1880 to measure the charge emitted by radium, it was not used for any practical applications for a third of a century [44]. However, the use of piezoelectric materials as actuators exploits the converse effect, i.e., gain of mechanical strain upon the application of an electric voltage. The converse piezoelectric effect, that is the change in dimensions of the crystal on the application of a voltage, was predicted theoretically by Lippman on thermodynamic principles [44]. Piezoelectric actuators made of ceramic PZT have been common for a long time, but recently thin-film actuators have started to appear in many applications [45].

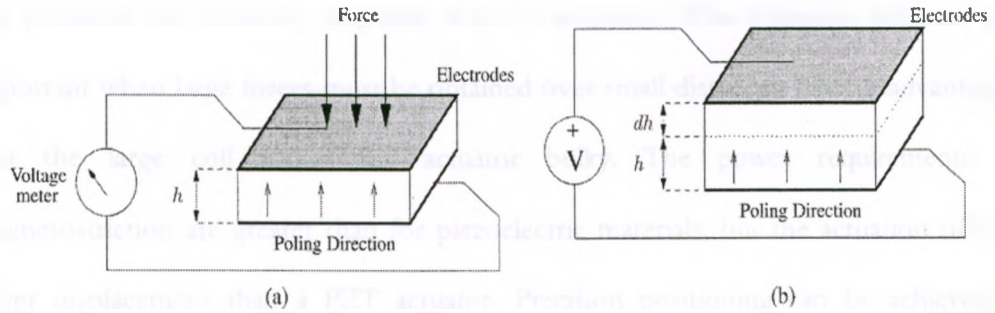

Fig. 1. 5. (a) Direct Piezoelectric effect, (b) Converse Piezoelectric effect [56].

Piezoelectric actuators have excellent operating bandwidth and can generate large mechanical forces in a compact design and for small amounts of power, but they have a relatively small displacement range. The electromechanical equations for linear piezoelectric material are given in [46], [47] as

$$S_i = s_{ij}^E T_j + d_{mi} E_m \tag{1.1}$$

$$D_m = D_{mi} T_i + \epsilon_{mk}^T E_k \tag{1.2}$$

where the indexes i, j = 1,2, …., 6 refer to electric field direction and m, k = 1,2,3 refer to the direction of reaction (e.g., strain). S, T, D and E refer to the mechanical strain, stress, electrical displacement, and electric field, respectively. The material properties s^E, d, and ϵ^T represent the elastic, piezoelectric strain, and dielectric constants respectively. The second equation describes the direct while the first one describes the converse piezoelectric effect. Depending on their electromechanical properties, different materials are considered either for sensor or actuation.

1.2.2.2 Magnetostrictive Actuators

Magnetostrictive material has the ability to convert electrical energy into mechanical energy due to magnetization which induces a dimensional change of the material [48]. Typically, current passing through a coil located around a magnetostrictive

rod produces the necessary magnetic field for actuation. This actuation mechanism is important when large forces must be obtained over small distances. The disadvantage is that the large coil makes the actuator bulky. The power requirements for magnetostriction are greater than for piezoelectric materials, but the actuation offers a larger displacement than a PZT actuator. Precision positioning can be achieved by precise control of the current. Nanometer-scale precision is also achievable with magnetic levitation systems [49] by using magnetic field to levitate an object. To keep the balance between magnetic force and gravity, graphite is used as diamagnetic materials.

A planar electromagnetic nanopositioner having a travel range of 60 μm with an average power consumption of 10 to 20 mW in each of X-Y axis is shown in Fig. 1.23. This design is suitable for parallel probe-based mobile storage devices or as a generic nanopositioning system for other nanotechnology applications.

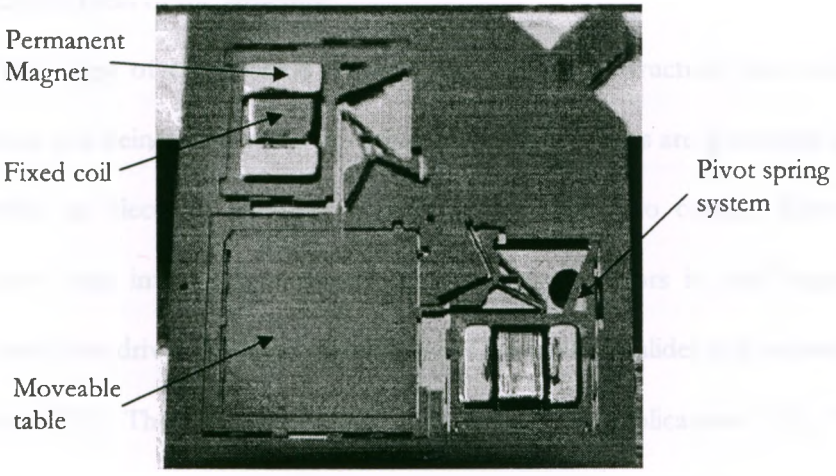

Fig. 1. 6. Silicon Microscanner [50].

1.2.2.3 Electrostatic Actuators

Electrostatic actuators [51] widely used in the MEMS field because of their ease of fabrication as only the structural material needs to be conductive. The electrostatic force generated by two parallel plates is given by (1.3)

$$F = \frac{1}{2}\frac{\varepsilon_0 A V^2}{d^2} \tag{1.3}$$

where A is the plate area, V is the voltage applied, d is a gap between the parallel plates, and ε_0 is the permittivity of free space. The maximum displacement of the moveable part depends on the initial gap d_0 as given in (1.4)

$$\Delta d_{max} = \frac{1}{3} d_0 \tag{1.4}$$

And the maximum voltage can be calculated by (1.5).

$$V_{max} = \sqrt{\frac{8kd_0^3}{27A\varepsilon_0}} \tag{1.5}$$

where k is the stiffness of the structure.

Another type of electrostatic actuator has comb like structure that consists of two capacitors, one being fixed while the other is movable. Forces are generated between the gaps while an electrical potential applied between the two combs. Electrostatic actuators have been intensively explored as secondary actuators in dual stage servo systems of hard disk drives (HDDs), particularly in the actuated-slider and actuated-head configurations [52]. They are also used in microgripper applications [53]. Vertical motions toward or out of a wafer surface are demonstrated in optical signal processing applications [54]. However, the drawbacks of interdigitated comb drives are they generate relatively weak force while they require high voltage [55].

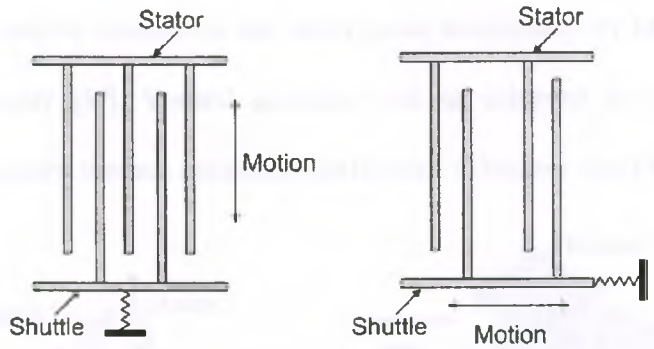

Fig. 1. 7. Electrostatic microactuators: (left) interdigitated comb actuator and (right) parallel-plates actuator [56].

Another type of actuator known as electrostatic surface actuator also consists of two periodic electrode structures: one fixed (to the stator) and the other movable (on the translator) [57]. In-plane forces are generated between them that cause the translator to move with respect to stable positions. These forces are determined by the spatial phase relationship between the two sets of periodic electrodes and the voltages applied to them [57]. For continuous motion, each surface has multiple periodic electrodes that can be successively activated to create a voltage wave to move the translator in the desired direction [56]. However, this type of actuator also exerts comparatively large forces, which must be taken into account in the design of flexure springs used to hold the translator above the stator. Still this range is too small to be utilized in many applications.

1.2.2.4 Thermal Actuators

The driving mechanism in thermal actuation is based on thermal expansion of material and mechanical amplification. Two types of thermal actuators are commonly available: the asymmetric type and the symmetric type. Asymmetric actuators include the bimorph effect using cantilever beams and the pseudobimorph effect using hot-cold arms [58]. Bimorph actuators consist of vertical bimorphs with silicon beams side-coated

with aluminum that can be actuated in the wafer plane horizontally by heating due to electrical current supply [59]. Vertical actuation can be achieved by stacking two materials and utilizing their thermal expansion coefficients difference (see Fig. 1.8a).

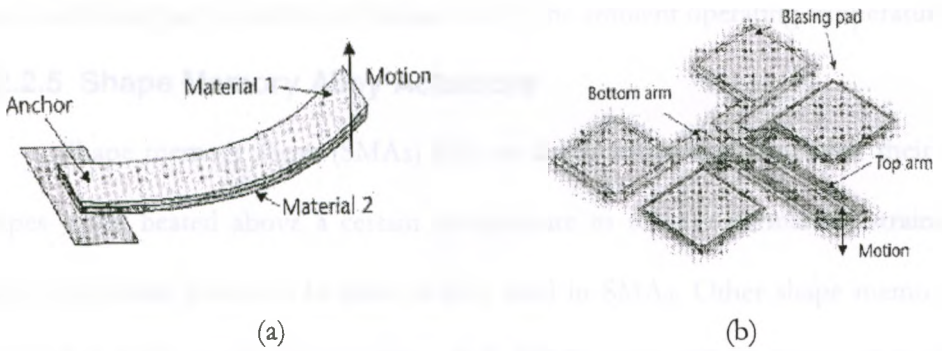

Fig. 1. 8. Vertical thermal actuators (a) Bimorph and (b) Pseudobimorph [59].

A vertical thermal actuator has been designed with two layers of arms vertically stacked [60] for out-of-plane actuation (see Fig. 1.8b). Here, microstructures with single-layer material can produce in-plane motion because of the difference in thermal expansion of a narrow hot arm and a wide cold arm. A MEMS hot-cold-arm thermal actuator design is described in [60] with bidirectional vertical motion. This design is a U-shaped structure with an active return current path that provides a larger deflection and better electrical efficiency than the traditional vertical thermal actuator does.

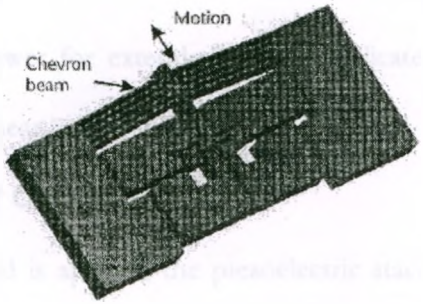

Fig. 1. 9. Chevron beam thermal actuator [61].

In chevron beam configuration, an array of buckled beams [61] are arranged close together and connected to two similar arms at the both ends. This provides linear deformation and force of millinewton range. However, the uses of thermal actuators in nanopositioning applications are limited due to the ambient operating temperature.

1.2.2.5 Shape Memory Alloy Actuators

Shape memory alloys (SMAs) [62] are metal alloys that remember their original shapes when heated above a certain temperature to recover permanent strains. Ni-Ti alloys have been found to be most widely used in SMAs. Other shape memory alloys include Cu-Al-Ni and Cu-Zn-Al alloys [63]. SMAs are useful for actuators that change shape, stiffness, position, natural frequency, and other mechanical characteristics in response to temperature or electromagnetic fields [64]. Bending, torsional, and extending actuations have been accomplished by SMA actuators depending on their designs. Some exploit integrated resistive heaters on the SMA films while some others directly utilize electrical currents on the SMA wires. The torsional mechanism utilizes a twisted SMA coil fixed inside a liner coil. When the SMA coil is heated above the transition temperature, it becomes untwisted. Thermal sensors are used to precisely control of the motions. Current SMA actuators suffer from some shortcomings such as vulnerability to excessive power for extended periods, delicate protection system, low bandwidth and highly non-linear behaviour.

1.2.3 Piezoworm Motor Concept

When an electric field is applied, the piezoelectric stack expands and produces the linear motion output. When the electric field is withdrawn, the stack contracts which causes the mechanism to return to its initial position. Piezoelectric actuators used in

piezoworm configuration can achieve centimeter scale range motion with nanometer scale accuracy by rapidly repeating a clamp-extend-clamp cycle. Fig. 1.10 shows six actuations result in one step motion of piezoworm motor. The energized piezostacks are shown by shaded color.

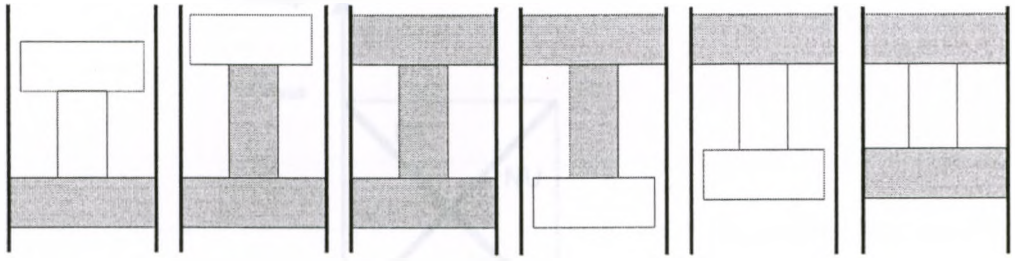

Fig. 1. 10. Actuation sequence of a typical piezoworm motor in vertical direction.

In conventional piezoworm actuation, the gripping clamp is completely engaged before the releasing clamp begins to unclamp. Each clamping action demands an individual actuation step. In complementary piezoworm, the intermediate steps are reduced since the unclamping and clamping occur at the same time as shown in Fig. 1.11. Here the both clamps can act simultaneously without losing contact with the guideway which is important in safe vertical positioning.

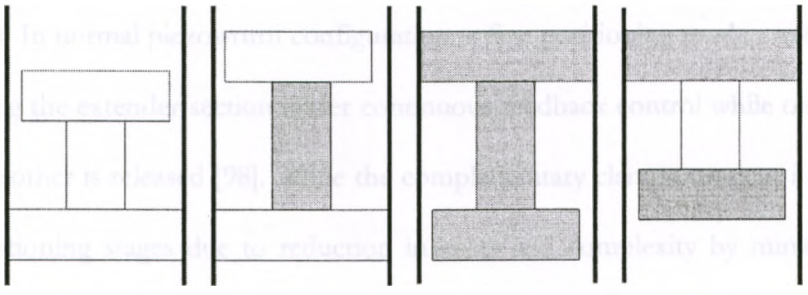

Fig. 1. 11. Complementary clamp configuration results in less actuation steps.

Considering a constant coefficient of friction, the restraining force vs. applied voltage characteristics for both NU and NC clamps are illustrated in Fig. 1.12. This

characteristic depends on the properties of the piezoelectric stack, the stiffness of the clamping flexure and the coefficient of the friction between the guideway and clamping surfaces.

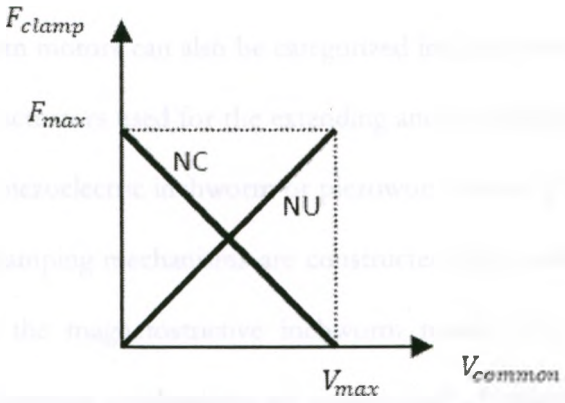

Fig. 1. 12. Force-voltage characteristics of the complementary clamps.

During each step of piezoworm operation, one of the two clamps grips while the other one releases. Each of the piezoworm's actuator can be operated independently, if driven by individual amplifiers. The complementary clamp configuration allows the clamps to share a common channel and, thereby, to reduce the required drive electronics. It is also possible to enter the fine positioning mode with both clamps unpowered. In normal piezoworm configuration, a fine positioning mode can be realized by activating the extender section under continuous feedback control while one clamp is on and the other is released [98]. While the complementary clamps concept is desired in planar positioning stages due to reduction in costs and complexity by minimizing the drive electronics, it becomes necessary in vertical positioning stages in order to hold the moving stage as well as the payload during unpowered state. Therefore, piezoworm based on complementary clamp concept allows safe vertical climbing by maintaining a

fixed position of the stage at any time. For smoother and continuous vertical positioning, it is important to slow down the unclamping relative to clamping during switching transient.

1.2.4 Piezoworm Motor Design

The inchworm motors can also be categorized into different categories based on the materials of the actuators used for the extending and the clamping mechanisms. The first category is the piezoelectric inchworm or piezoworm motor [65], in which both the extending and the clamping mechanisms are constructed of piezoelectric actuators. The second category is the magnetostrictive inchworm motor [66], in which both the extending and the clamping mechanisms are constructed of magnetostrictive actuators. The disadvantage is that the actuator that uses magnetostrictive material requires a large coil around it to create the magnetic field which makes the actuator bulky. Another catergory is the electrostatic inchworm actuators [67] which make use of electrostatic gap-closing actuators to generate high force densities at small displacements with low power consumption. The last category is the hybrid inchworm motor [68], in which the extending and the clamping mechanisms are made of the different types of actuators.

Piezoworm actuators operate by incrementally summing up micron-sized displacements into a single large displacement. Due to the advantages of the piezoelectric actuator and amplifier costs being significantly reduced in mid-90s, the piezoworm development has been actively increased afterwards. The piezoworm designs are generally of four types as shown in Table 1.1.

Table 1. 1. Different piezoworm actuator configuration

Type	Shaft/Guideway	Clamps Translate
I	Shaft	No
II	Guideway	Yes
III	Guideway	No
IV	Shaft	Yes

Types I and III are simpler than type II to produce. In the type I and III piezoworm, the fixed clamps reduce the complexity during large step positioning. Nonetheless, the type II has advantage of providing higher load capacity for the same size motor because there is more surface area for the clamps to contact which means higher friction forces.

One of the original piezoelectric piezoworm motors of type I was introduced by Hsu in 1966 [69]. The extending mechanism utilized a piezoelectric tube to create the motion forth and back. The clamping mechanisms used a one-way clamping technique, by means of two annular wedge surfaces inclined to the shaft's axis such that the wedged members could prevent motion in either direction (see Fig. 1.13).

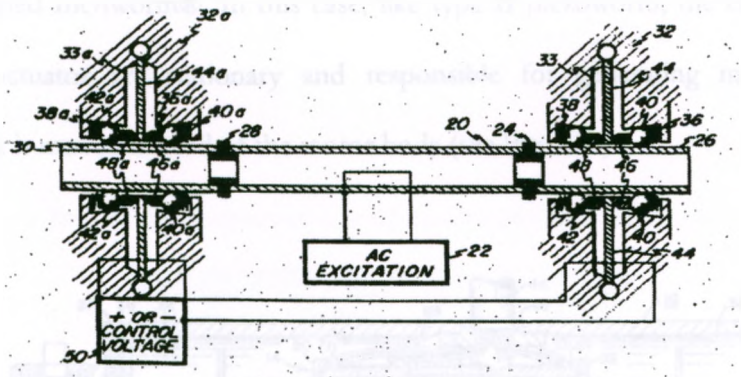

Fig. 1. 13. Hsu piezoworm design [69].

Galutva et al. in 1972 [70] is the first example to use piezoelectric stacked actuators to create a piezoworm motor of type II. The piezoelectric stacked actuators were used both to create the forward motion and to directly clamp the walls of the guideway (see Fig. 1.14). The motor moves through a guideway by utilizing its clamps and extension parts.

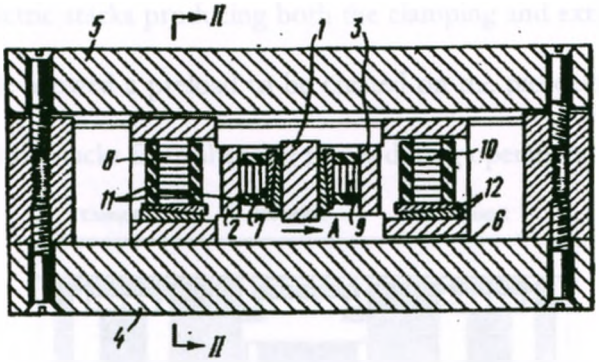

Fig. 1. 14. Galutva piezoworm design [70].

One of the most revolutionary piezoworm motors of type I was introduced by R.A. Bizzigotti and W.G. May. The design created for Burliegh Instruments, Inc. [71] was used as a basis for their production Inchworm motors in 1975 under the

trademarked named Inchworm®. In this case, like type II piezoworm, the clamps and the extension actuator are stationary and responsible for generating movements. However, a shaft is moved instead of the motor body (see Fig. 1.15).

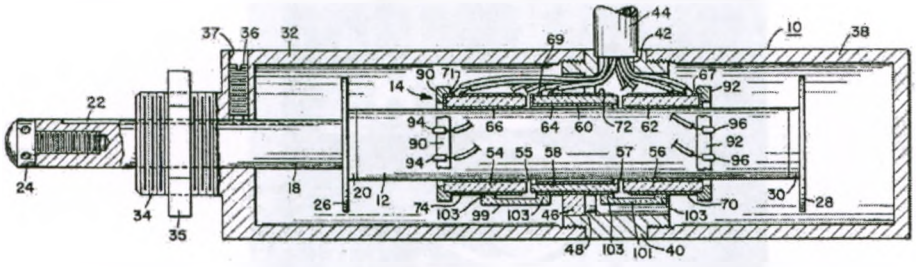

Fig. 1. 15. Burleigh Inchworm® design [71].

Zhang and Zhu [2] have proposed an piezoworm actuator (see Fig. 1.16) which has very large output force 200 N with range of 300 mm and operates at 6 mm/s. Their design included a structure created from a single flexural block. The flexure frame contains three piezoelectric stacks producing both the clamping and extending motions. Using the flexure frame allowed a preload to be created on the piezoelectric stacks and protected the piezoelectric stacks from shearing forces during operation.

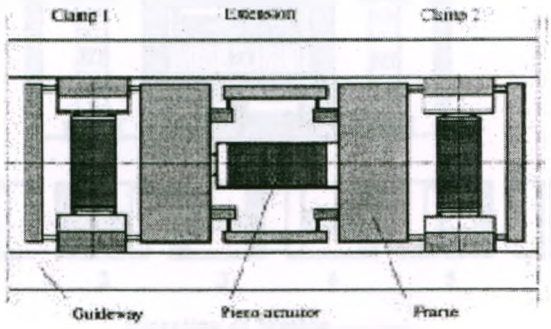

Fig. 1. 16. Zhang & Zhu piezoworm design [2].

To achieve smooth and continuous motion, many researchers employed more piezoelectric actuators in their piezoworm configurations, while in some cases the

researchers [72] used as many as 12. Amplified piezoelectric actuator (APA) was used to provide extending motion in the piezoworm designed by Vaughan [73]. Their motor produced a velocity of 4.9 mm/s at a drive frequency of 50 Hz and a stall load of 17 kilograms. The stall load of the design was severely limited by clearance losses.

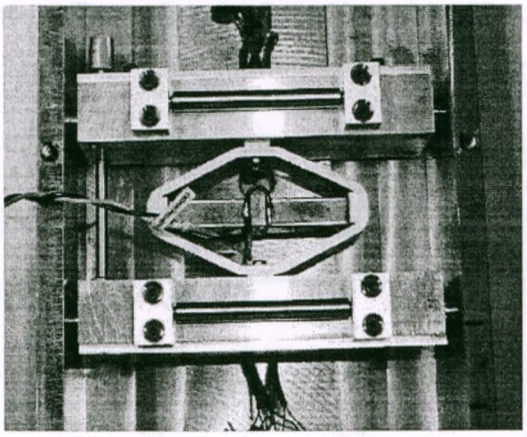

Fig. 1. 17. Vaughan piezoworm motor [73].

Piezoworm based positioner designed by Tenzer and Ben Mrad [3] has also large output force 150 N with long range of 200 mm at relatively higher speed of 8 mm/s (see Fig. 1.18).

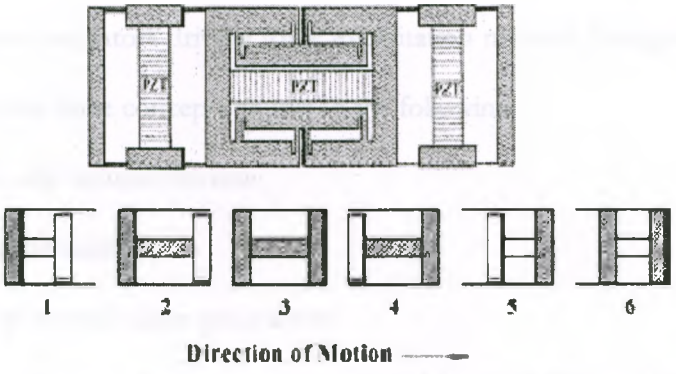

Fig. 1. 18. Tenzer piezoworm design and operation principle [3].

While numerous piezoworm motors have been proposed in literature as shown in Table 1.2, none of the approaches provide the large vertical travel actuation that is required.

Table 1. 2. Survey of different piezoworm actuators performances

Researcher	Type	Range(mm)	Speed(mm/s)	Thrust(N)	Year
Burleigh [71]	I	25	1.5	15	1975
Zhang [2]	II	300	6	200	1997
Galante [74]	II	6	8	200	1999
Vaughan [73]	II	N/A	5	170	2001
Tenzer [3]	II	200	8	150	2004
Salisbury [65]	I	50	8.5	10	2006
Moon [75]	III	100	10.2	10	2006

1.2.5 Stage Driving Principles

The piezoelectric actuator based positioning stages can broadly be divided into three types in terms of actuators driving force exploitation method. Designing of stages are based on one of the three concepts shown in the following:

I. stick–slip induced friction,

II. lever mechanism,

III. clamp-extend-clamp piezoworm.

The first notable type I stage was investigated by Pohl [76] in 1987 where the principles of inertial and frictional force were utilized in driving a stage by means of a piezoelectric actuator. The stage provides step sizes of 0.04 - 0.2μm, speeds of up to 0.2

mm/s and load capacity of 1 kg. The stick–slip friction principle to drive the stage was also adopted by Niedermann et al. [77], Renner et al. [78], Smith et al. [79], Chang and Li [80].

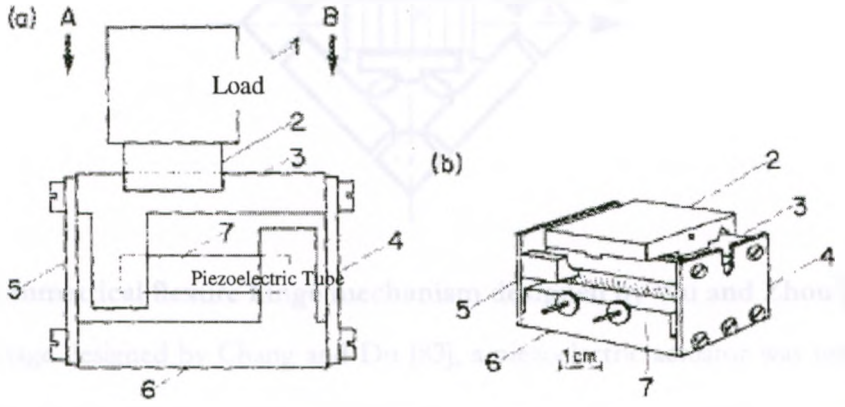

Fig. 1. 19. The stage designed by Pohl [76] can slide between end points A and B.

The first notable type II stage was designed by Scire and Teague [81] in 1978. Fabricating the flexure-pivot-lever system stage involved machining the flexure pivots and levers from a metal blank and integrating the piezoelectric actuator that produces the required displacement input to the lever magnification system. They measured a displacement travel of 50 μm and a displacement resolution of 1 nm. An XYθ_z positioning stage was developed by Wu and Zhou [82] in which 3-DOF motion in plane could be obtained with one actuator. The piezoelectric actuator P causes block A to move in X direction, block B to move in Y direction, and block C rotates round center. Their results indicated that the three axis positioning stage was capable of displacements of 10.6 and 10.3 μm in the X and Y directions, respectively, and had a yaw motion of approximately -27.5 μrad.

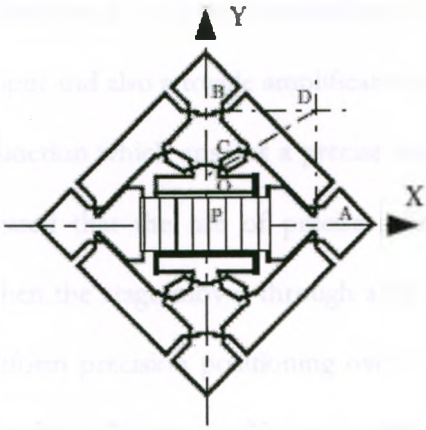

Fig. 1. 20. Symmetrical flexure hinge mechanism designed by Wu and Zhou [82].

In a stage designed by Chang and Du [83], a piezoelectric actuator was used to drive two sets of Scott-Russell straight-line mechanisms to amplify the output displacement of the piezoelectric actuator and to ensure a linear displacement of the positioning device output. They developed a compact positioning stage by forming the flexure hinges and levers in one piece of metal linking a parallel guide spring to the output end of the positioning device (see Fig. 1.18).

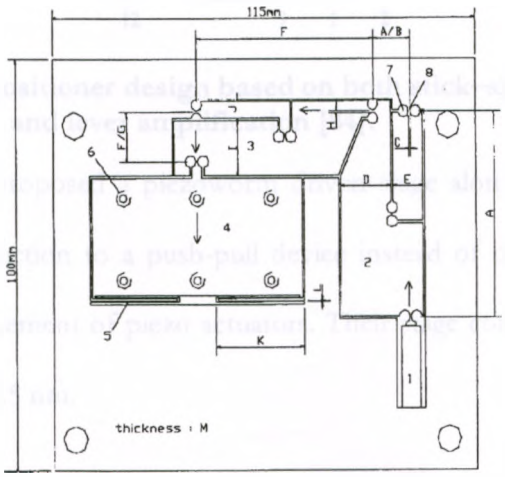

Fig. 1. 21. Chang and Du positioner design with flexure pivoted multiple linkages [83].

Chu and Fan [84] employed a lever mechanism to perform an initial amplification of the actuator input and also a toggle amplification mechanism to perform a second stage amplification function which ensures a precise straight line displacement output. The results demonstrated that the use of precise cylindrical guides reduced straightness error of 50 nm when the stage moves through a 10 mm displacement. (see Fig. 1.19). Their stage can perform precision positioning over a displacement range in incremental step sizes ranging from 70 nm to 35 μ m in the stepping mode and a scanning motion over a displacement range of 50 μ m in the scanning mode.

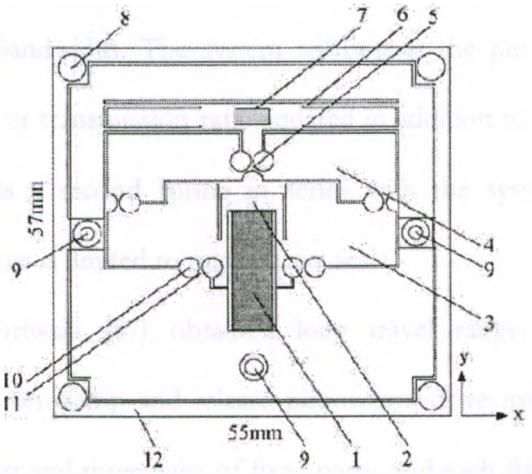

Fig. 1. 22. Chu and Fan positioner design based on both stick–slip friction effect and lever amplification [84].

Kihwan et al. [85] proposed a piezoworm driven stage along with hinge-lever mechanism for motion reduction to a push-pull device instead of conventional hinge levers amplifying the displacement of piezo actuators. Their stage could perform a step movement of 1 nm up to 82.5 nm.

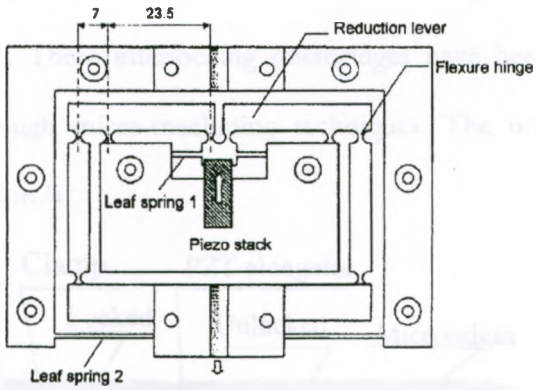

Fig. 1. 23. Kihwan stage design with lever mechanism [85].

Travel amplification can be achieved using levers at the expense of force capability, stiffness, and bandwidth. The system stiffness is the piezoelectric element stiffness divided by the lever transmission ratio squared in addition to the lever stiffness which can be modeled as a second spring in series with the system stiffness [86]. Nonetheless, the travel range is limited to micrometer scale.

Shamoto and Moriwaki [87] obtained long travel range with positioning resolution of 5 nm based on clamp and release piezoworm drive method. The device consists of one moving part and three pairs of fixed parts, and each fixed part has a feed actuator and a clamp actuator. Each pair of the feed and clamp actuators produces the feed and clamp motions within a short stroke by displacing a clamping block supported by eight parallel beams.

Chen et al. [88] presented a Mesoscale Actuator Device (MAD) device of 50 mm size and a pair of 25 mm^2 interlocked area for particular microridges that would support large force output as large as 500 N. This design has similarity to the designs introduced by Murata [89] and Lee et al. [90]. Mechanically interlocking microridges has been

proposed for clamping sections instead of the traditional frictional clamping mechanisms in the typical piezoworm. These interlocking microridges have been produced from single crystal silicon through micro-machining techniques. The motor can produce unloaded speeds up to 5 mm/s.

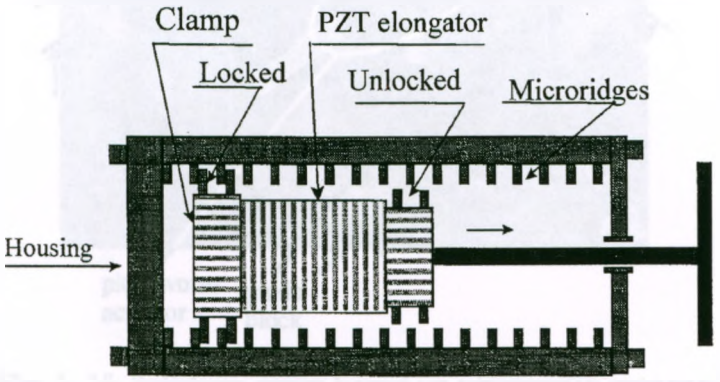

Fig. 1. 24. Piezoworm positioner with microridges interlocking [88].

Salisbury et al. [63] designed compact piezoworm actuators which were integrated into commercially available planner positioning stages. The flexure frames of the clamps and extender are based on improved stiffness model where the effect of shear stress was taken into consideration. A complementary clamp concept is employed so that one voltage signal drives both clamps instead of an individual signal for each clamp. This reduces the driving requirements and control complexity. The stage is capable of providing speed of 8.5 mm/s and load capacity of 10 N.

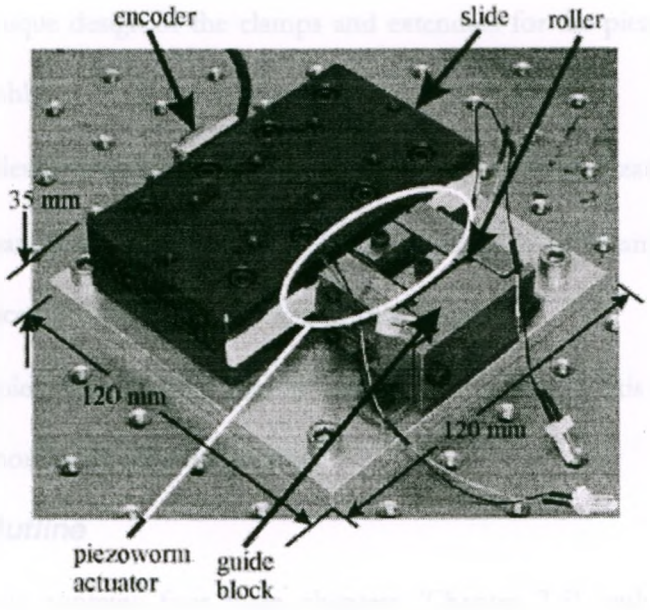

Fig. 1. 25. Salisbury stage based on piezoworm actuator.

From a detailed survey of the literature relating to the development of precision positioning stages, it can be concluded that the clamp release piezoworm type stage has the ability to perform long travel positioning. Conversely, both the stick–slip induced friction drive stages and the elastic deformation type stages have the disadvantage of limited positioning travel range. In addition, using a lever has its disadvantage since the stiffness is inversely proportional to the square of the lever ratio.

1.3 Thesis Objectives

The main objective of this thesis is to develop a Z axis linear positioning system capable of 20 mm stroke with nanometre accuracy and load capacity of 8 N. This can be achieved through the following phases:

- Develop analytical tools to aid piezoworm motor design for travel in vertical direction

- Present unique design of the clamps and extenders for the piezoworm motor to ease assembly.
- Integrate design features that facilitate stage design and optimization.
- Deploy mating drive surfaces through the application of ceramic drive strips to maintain accuracy and minimize wear of the clamps
- Integrate piezoworm motor into an effectively designed Z-axis stage in order to enable a more compact configuration

1.4 Thesis Outline

This thesis contains four main chapters (Chapter 2-5) with an introductory chapter (Chapter 1) and concluding chapter (Chapter 6).

Chapter 2 presents an enhanced stiffness model for Normally Clamped (NC) clamp to achieve high restraining force capacity as compare to the previous designs. This model includes the effect of preloading and analyzed the forces transmitted through the clamp flexure. The deformation induced by blocking force of the moving platform is also considered. This model aids to achieve good performance from flexure system by estimating accurate stiffness and to avoid the instabilities such as buckling or even the component fail down during operations.

Chapter 3 is an overview of the process used to design the piezoworm motor based on flexure mechanism and complementary clamp configuration. This chapter describes a wide range of design configurations to aid in the development of novel vertical positioner. In case of clamp design, symmetrical configurations are preferred to utilize the piezoelectric stack displacement on both sides. The amplified piezoelectric

actuators are proposed as extenders to provide long range vertical motion during fine positioning.

Chapter 4 describes the design and optimization of a novel vertical nano-motion positioner. This design strategy is focused on the light piezoworm actuator as well as compact positioning stage that can be readily configured into multi-coordinate systems to form unique precision manipulators with high speed. A complementary piezoworm configuration based on three piezoelectric stacks and two amplified piezoelectric actuators for Z-axis motion has been described. The moving platform of the vertical positioner consists of a top plate, two friction surfaces and two side plates.

Chapter 5 presents a prototype of the vertical positioning stage which is subjected to static and dynamic evaluations. An experimental assessment of the effects of the frequency and applied force on the piezoworm performance is demonstrated. The similarities and differences between the analytical and experimental results are discussed with possible explanations.

Chapter 6 summarizes the entire project, and proposes future work.

1.5 List of Contributions

The project presented in this thesis makes the following contributions:

- An analytical tool is developed to facilitate rapid design iterations for vertical positioner.
- An improved model of flexure stiffness for Normally Clamped (NC) clamp with effects of preloading has been taken into consideration. The deflection on the flexure induced by the platform during assembly is considered.

- A piezoworm actuator in which the extending mechanism uses two compliant amplified piezoelectric actuators is designed. Three piezoelectric stacks are deployed for the clamps which make a total of five piezoelectric actuators in Z axis configuration. This is due to achieve the objectives of large load capacity and compactness of the structure.
- New configurations of clamp flexure-based frame design are presented. Complementary extension concept is implemented which allows both amplified piezoelectric actuators to extend and compress at the same time by one control signal. This arrangement allows uniform upward and downward movement of the Normally Unclamped (NU) clamp and reduces the number of amplifiers required to drive the extender section and complexity of control. The symmetrical designed clamps normally hold the payload against the force of gravity and do not require power to maintain a fixed vertical position of the platform.
- The stiffness and weight of the positioning platform design is optimized. Both the platform and the piezoworm actuator are designed to be easily assembled which makes the Z-axis stage compact.
- A prototype of the vertical positioning stage based on compliant piezoworm actuator is developed. The prototype is subjected to several tests to assess its performance.

Chapter 2

2 An Improved Analytical Stiffness Model for NC Clamp Flexures

2.1 Introduction

In Chapter 1, we discussed piezoelectric actuators based precision positioning systems used in applications ranging from semiconductor lithography to photonics packaging automation to biomedical research. Such systems require accurate displacement over short distances. The first design rule in nanopositioning is that friction has to be eliminated. It eliminates all devices with ball, roller, or sliding bearings except frictionless air bearings and flexures. A flexure is a frictionless device with high stiffness that relies on the elastic deformation of a solid material to permit motion. They are relatively simpler to manufacture and assemble as the complete mechanism can be produced from a single monolithic block. They do not undergo irreversible deformations which make them free of wear, but at the same time, act as springs. If the stiffness is

known, the spring action is utilized in sensors like accelerometers to get a force or acceleration measurement after measuring the displacement [91]. The reason behind the use of the flexure is that the piezoelectric actuator can withstand large compressive force but generally vulnerable to shear and tensile stresses. Moreover, the piezoworm motor shifts back and forth at a micrometer level during each clamping motion. This phenomenon is known as glitching which is due to the dimensional change of the interface areas between clamp and wall during a clamping motion. The spring action of the flexure is used to preload and protect the actuator from tensile and shear loads [2] by maintaining contact condition during the motion. On the other hand, flexures cannot tolerate overload. If the stress is relatively higher than the ultimate tensile stress, failure can occur after a few hundred cycles or less. Moreover, significant stresses could create some hysteresis in the stress-strain characteristics. For flexure designs, it is desirable that a design will be subject to stresses much lower than the yield stress. Therefore, it is essential for a designer to consider the material properties, nature of applied load and geometric dimensions to predict the force-displacement characteristics accurately.

The concept of complementary clamps in piezoworm is given in [65]. However, the stiffness estimation for Normally Clamped (NC) clamp is based on the same stiffness model considered for the Normally Unclamped (NU) clamp. This is not suitable for the NC clamp flexures used in complementary clamp concept because its clamping force mainly depends on its flexure stiffness, while the piezoelectric stack actuation has less contribution to it, which is opposite to the NU clamp flexure working principle. The displacement of clamp surface depends not just on the kinematics of the mechanism but also on the installation method, which might impart a preload to the flexure in addition

to driving actuation. To date, the effects of preload and driving force on stiffness estimation of the flexures used in complementary piezoworm design have not been reported.

This chapter presents an enhanced stiffness model for a flexure system used in mechanically complementary clamp configuration in piezoworm motors. The long-term linearity and repeatability of the flexure system is ensured by this improved model by good compromising between stiffness the flexure and allowable stress of its material. The stiffness obtained from the model is compared to FEA results.

2.2 Simple Flexure Stiffness Analysis

Flexures are monolithic with the mechanisms they are part of and the mechanisms continue to operate until something fails due to fatigue or overloading. Since repair cannot be done in the flexures, it is necessary to estimate their stiffness accurately during design and to inspect the errors induced in the ideal geometry by machining during fabrication.

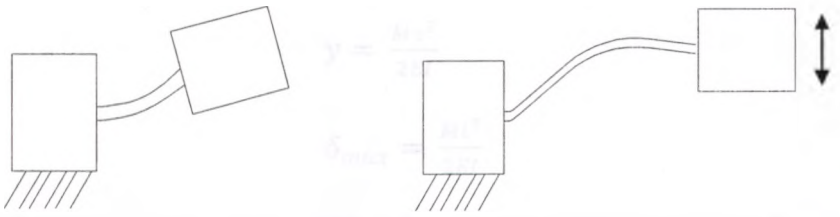

Fig. 2. 1. Common types of flexure mechanisms, (a) flexure hinge and (b) flexure link.

The simplest flexure mechanism is the cantilever beam with both ends built in (no rotation) and linear mechanism, i.e., only the vertical direction movement is permitted. If the supporting structures on the ends of the beam are sufficiently stiff then

the beam can be considered as a single flexure element [94]. In simple cantilevers, greater deflection is achieved by making a longer and proportionally wider flexure.

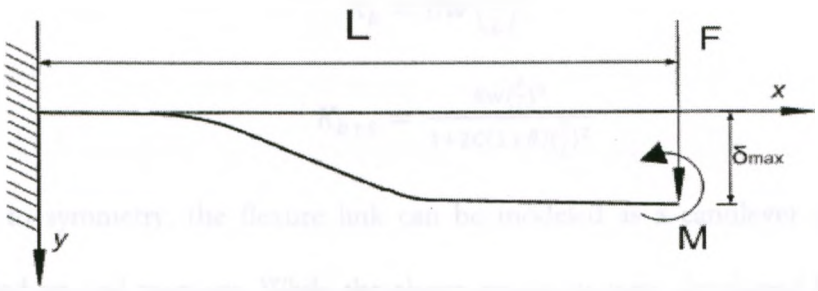

Fig. 2. 2. One end fixed cantilever beam model of simple flexure mechanism.

A load F is applied to the end of the beam of length L and its subsequent displacement in the y direction is obtained by (2.1). In case of a moment M applied to the beam end, the displacement is obtained by (2.3).

$$y = \frac{Fx^2}{6EI}(3l - x) \tag{2.1}$$

$$\delta_{max} = \frac{Fl^3}{3EI} \tag{2.2}$$

$$y = \frac{Mx^2}{2EI} \tag{2.3}$$

$$\delta_{max} = \frac{Ml^2}{2EI} \tag{2.4}$$

If the applied force (F) or moment (M) is known, this deflection is used to determine stiffness of the beam according to (2.5).

$$K = \frac{F}{y} \tag{2.5}$$

Alternatively, the stiffness of the beam with width (w), thickness (t) and modulus of elasticity (E) is given by (2.6) without considering the effects of shear stress. An improved model for the stiffness of a single beam is given in [93] where the effect of

shear stress is considered along with bending stress. Equation (2.7) shows beam stiffness (K_{b+s}) with shear stress correction factor (C).

$$K_b = Ew\left(\frac{t}{L}\right)^3 \tag{2.6}$$

$$K_{b+s} = \frac{Ew(\frac{t}{L})^3}{1+2C(1+\vartheta)(\frac{t}{L})^2} \tag{2.7}$$

Due to symmetry, the flexure link can be modeled as a cantilever beam with point load and an end moment. While the above equations were developed for free or unloaded state of the compliant mechanisms, addition stress occurs in flexure links due to the preload is not taken into consideration. Consequently, the offset of the deflection during the motion of the flexure links is also neglected during the analysis. This causes alternations of flexure mechanism performance to the predicted results. The variation in dynamic fatigue strength of the flexures due to the preloading is shown in [94]. The driving force by actuator cause additional stress in the flexure.

If the stress induced during deformation exceeds the yield stress of the material, permanent deformation or even fracture of the flexure will take place. Therefore, the dimensions of the flexure links has to be chosen carefully since they significantly influence the clamping force and effectiveness of the preload.

2.3 Normally Clamped (NC) Clamp Flexure Analysis

During installation of piezoelectric stack inside the flexure frame for NC clamp, the gap between the stack and frame is adjusted with micron level compression by set-screw rotation. Preloading causes compression within the actuator and tension within the frame. During the preload step, an amount of deflection is occurred the NC clamp

flexure as shown in Fig. 2.3(b). The stress is amplified in several times during driving actuation in energize step as illustrated in Fig. 2.3(c). Furthermore, blocking force of the stage slide wall during assembly generates an additional stress on the NC clamp flexure. From a kinematic perspective, the effect of preload would be lost completely if the flexure stiffness represented by K_f are not strong enough to withstand the wall stiffness represented by K_{fa} as shown in the Fig. 2.3 (d). If the internal dynamic forces are above the preload, the actuator is in danger because of it goes in tensile stress and also the stack loses contact with the frame interface.

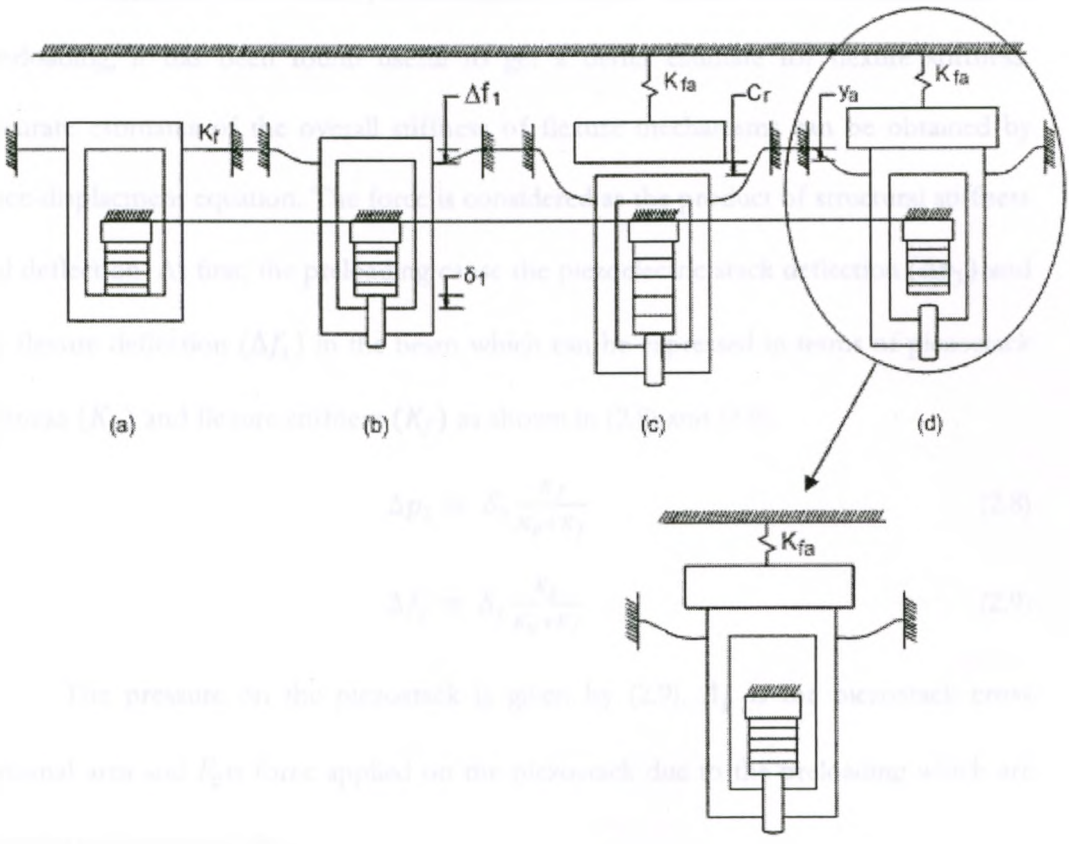

Fig. 2. 3. Installation steps of Normally Clamped (NC) Clamp with improved stiffness model: (a) at rest, (b) preload, (c) energize, and (d) de-energize.

From Fig. 2.3, it is noted that a high stiffness flexure mechanism reduces the actual working range of the clamp mechanism while increases the clamping force, indicating that the deformation of the links will become larger under the same output displacement. This helps the NC clamp to move the wall along its driving direction and the preloading of the piezoelectric actuator is maintained (see Fig. 2.7(d)) in Complementary Clamp configuration. On the other hand, if the flexure stiffness is low, it reduces the output clamping force and adversely affects the preloading of the piezoelectric actuator (see Fig. 2.3(d)).

To maintain the actuator preloading and to avoid flexure structural failure due to overloading, it has been found useful to get a better estimate for flexure stiffness. Accurate estimates of the overall stiffness of flexure mechanisms can be obtained by force-displacment equation. The force is considered as the product of structural stiffness and deflection. At first, the preloading cause the piezoelectric stack deflection (Δp_1) and the flexure deflection (Δf_1) in the beam which can be expressed in terms of piezostack stiffness (K_p) and flexure stiffness (K_f) as shown in (2.8) and (2.9).

$$\Delta p_1 = \delta_1 \frac{K_f}{K_p + K_f} \tag{2.8}$$

$$\Delta f_1 = \delta_1 \frac{K_p}{K_p + K_f} \tag{2.9}$$

The pressure on the piezostack is given by (2.9). A_p is the piezostack cross sectional area and $F_p$is force applied on the piezostack due to the preloading which are given by (2.11) and (2.12).

$$P_p = \frac{F_P}{A_p} \tag{2.10}$$

$$A_p = bh \tag{2.11}$$

$$F_p = K_p \Delta p_1 \tag{2.12}$$

As the piezoelectric stack expands (Δp_0) upon application of voltage, additional piezostack deflection (Δp_2) and flexure deflection (Δf_2) are induced as shown in (2.13) and (2.14).

$$\Delta p_2 = \Delta p_0 \frac{K_f}{K_p + K_f} \tag{2.13}$$

$$\Delta f_2 = \Delta p_0 \frac{K_p}{K_p + K_f} \tag{2.14}$$

These deflections cause the resultant forces on piezostack (F_p) and on flexure (F_f) which can be expressed in terms of total piezostack deflection (Δp) and flexure deflection (Δf) as shown in (2.14) and (2.15)

$$F_p = K_p \Delta p = K_p(\Delta p_1 + \Delta p_2) \tag{2.15}$$

$$F_f = K_f \Delta f = K_f(\Delta f_1 + \Delta f_2) \tag{2.16}$$

Next, the piezostack returns to its initial form upon withdrawn of voltage. Therefore, the remaining piezostack deflection can be obtained by (2.17) which is used in deriving net force on piezostack (F_{pa}) as presented in (2.19).

$$\delta_p = \Delta p - \Delta p_0 \tag{2.17}$$

$$F_{pa} = K_p \delta_p \tag{2.18}$$

$$F_p = \frac{K_p}{K_f + K_p}\left[\delta_1 K_f + C_r\left(K_p + K_f\right) - \Delta p_0 K_p\right] \tag{2.19}$$

By deducing the total force on flexure from the net force on piezostack, we obtain the clamping force (F_c) as presented in (2.20).

$$F_c = F_f - F_{pa} \tag{2.20}$$

$$F_c = \frac{K_{fa}}{K_{fa}+K_p+K_f}\left[\Delta p_0 K_p - C_r\left(K_p + K_f\right)\right] \tag{2.21}$$

Using the properties of steel (E = 193 GPa, ϑ = 0.27), a comparison of the improved flexure model to the simple model is shown in Fig. 2.4. It shows the simple model greatly under estimate the stress that can be produce by preloading. The stiffness obtained by the improved model is validated to FEA results (see Fig. 2.5).

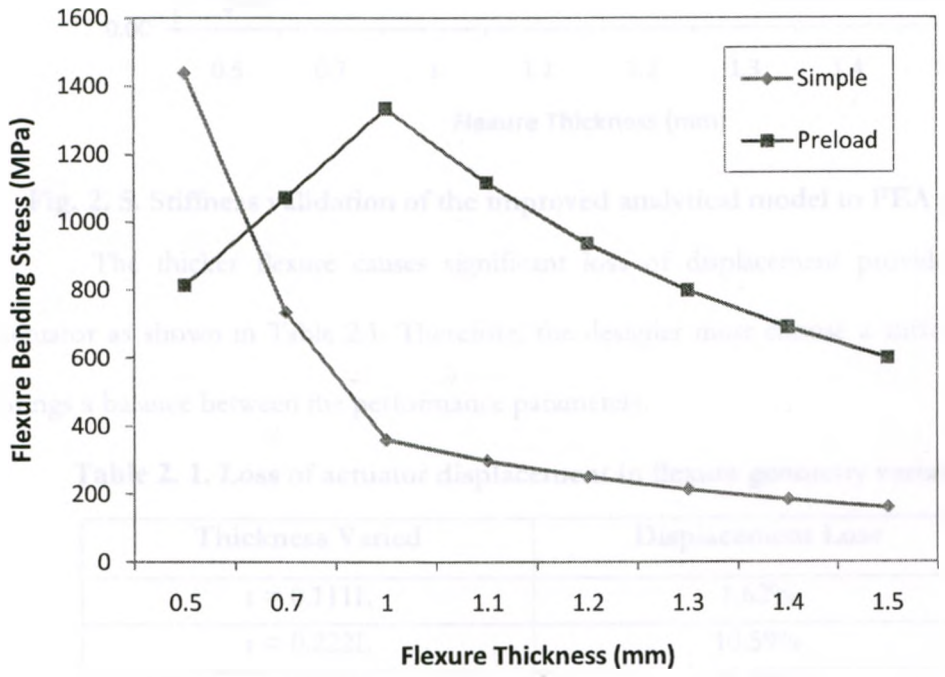

Fig. 2. 4. Stress comparison of the improved model to the simple model.

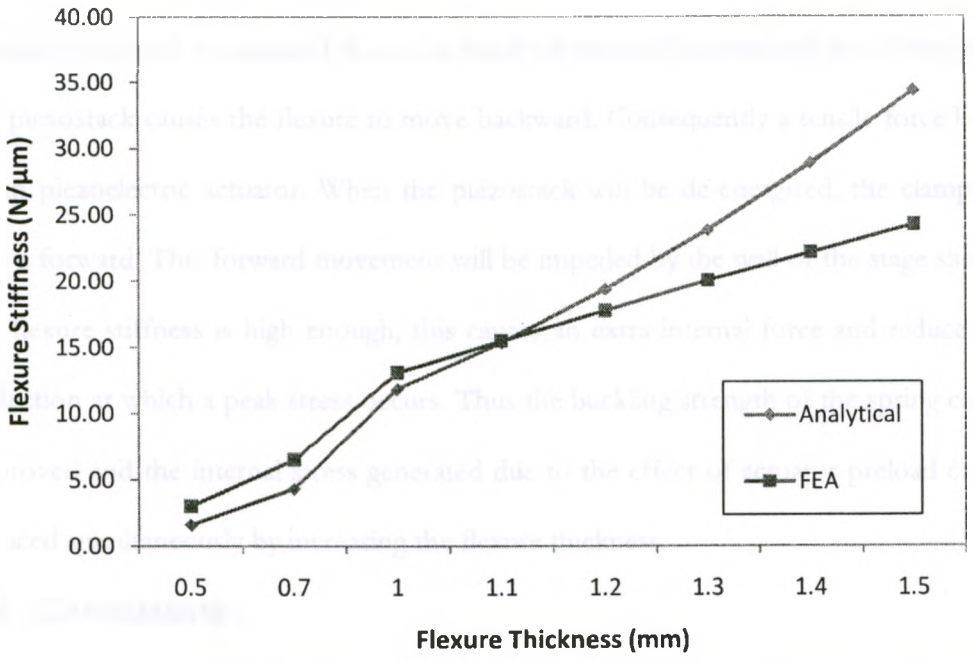

Fig. 2. 5. Stiffness validation of the improved analytical model to FEA results.

The thicker flexure causes significant loss of displacement provided by the actuator as shown in Table 2.1. Therefore, the designer must choose a stiffness which brings a balance between the performance parameters.

Table 2. 1. Loss of actuator displacement in flexure geometry variation

Thickness Varied	Displacement Loss
t = 0.111L	1.62%
t = 0.222L	10.59%
t = 0.233L	11.92%
t = 0.267L	16.22%
t = 0.280L	18.04%
t = 0.312L	22.41%
t = 0.351L	27.94%
t = 0.467L	43.14%

During assembly when the guide slide is loaded directly to the clamp surface, the piezoelectric stack is energized. Since the fixed tab remains constrained, the deflection of the piezostack causes the flexure to move backward. Consequently a tensile force builds up in piezoelectric actuator. When the piezostack will be de-energized, the clamp will move forward. This forward movement will be impeded by the wall of the stage slide. If the flexure stiffness is high enough, this causes an extra internal force and reduces the deflection at which a peak stress occurs. Thus the buckling strength of the spring can be improved and the internal stress generated due to the effect of actuator preload can be reduced simultaneously by increasing the flexure thickness.

2.4 Conclusions

Flexure mechanisms are often used in nanopositioning to provide accurate linear motion upon application of a force. The main aim of the flexure design is not only limited to achieve precise displacement upon application of a specific applied force, but also to achieve accurately known force upon application of a specific applied displacement. The range of deflection of a flexure depends on by either its stiffness or its elastic properties. Increase in stiffness causes increase in response time and resonant but decreased deflection range. Slight alterations in geometry can produce results that are sensible at the response level. This is particularly important in flexure mechanisms where precision is a key performance parameter and the output is expected in terms of displacement, force or frequency response. This model will help the designer to achieve good performance from flexure system by estimating accurate stiffness and to avoid the instabilities such as buckling or even the component failure during operations. This new model included the effect of preloading and analyzed the forces transmitted through the

clamp flexure. The deformation induced by blocking force of the moving platform is also considered. This led to better estimation of the stiffness for Normally Clamped (NC) clamp as compare to the previous designs which has low clamping force capacity. The flexure stiffness is validated using FEA and allows the designer to choose suitable preload and acceptable bending deformation of the links.

Chapter 3

3 Design Considerations for Z Axis Positioning Stage

3.1 Introduction

Actuation is an extremely important topic in assessing the overall performance of precision positioning stage. In Chapter 1, we discussed several means of actuation that can be utilized for precise positioning, depending on the applications and design requirements. PZT ceramics achieve a high performance actuation because of high piezoelectric properties through polarization produced by their morphotropic composition that is coupled between two phases (tetragonal phase and rhombohedral phase) [95]. However, high resolution is not the only issue for vertical positioning stage. The effect of gravity has to be taken into consideration for vertical nanopositioning. A pair of vacuum cylinders with noncontact seals has been proposed as gravity compensator for a voice coil motor driven vertical nano-motion platform [96].

Counterbalances with pneumatic cylinders are also widely used to minimize the gravity effects. However, such systems suffer from friction and force fluctuations. An alternative way is that the actuator responsible for the vertical motion must provide enough output force. In the piezoworm motor configuration, all loads are ultimately supported by the frictional forces between the guideway and clamps. Many researchers proposed different actuation technologies for the clamp and extender sections [68], [97] to improve the performance. Most of the piezoworm motors that have been designed so far use two clamp sections and one extender sections.

This chapter is dedicated to designing a range of piezoworm configurations based on mechanically complementary clamp concept for Z-axis motion. Some unique designs for the clamp and extender are introduced and discussed in Section 3.2. Section 3.3 proposes the amplified piezoelectric actuator for the extender of piezoworm motor. Then the section 3.4 presents the clamp model and its performance analysis. Several design configurations for vertical positioning stage have been proposed in section 3.5. It also describes the advantages and disadvantages of the configurations. The conclusions are drawn in section 3.6.

3.2 Conceptual Designs

The compact vertical positioner with high speed and long travel range can be achieved through the proper piezoworm motor design. In order to achieve the design objectives shown in Table 3.1, the design tasks have been split into two major factions: design of the basic components of the piezoworm motor and design of the basic components of the positioning platform with compliant base.

Table 3. 1. Stage Design Goals

Criteria	Value
Range	20 mm
Force	10 N
Speed	6 mm/s
Capacitance (for amplifier load)	1.5 μF
Size	100x115x50 mm^3

3.2.1 Clamping System Design

The clamping system as the key part in the piezoworm actuator determines the force output. In recent years, considerable design effort has been devoted to improving active clamps in order to acquire output force as high as possible. Since piezoelectric actuators provide very small displacements, the clamp flexure frame has to be made with tight tolerances in order to exploit the performance of the piezoelectric actuator.

A conceptual design configuration for the NC clamp for vertical positioning is illustrated in Fig. 3.1. The clamp consists of a monolithic block with proper thickness of two flexures inside. Two moving members are attached to the top and bottom sides of the block by their ends so that they would act as cantilever beams. The mechanism is further sandwiched by two covers. In this configuration, only one piezoelectric actuator is required to provide actuation to both sides. The drawback of such mechanism is that the cantilever beams will always have deflection at the ends which worsen the positioning accuracy provided by the piezoelectric stack. Straightforward integration of the moment distribution along a beam will result in the deflection shape of a beam for

any load conditions. The driving force is transmitted through the beams, rather than acting directly to the guide way. This results in low force which is detrimental to vertical positioning.

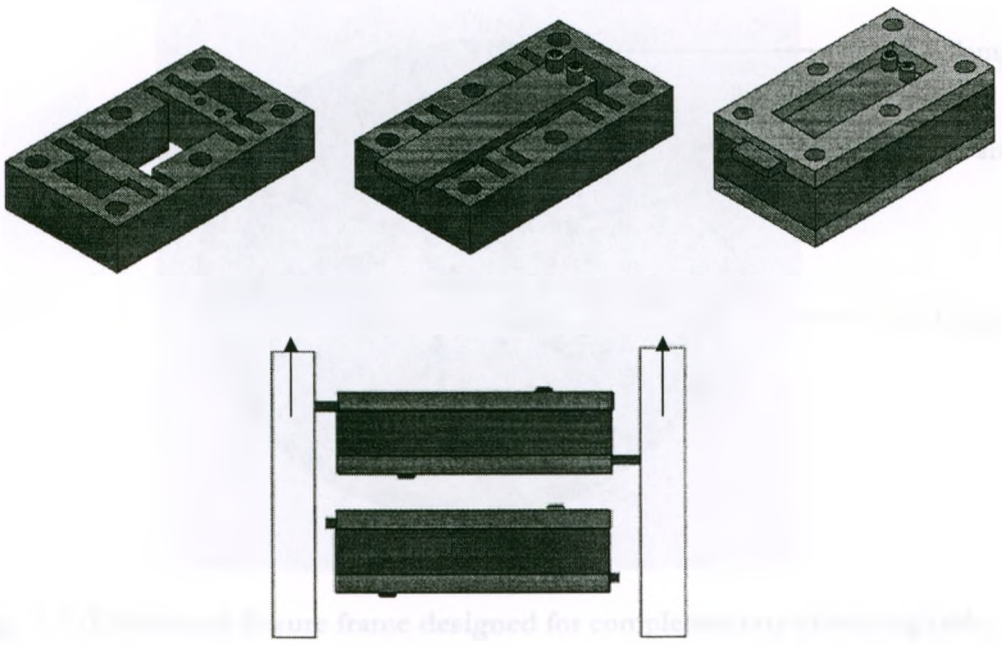

Fig. 3. 1. Conceptual design and operation of a normally Clamp (NC) clamp.

Good design practices for precision positioning suggest that friction inside the clamp mechanism has to be eliminated. Therefore, design for precision positioning relies on highly stiff flexures. In particular, a broad range of flexures utilizing deflection of slender and symmetric beams of uniform cross section can be fabricated. A unique approach for complementary clamping task has been designed that allows all the NU and NC clamps to be fabricated from a single metal circular block (see Fig. 3.2). The two NC clamps are stationary and situated evenly among the three fixed parts by flexures. The fixed parts can be attached to the base while the NU clamp frame can be attached to the extender. The direction of the NU clamp driving force is toward the center of the

cylindrical frame while the NC clamp driving force direction is outward from the center. This allows the moving member at the center of the cylindrical frame to move upward and downward.

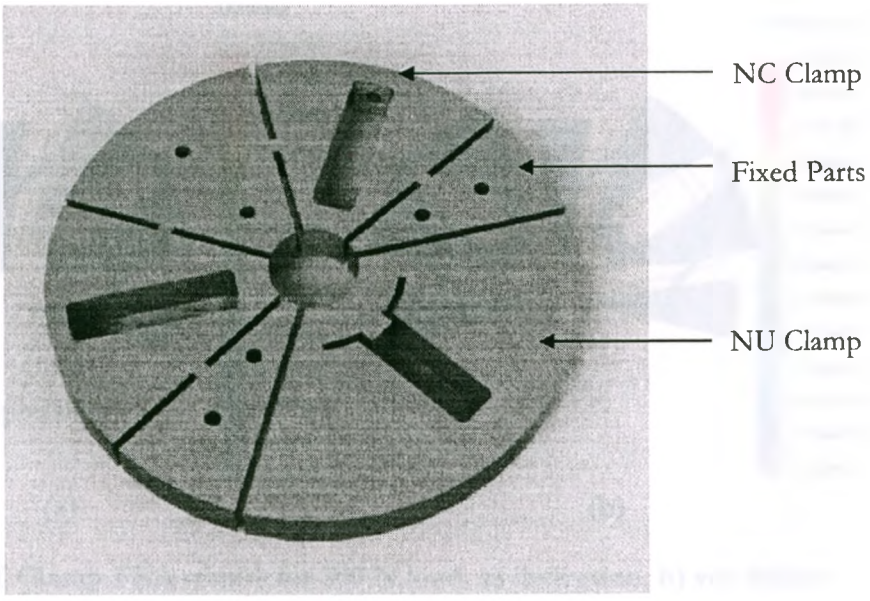

Fig. 3. 2. Cylindrical flexure frame designed for complementary clamping task.

The flexures require the prediction of maximum stresses and strains as well as deflections relative to a fixed frame (see Fig. 3.3 and Fig. 3.4). For the parts to remain stationary, it is necessary that the total force due to the distributed stress is zero. Consequently, the total sum of compressive stresses must equal to the tensile ones. Also it is apparent that there will be a compressive stress at the outer surface and a tensile stress on the inner one. Hence, there must be a plane running along the axis of the beam in which the stress is zero which is termed as the neutral plane. If a cross section is taken through the beam, the neutral plane would intersect along a line in the Z direction and this is the neutral axis. This leads to a generalized method for the solution of beam deflections in terms of the load distribution. Normally, for the purpose of deriving the

shape of a flexure, it is necessary that the equation satisfies the boundary conditions at each end or support or constraint. The simplest and often most usable conditions are those having zero value.

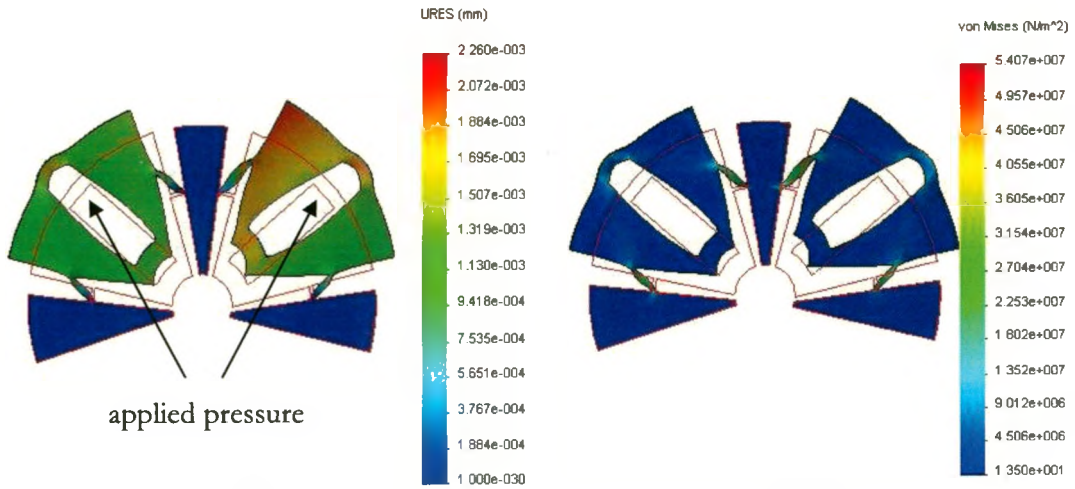

Fig. 3. 3. NC Clamp FEA results for 200 N load. a) deflection, b) von Mises stress.

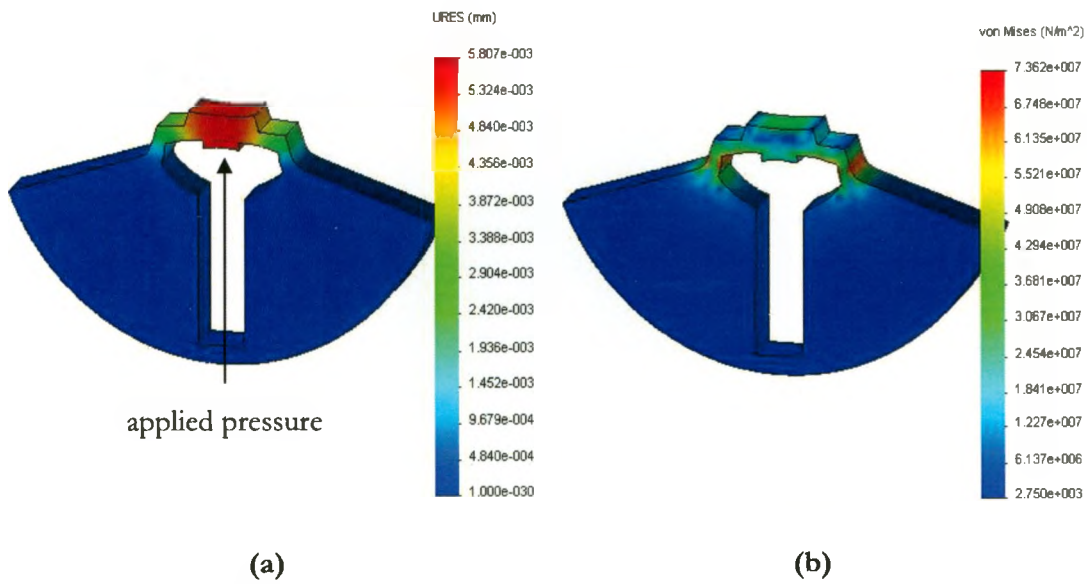

Fig. 3. 4. NU Clamp FEA results for 200 N load. a) deflection, b) von Mises stress.

3.2.2 Extender System Design

Designing a proper flexure frame for extender in nanopositioning is challenging. Slight alteration or rotation of the flexure could adversely affect the positioning accuracy. Designing flexures with extremely tight tolerances may not feasible in terms of manufacturability and cost effectiveness. Symmetrical I-shape extender frame design allows the piezoelectric stack as a central drive as shown in Fig. 3.5. Since the compound spring consists of two simple springs in series, its maximum stress is equal in each section and governed by half of its total displacement. Hence, symmetrical drives will lead to minimum stresses. The deflected shape of the platform reveals that most of the bending occurs near the top, with the middle sections remaining relatively straight.

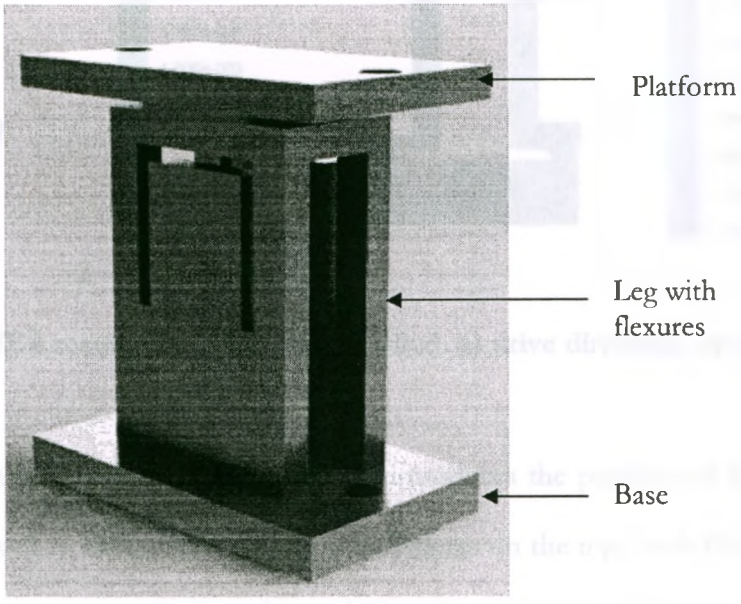

Fig. 3. 5. Extender frame design with platform on top.

The ideal extender mechanism will deflect without rotation. However, the platform or the free end of an extender mechanism will always show some rotation as it

deflects under transverse load. This imbalance cause some increase in susceptibility to parasitic forces from the drive (see Fig. 3.6). If the drive is applied directly to the platform from its bottom side and the legs constrain prevent end rotations each other, a tensile force builds up in one side and a corresponding compressive force in the other to provide a moment that bends the springs back into the symmetrical I-shape. Even though this reduces the maximum bending moment in the springs, the platform can still tilt which is detrimental to vertical nanopositioning.

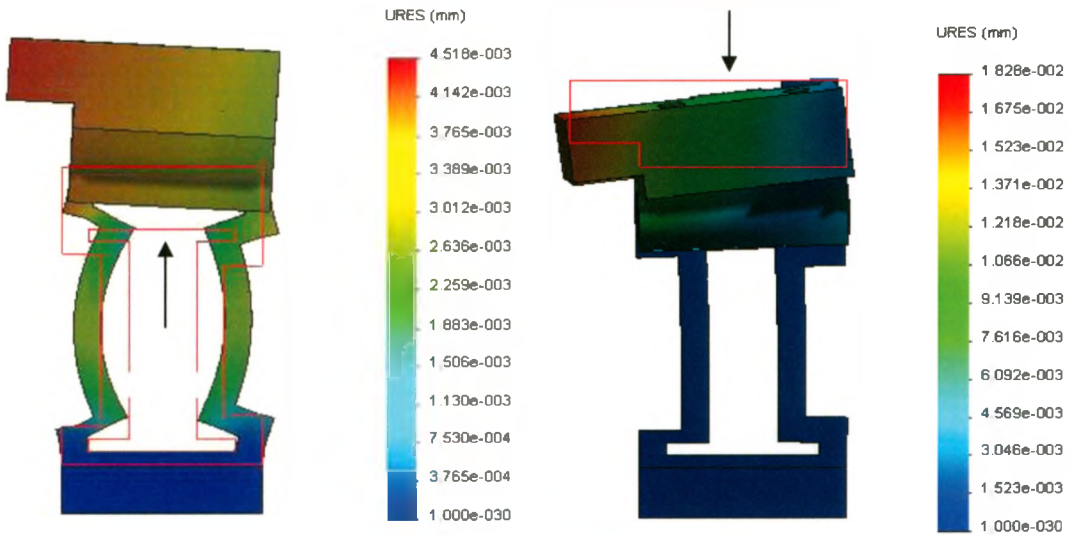

Fig. 3. 6. Extender FEA results for 200 N load applied. a) drive direction, b) top.

The fabrication of compound flexure devices introduces the problem of fixing the component parts such as base at the bottom and platform on the top. Such flexures will always cause some uncertainty both in the analysis with which they simulate a truly built-in beam end. One way of overcoming these difficulties is to use a monolithic

structure. However, it requires good machining quality flexure guidance, and so is complex mechanism as well as expensive.

3.3 Amplified Piezoelectric Actuator

If an application requires a piezoelectric actuator with the larger travel motion in a pulling or contracting mode, Amplified Piezoelectric Actuator (APA) is a good option. Here the kinematic design of actuator is reversed and causes the output or contact faces of the frame to contract as the piezoelectric stack expands. In APAs, displacements are amplified while forces are compressed. The amplification efficiency η is obtained by (1) as given in [99].

$$\eta = \frac{u_a F_a}{u_p F_p} \tag{3.1}$$

where F_p is the piezoelectric stack block force, F_a is the actuator block force when both faces are clamped, u_p is the piezo stack free stroke and u_a is the actuator free stroke. From the equation, it is realized that the higher the amplification of displacement, the lower the amplification efficiency.

Piezoelectric stacks can bear large compressive stress but they cannot bear tensile forces with a good reliability. Therefore, the APA shells are designed to preload the piezo stack in addition to the amplification function as shown in Fig. 3.7.

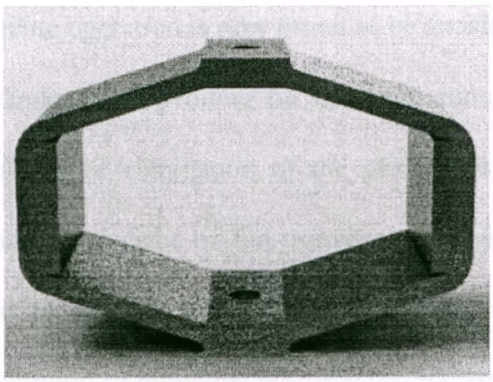

Fig. 3. 7. Flexure shell for amplified piezoelectric actuator.

APAs can be a good choice to address the limitations of compound extender frame since they provide specified output displacements and forces. If one side of an APA is attached to the base and another to the NU clamp, it can move the clamp in straight line with larger step size than typical piezostacks can. Fig. 3.8 shows an improved piezoworm actuation in vertical direction that contains APA as extender and complementary clamp mechanism.

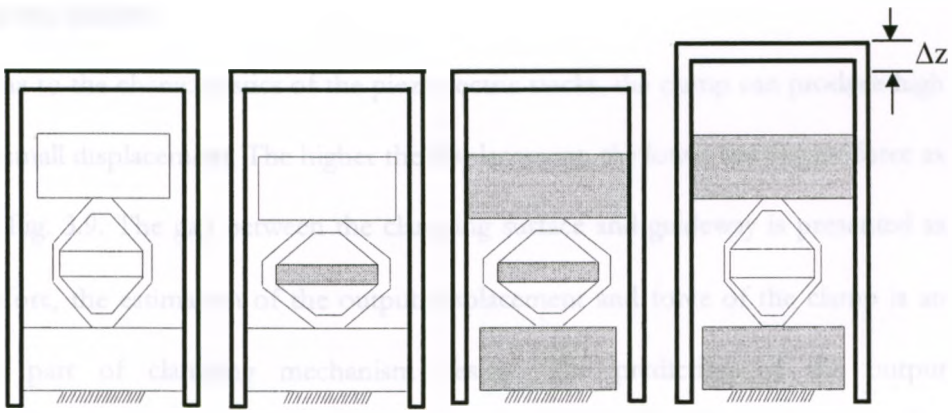

Fig. 3. 8. Motion principle of a Z-axis positioning stage.

Use of two amplified piezoelectric actuators in parallel position eliminates the necessity of guiding rods. The complex flexure mechanism originally thought to be

needed to support the extending operation is now found to be avoidable. The guide rods can be reduced or even eliminated depending on the application. The reduction of extender mechanism complexity or elimination of the guide rods will greatly reduce production cost, the size and the weight of the overall stage. Using direct extending actuators would increase the piezoworm actuator's thrust and performance under high loading conditions. The application of amplified piezoelectric actuator will most likely to prevent deflection of the clamp and reduce in the piezoworm actuator's height as well as the stage height, but more importantly will allow space for the NC clamps. The amplified piezoelectric actuator as extender also allows the reduction in the height of the actuator and improves the actuator's ability to be packaged and integrated into the stage. The displacement range of the extender determines the step size and speed of the stage. Amplified piezoelectric actuator provides extended displacement range which maximizes the speed of the stage.

3.4 Clamp Model

Due to the characteristics of the piezoelectric stacks, the clamp can produce high output in small displacement. The higher the displacement, the lower the output force as shown in Fig. 3.9. The gap between the clamping surface and guideway is presented as C_r. Therefore, the estimation of the output displacement and force of the clamp is an important part of clamping mechanism design. The prediction of the output displacement and force requires the mechanical model of the mechanism. The mechanical model for the NU clamp from Fig. 3.7 is considered and has fully complementary characteristics.

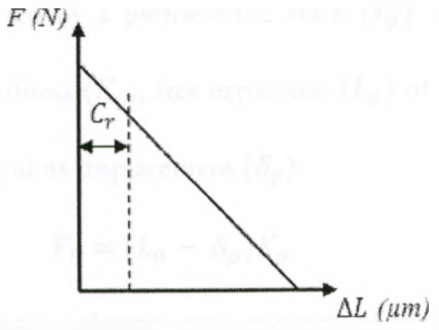

Fig. 3. 9. Force-displacement characteristics of a piezoelectric stack.

The static model of a compliant mechanism is expressed by

$$F = Kx \tag{3.2}$$

where F, K and x are the force vector, stiffness matrix, and displacement vector, respectively.

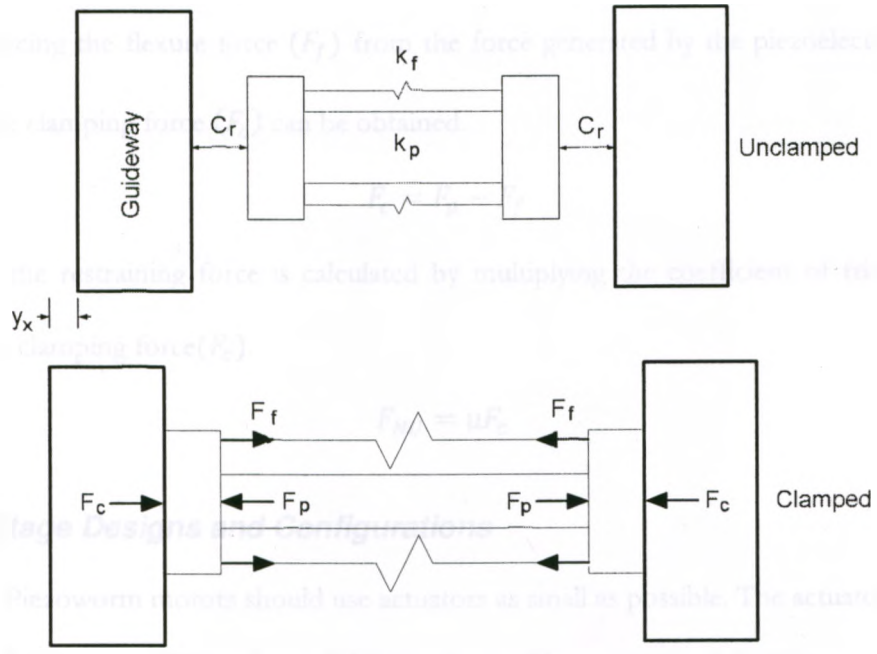

Fig. 3. 10. NU clamp model in unclamped ($V = 0$) and clamped ($V = V_p$) states.

From [100], the force generated by a piezoelectric stack (F_p) can be expressed as a function of its voltage (V), stiffness (K_p), free expansion (L_p) of the piezoelectric stack at maximum voltage (V_{MAX}) and its displacement (δ_p).

$$F_P = (L_0 - \delta_p)K_p \tag{3.3}$$

The total displacement of the piezoelectric stack is a sum of the displacement to cover the gap (C_r) and the deflection of the platform surfaces (y_x) on both sides.

$$\delta_p = 2(C_r + y_x) \tag{3.4}$$

Using the simple linear spring equation, the flexure force can be presented as a function of its stiffness (K_f) and the piezoelectric stack displacement(δ_p).

$$F_f = K_f \delta_p \tag{3.5}$$

By balancing the flexure force (F_f) from the force generated by the piezoelectric stack (F_p), the clamping force (F_c) can be obtained.

$$F_c = F_p - F_f \tag{3.6}$$

Finally, the restraining force is calculated by multiplying the coefficient of friction (μ) with the clamping force(F_c).

$$F_{NU} = \mu F_c \tag{3.7}$$

3.5 Stage Designs and Configurations

Piezoworm motors should use actuators as small as possible. The actuator shown in Fig. 3.11 has one NC and one NU type clamp. Moreover, since the piezoworm is to serve as a positioner, it must be capable of generating a certain amount of thrust. The displacement range of the extension flexure frame determines the step size and speed of

the stage. The upper section of the extension frame is attached to the base wall and the lower section is attached to the NU clamp so that its operation creates the motion. The NC clamp is fixed to the base wall on the other side. The clamps are oversized to avoid clamping force or applied force induced deflections. The motor is guided by a vertical rail surface in the middle which supports a horizontal plate on top. Each guide and contact surface is readily surface ground and finished smooth and flat. In this design, the interface of slide-clamp has relative motion during the clamping motion.

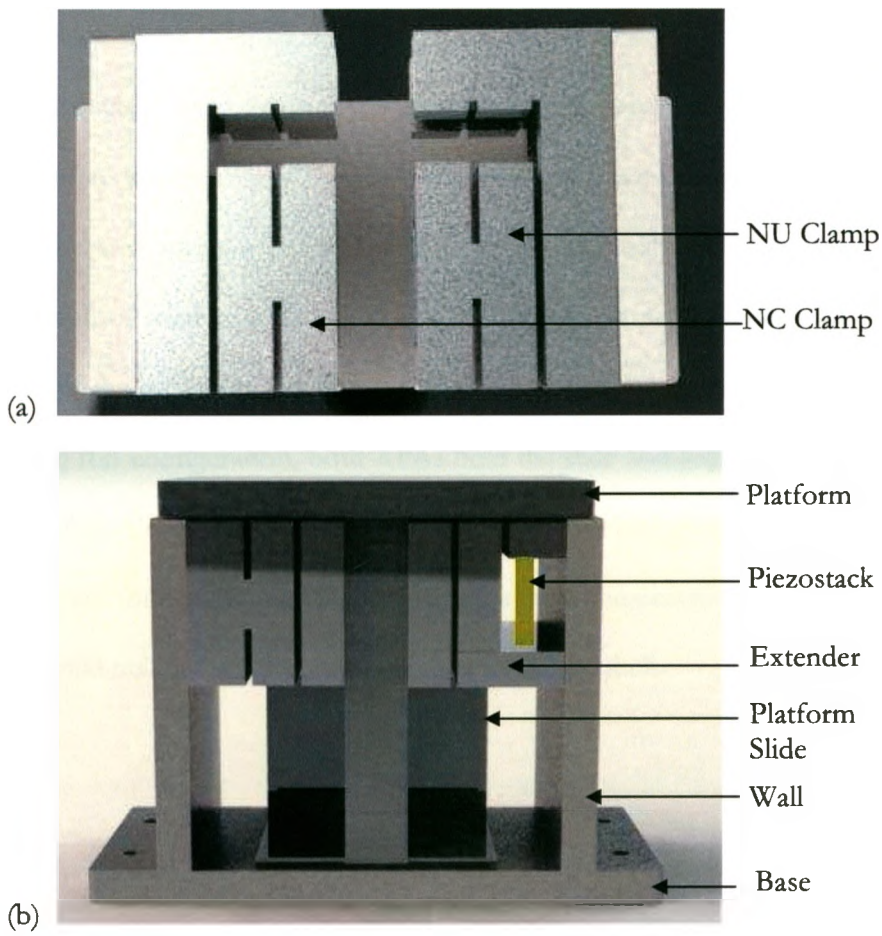

Fig. 3. 11. Conceptual design of a vertical positioner: (a) top view, (b) front view.

In the design illustrated in Fig. 3.12, two APAs are used for both NU and NC type clamps. The NC clamp is attached to a fixed frame and the NU clamp is placed on top of the extender flexure frame. A multilayer piezoelectric stack is supported in a flexure frame in order to maintain a moderate pre-stress and protect the stack from external force stress. Thus both clamps are kept separate. The extender causes the slide move upward with the help of NU clamp and the spring mechanism of the extender frame returns it to the original position when it is de-energized. Both APAs normally hold the slide and payload when de-energized. The NC clamp is used in such that no power is needed to maintain a fixed vertical position, holding the payload against the force of gravity. Both APAs have common surfaces with their contacts on each side. The parallel tolerance of the two surfaces must be smaller than the maximum clamping stroke, with consideration of some margin has to be saved for the flatness tolerance of the surfaces, the wear of the surface-clamp interface, and the elastic deformation of the clamps and surfaces. In this configuration, both APAs hold the slide and payload when they are de-energized and release the slide and payload when they are energized. The challenges with APAs used for clamping applications are the large compressive stress on their output surfaces could nullify the effect of preloading inside the shell.

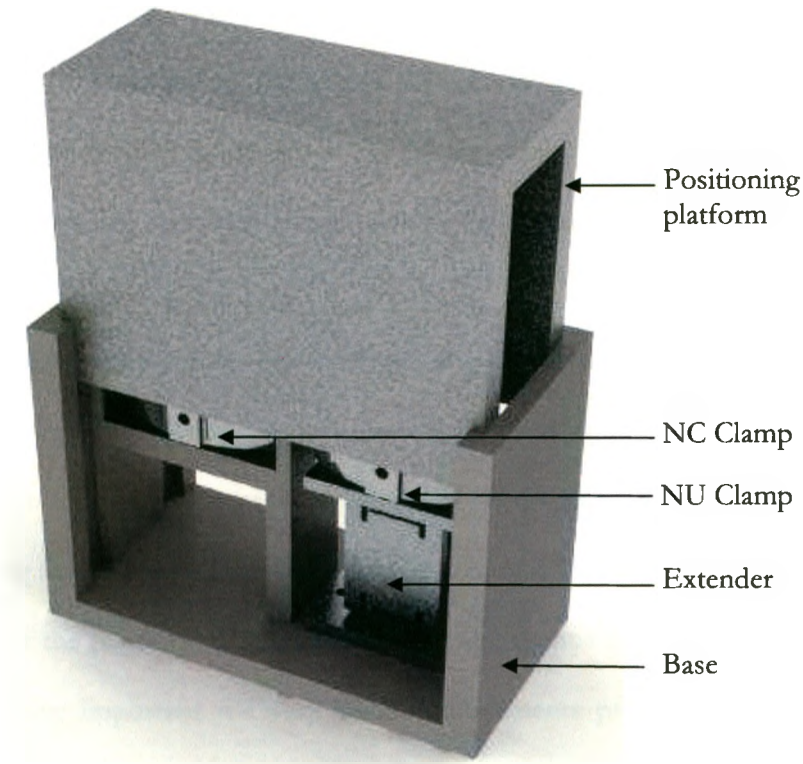

Fig. 3. 12. Conceptual design of a vertical positioner that uses APAs as clamps.

Some other configurations of vertical positioner based on complementary piezoworm actuator are shown in Fig. 3.13. The symmetric frame simplifies the piezoworm motor analysis, provides better performance and offers design flexibility. The piezoworm in the first positioner uses two APAs for extender section (see Fig. 3.13(a)). This design aims to make the positioner compact by utilizing the space between two APAs used for extender section. The NC clamp will be attached to the middle section of the base and each APA to the each side of the section. This increases the manufacturing complexity and costs since both inside and outside surfaces of the slide are needed to fabricated precisely with surface flatness of no more than 1μm. The parallel tolerance of the all four surfaces and the elastic deformation must be smaller

than the total clamping stroke. The alignment of NC clamp and the slide surface gap during installation may also be a problem. The size of the NU clamp becomes bigger to allow wider space for NC clamp in between two APAs. These problems make the design difficult for microfabrication and thus may not be able to fulfull its ultimate role as a precision positioner.

Both NC and NU clamps can be created from singular circular metal disk as illustrated in Fig. 3.16(b). This allows more compactness and unique cylindrical configuration where the clamping forces are pointed towards the center of the positioner. The clamping forces will be exploited for vertical movements of the rigid rod connected to the base of the platform. The disadvantage is the clamps do not have flat surface which is extremely important for very small displacements provided by the piezostacks.

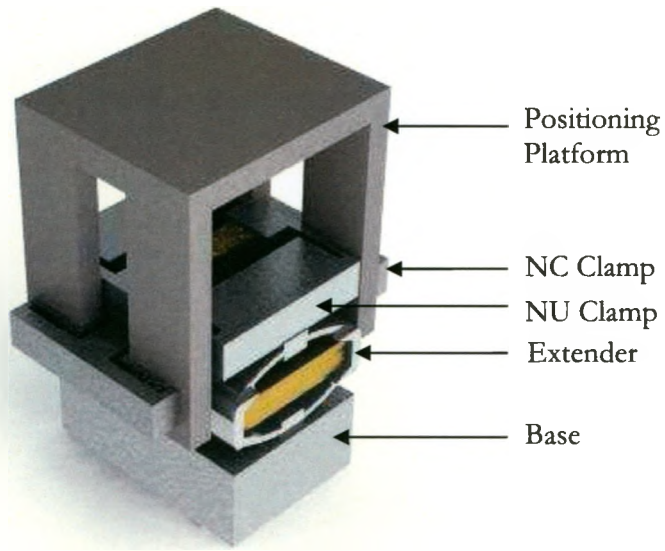

(a)

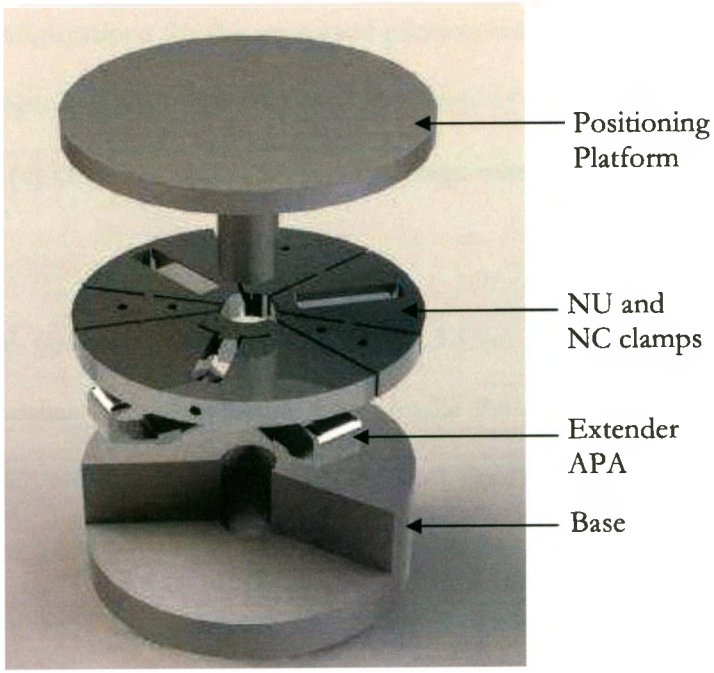
Positioning
Platform
NU and
NC clamps
Extender
APA
Base

(b)

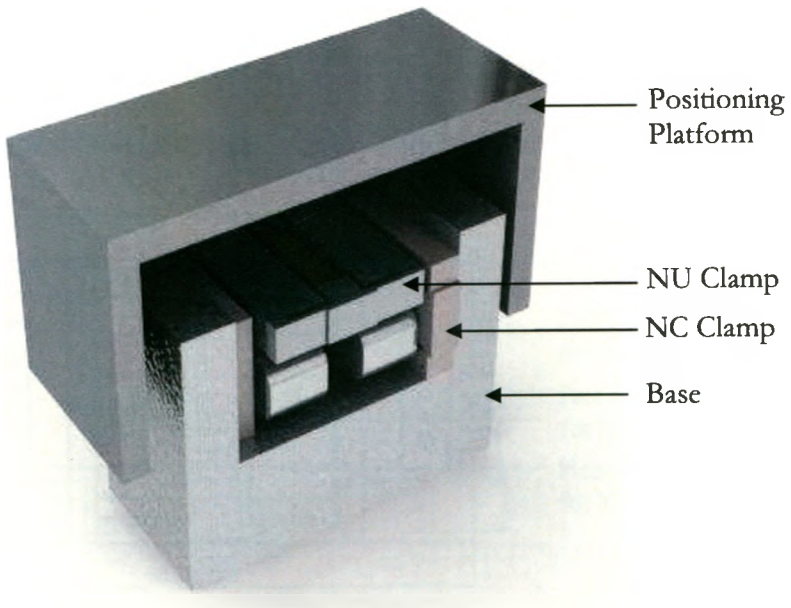
Positioning
Platform
NU Clamp
NC Clamp
Base

(c)

Fig. 3. 13. Several configurations for the proposed piezoworm vertical positioner (a) external NC clamping mechanism, (b) exploded view of cylindrical shaped vertical positioner (c) cross section of box-shape stage where piezoworm is housed inside.

Another vertical positioner is proposed in Fig. 3.13(c). Here the fixed NC Clamps are attached parallel to the base walls which make the positioner a box like shape. In this design, both NU and NC clamp on each side have a common surface with their contacts. This principle allows higher tolerances to surface flatness errors during the linear motion of the slide caused by the clamps and extenders than the previous design. Therefore, high precision can be assured. Cross rollers can be used in between the surfaces of base and slide for smooth motion and to withstand normal and moment load. This design requires two NC clamps instead of one as illustrated in the previous designs. The drawback of such configuration is that the difficulty in the adjustment of the NC clamps positions during assembly.

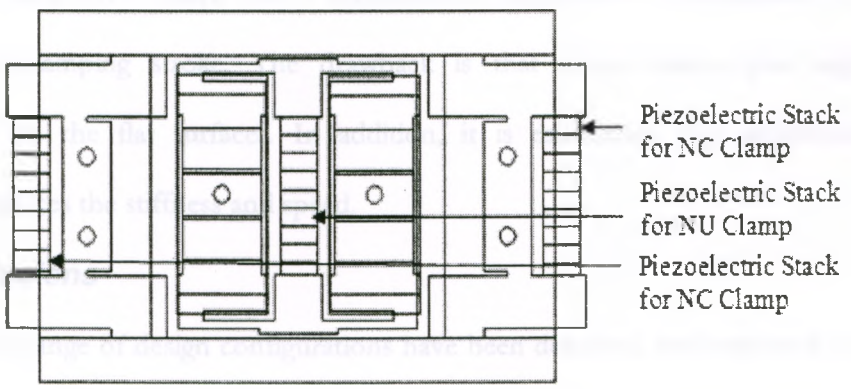

(a)

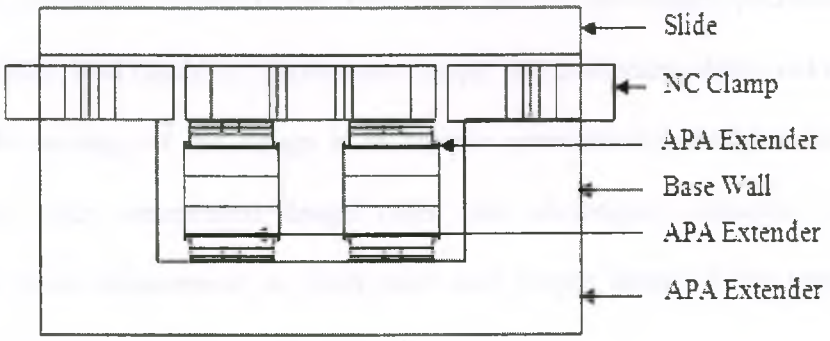

(b)

Fig. 3. 14. Conceptual design of vertical positioner with both types of clamps in same level (a) top view and (b) side view.

Improving in the last design in which the NC Clamps are attached parallel to the base walls, this symmetrical design presents the NC clamps normal to the base walls and in the same level as NU clamp (see Fig. 3.14). Thus the configuration allows the positioner to be more compact, but with compromising the increase in length. Like the previous design, it allows enough tolerance to surface flatness errors. The interfaces of slide-clamp have been increased as each NC clamp has two contact surfaces. Furthermore, each NC clamps has a displacement amplification mechanism which increases the clamping stroke. The drawback is that these clamps give angular displacement on the flat surfaces. In addition, it is established that amplification mechanism reduces the stiffness and speed.

3.6 Conclusions

A wide range of design configurations have been described and evaluated to aid in the development of novel vertical positioner based on piezoelectric actuators. Since the optimal designs are based on flexure mechanism and complementary clamp

configuration, substantial considerations have been given to the design specification in terms of accuracy, load capability, displacement range, size, manufacturability and ease of assembly. The strategy of the design is to achieve symmetrical balance in centered compositions. Such symmetrical design offer two advantages: utilization of the piezoelectric stack displacement on both sides and proper lifting of the positioner platform without tilt or rotation in any side.

An amplified piezoelectric actuator is proposed to perform the vertical motion of a piezoworm motor which allows the designer to avoid complex flexure-based mechanism design for extender section without compromising high resolution and displacement. A mathematical static model for flexure based clamping mechanism driven by piezoelectric stack is derived. This model is useful to predict the static characteristics of a clamp and to determine the stiffness of the flexure. The force and the displacement of the clamps are decided by the relation between the stiffness of the piezo stack, the stiffness of the flexure and the voltage applied to the piezo stack.

surface to the actuator is carefully designed so that the slide and clamps are in proper alignment in order to avoid backlash or binding.

In section 4.2, the piezoworm actuator configuration is presented. The simulation model based design of NC type and NU type clamps are described in section 4.3. Section 4.4 asserts on stage design and its sliding mechanism. The stiffness of the positioning platform is analyzed in section 4.5. For the given stiffness of the positioning platform, the restraining forces provided by the both types of clamps are analyzed in section 4.6. Conclusions are drawn in section 4.7.

4.2 Actuator Configuration

The configuration of the complementary piezoworm actuator is shown in Fig. 4.1. The actuator is mounted on a base plate and has two NC type and one NU type clamp. Two amplified piezoelectric actuators (APA) act as the extenders of the piezoworm actuator. The NU type clamp is directly connected to one-side face of each APA shell while the other face is connected to the base. This allows the APAs to control the movement of the NU type clamp. On the other hand, two NC type clamps are attached to the chassis which is further attached to the base. The NU type clamps are designed such that they can be accommodated in between two APAs. This reduces the vertical distance between two clamping sections and thus aids the compactness of the structure. The gap between two clamping surfaces is perfectly aligned by adjusting the position of the chassis with respect to fixed base. In most of the piezoworm actuators, two clamps are attached to the extender frame. To design more compact piezoworm as well as positioner for vertical motion, the space in between two APAs is utilized here.

Each component of the piezoworm actuator is separate and if a component is damaged, it can be replaced by new one instead of replacing the entire piezoworm.

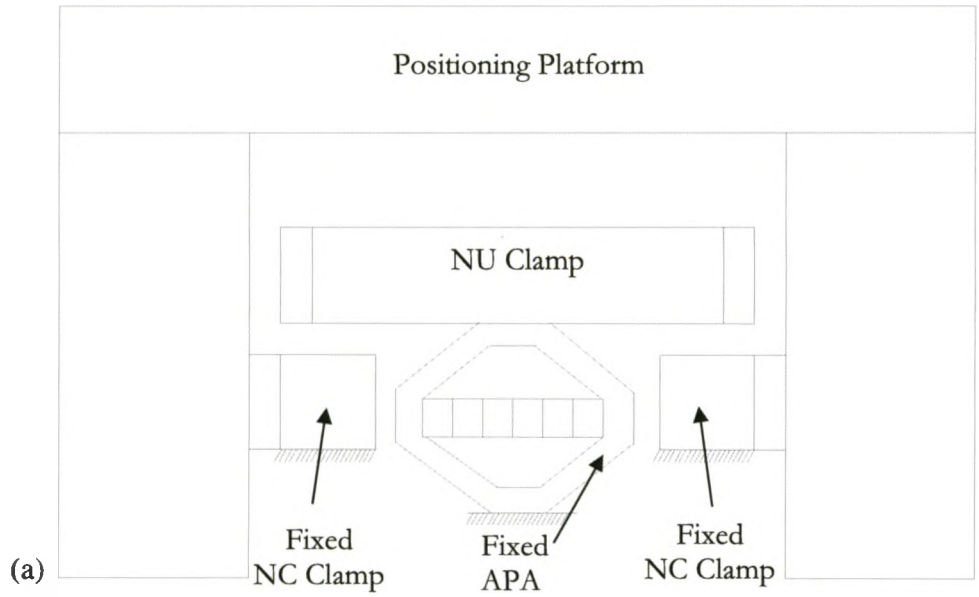

(a)

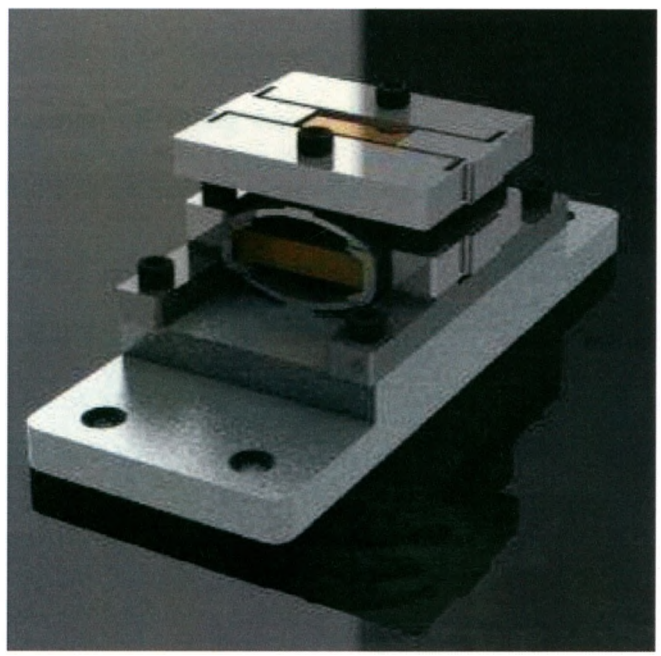

(b)

Fig. 4. 1. Piezoworm actuator a) general configuration, b) CAD 3-D model.

To step to the up, the APAs are energized to lower the NU type clamp and then the NU type clamp grasps the slide while the NC type clamp releases it as both clamps are energized at the same time. Then the voltage is withdrawn from the APAs the upper clamp moves the slide to the up approximately total the displacement of the APAs. The clamps switch such that the lower clamp now holds the slide and secure the position. Thus by repeating this step large range can be achieved. Since the NU type clamp is mobile, the fine positioning mode is performed with high voltage on both clamps. Here, both clamps are driven by the common clamp signal due to mechanically complementary clamp configuration. This permits the piezoworm actuator to hold the platform all the time, no matter which clamp is gripping it, which is crucial for safe vertical positioning.

4.3 Clamp Design

A total of three flexure based frame are required for two NC type clamps and one NU type clamp. Machined flexures are used to provide precise linear motion and spring actions simultaneously. Bringing variation in the flexure geometry, sufficient stiffness can be achieved to ensure the frame resonant frequency is more than the excitation frequency. Both NC type clamps have identical flexure frame. Each of them uses identical ceramic monolithic multilayer piezostack made of Physik Instrumente (P-885.10) having dimension of 5x5x9 mm. The selected piezoelectric actuator can generate a nominal displacement of 6.5 μm at 100 V, has stiffness of 100 N/μm and can deliver a maximum driving force of 800 N. The NC type clamps are located in the same level in the piezoworm arrangement. On the other hand, the NU type clamp uses longer monolithic multilayer piezostack made of Physik Instrumente (P-885.50) having dimension of 5x5x18 mm which can generate a nominal displacement of 15 μm at 100

The goal of the NU type clamp flexure design is to minimize the stiffness as much as possible so that the piezostack displacement is properly utilized. In contrast, the clamping force direction in NC type clamp is opposite to the driving force direction of the piezostack. Hence high flexure stiffness is required to provide considerable clamping force. This tradeoff between clamping range and clamping force is solved by estimating the correct stiffness model which is presented in Chapter 2. The stiffness is first estimated from (2.7) at 28.88 N/μm and then finite element analysis (FEA) is performed using Abaqus [101] where the stiffness is found as 24.17 N/μm. The clamp range can be obtained by (4.4) where K_p, K_f, L_0, L_f represent the piezostack stiffness, flexure stiffness, piezostack expansion and flexure expansion respectively. Each NC type clamp range is estimated to be 5.23 μm which will results a total clamping range of 10.46 μm in the lower clamping section. The maximum von Mises stress in the flexure using Abaqus is 112.9 MPa which gives a factor of safety 9.16. The FEA results for the NC type clamp deflection and stress are shown in Fig. 4.3 with force of the piezostack is applied in the form of pressure on the inner surface at the rear side only.

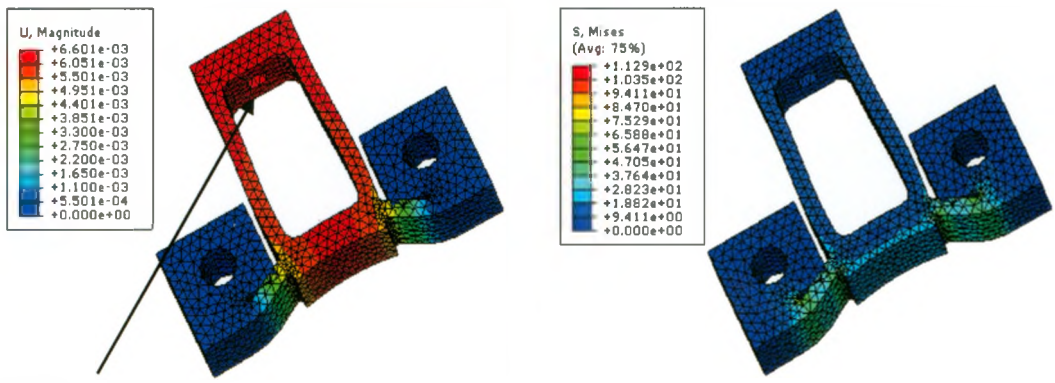

Fig. 4. 3. NC Clamp FEA results for 160 N load. a) deflection, b) von Mises stress.

In NU type clamp, the expansion of the piezostack will cause the clamping surface to move toward the friction surface of the platform. The symmetric design is applied to the NU type clamp in order to exploit the piezoelectric stack displacements on both sides. This allows it to directly act from both sides on the positioning platform which functions as the moving member. When the NU type clamp begins to push on the platform, the extender shells help the clamp to balance itself by adjusting the deflections on both sides. The stiffness is first estimated from (2.7) at 3.78 N/μm and then FEA is performed using Abaqus where the stiffness is found as 4.44 N/μm. The NU type clamp range is estimated to be 13.94 μm. The maximum von Mises stress in the FEA is found as 881.1 MPa which gives a factor of safety 1.17. The FEA results for the NC type clamp deflection and stress are shown in Fig. 4.4 with force of the piezostack is applied in the form of pressure on the inner surface at the both sides.

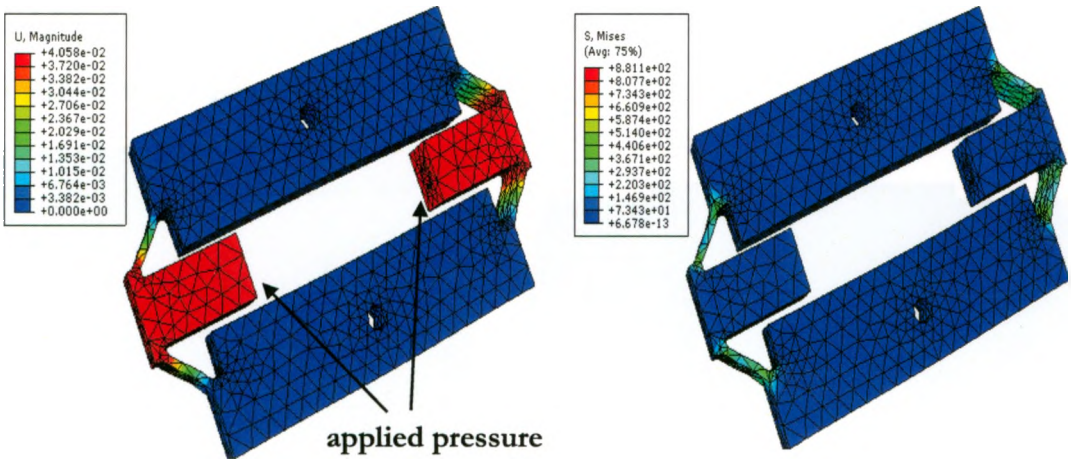

Fig. 4. 4. NU clamp FEA results for 180 N load: a) deflection, b) von Mises stress.

4.4 Stage Design

The objective is to design a stage to have a range of around 20 mm in Z-axis direction, maximize speed, stiffness and thrust while minimizing the mass and size. After selecting the proper configuration for piezoworm motor, the decision that has to be made is how extensive the stage should be. The stage consists of a positioning platform, a base, and chassis for each NC clamp. The chassis affects the positioner's ease of assembly, the adjustments between the NC clamps and the frictional surfaces, and how effectively it accommodates the NC clamps in such compact piezoworm configuration. The design of the NC clamp easily determines the chassis configuration as shown in Fig. 4.5. The orientation of the tab that extends from the chassis frame dictates the performance of the NC clamp. While the base supporting the piezoworm actuator and the platform seems to be simple, the ease of access to all components for accommodation and adjustment heavily depends on it. The design of base aims to lower weight and simpler fabrication. The base affects the positioner's ease of handling and installation to an automated stand.

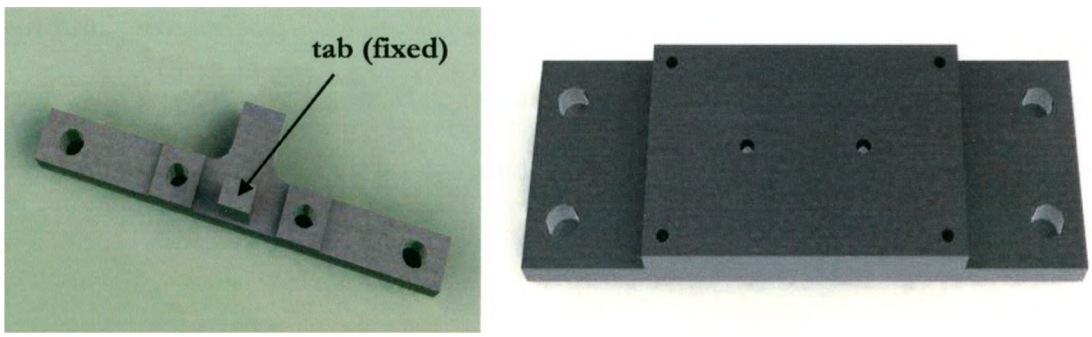

(a) (b)

Fig. 4. 5. CAD models of stage components: a) Chassis, b) Base.

The moving platform of the vertical positioner consists of a top plate, two friction surfaces and two side plates. It has to perform two important tasks: to act as guide way for the piezoworm motor while, at the same time, to provide truly straight sliding. To aid the sliding mechanism, two commercially available precision ball slide guides built for immediate installation are proposed as shown in Fig. 4.6. The slide guides are attached to the base plate to guide the platform straight and provide extra rigidity. It also prevents the moments applied to the platform which may twist the actuator inside and cause it to bind. Cross roller slides provide better accuracy. However, they cannot provide accuracy less than 10 μm which is not good enough for nanopositioning applications. For a given size, they also have limited stroke ranges which adversely affect the compactness of the stage. High force applied to the cross roller slide causes degradation in its resolution while the piezoworm for vertical positioner is aimed to provide high output thrust. Therefore, the positioning platform uses two side metal plates instead of roller sliding mechanism as shown in Fig. 4.7. These side plates are attached to the friction slides at the ends. This increases the stiffness and mass of the structure. Being compact, the platform provides stable adjustment of height and width. It can provide long travel range, and support large loads. While moving the platform stays parallel to the base and thus eliminates the twist of the actuator during motion.

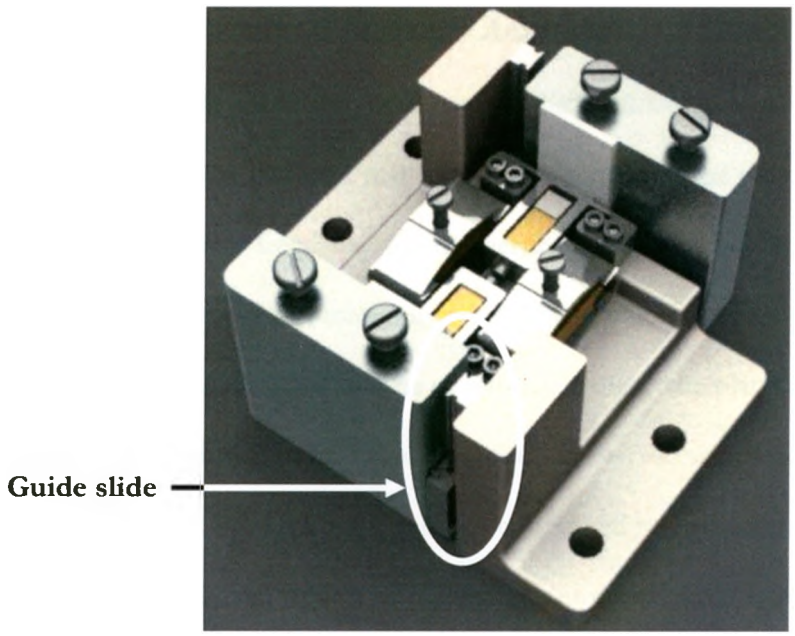

Fig. 4. 6. Vertical stage with guide sliding mechanism.

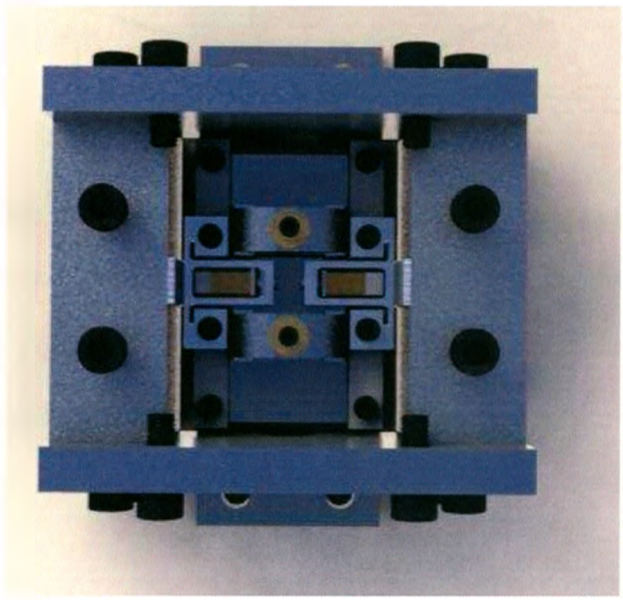

Fig. 4. 7. Internal structure of the vertical stage (top view).

4.5 Positioning Platform Stiffness Analysis

To exploit the small displacements of the piezoworm actuator, it is extremely important to design the platform that has high stiffness. On the other hand, in order to achieve a high dynamic frequency for the vertical positioner, the mass of the moving platform should be limited to minimum level. This tradeoff between stiffness and mass can be solved by analysis that allows us to estimate appropriate platform geometry where the deformation induced by the clamping forces must be restricted to an acceptable level. The platform, in instances, can be considered as the beam which is simply supported at the ends, and subject to the bending moments from attachments occupying a short span of the total beam length as shown in Fig. 4.8.

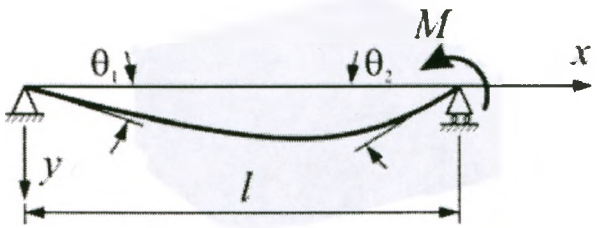

Fig. 4. 8. Deflection of simply supported beam with moment applied at the end.

Under these conditions it can be assumed that the load or bending moment (M) appears at a point along the beam of *l* length. This can be included in the bending equation and integrated to determine the displacement.

$$\theta_1 = \frac{Ml}{6EI} \tag{4.1}$$

$$\theta_2 = \frac{Ml}{3EI} \tag{4.2}$$

$$y = \frac{Mlx}{6EI}\left(1 - \frac{x^2}{l^2}\right) \tag{4.3}$$

where, E and I are modulus elasticity of the material and moment of inertia respectively.

Finite element analysis is one of the effective methods to examine dynamic performance of mechanical structures. The boundary conditions for finite element model are chosen as: the top edges of both sides of top plate are fixed and constrained for all degrees of freedom as shown in Fig. 4.9. The force is applied to the ceramic strips of 1.5 mm thickness placed inside and in the middle of the both frictional plates.

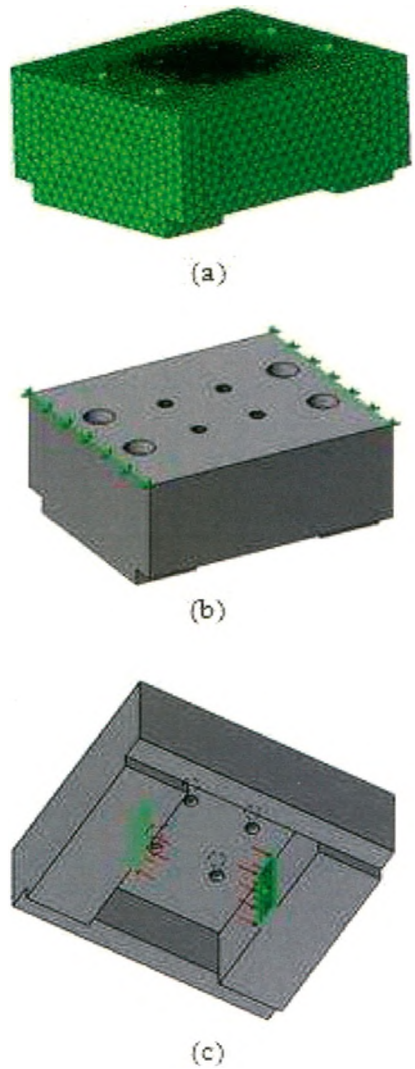

Fig. 4. 9. Finite element analysis of the stage platform: (a) meshed model, (b) boundary condition, (c) applied load.

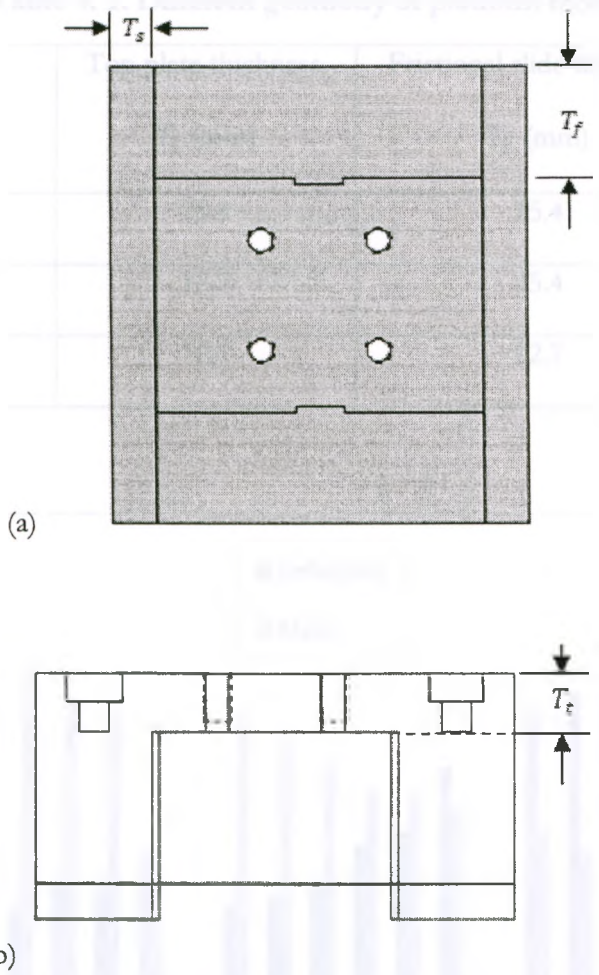

Fig. 4. 10. Dimensions of the stage platform: (a) bottom view, (b) side view.

Using the properties of stainless steel 316L (E = 207 GPa,$\vartheta = 0.27$), a comparison of the platform model among the following three cases is shown in Fig. 4.11. The side plate thickness T_s has been varied in the plot.

Table 4. 1. Different geometry of platform model

Case	Top plate thickness, T_t (mm)	Frictional slide thickness, T_f (mm)
1	25.4	25.4
2	12.7	25.4
3	12.7	12.7

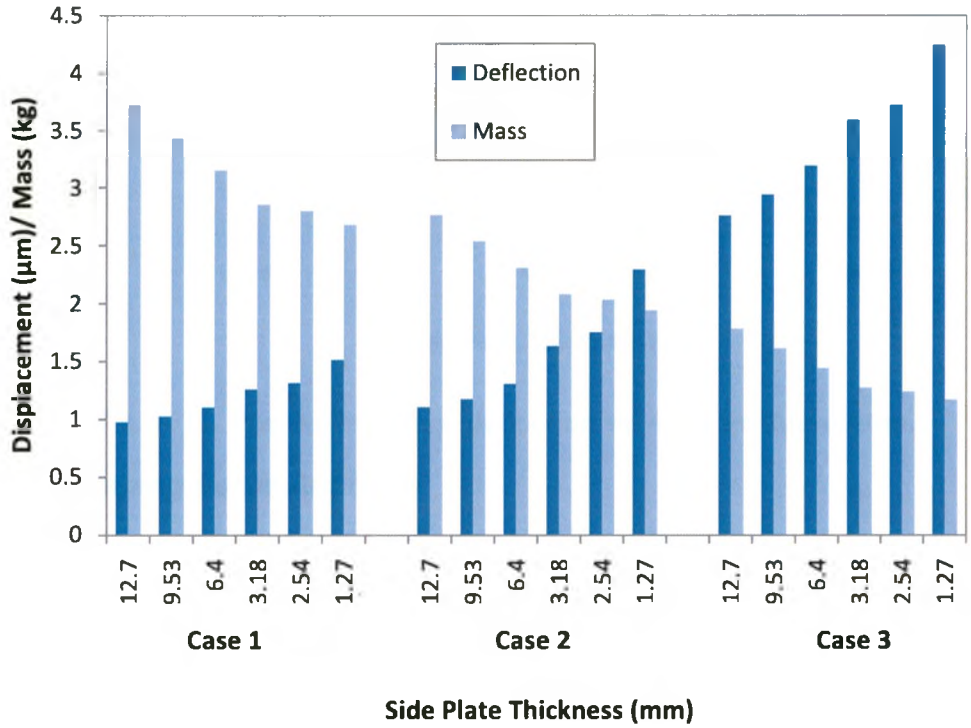

Fig. 4. 11. Positioning stage deflection vs. mass for Stainless Steel.

Similarly, the properties of aluminum 2024 (E = 68 GPa, $\vartheta = 0.33$), a comparison of the platform model among the three cases in shown in Fig. 4.12. It is noted that platform models that are made of stainless still and having Case 2 geometry show better

balances between deflection and mass. The aluminum platforms are lighter in weights but the deflections are too large to be acceptable.

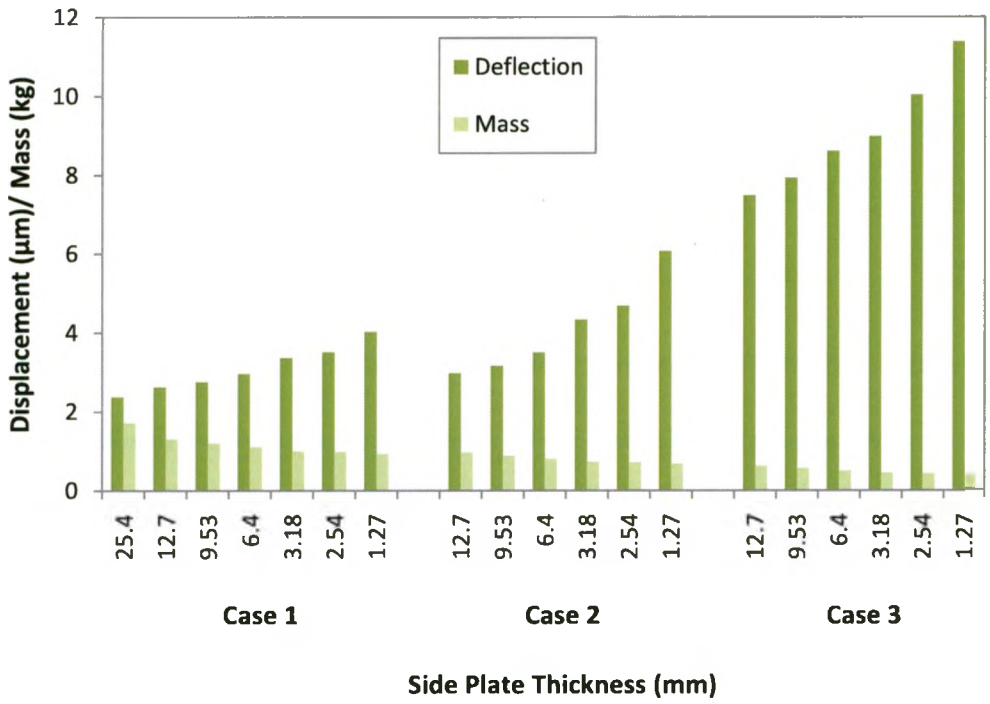

Fig. 4. 12. Positioning stage deflection vs. mass for Aluminum.

4.6 Clamping Force Analysis

The analysis done previously used to design the platform frame geometry provided only a first approximation of the clamp performance. However, the effects of the stiffness on the clamping forces were not considered. To determine the thrust force for a given platform geometry, we select two piezostacks for the two clamps. The NU clamp uses PZT stack that has 5mm×5mm×18mm of dimension, 900N of blocking force and 15μm of nominal displacement. To maintain the compactness, the NC clamp uses another PZT stack that has 5mm×5mm×9mm of dimension, 800N of blocking force

and 6.5μm of nominal displacement. The equation for determining the restraining force can be obtained by (2) as given in [8].

$$F = \left[\frac{K_{fa}}{K_p + K_f + K_{fa}} \{K_p L_0 - (K_p + K_f)C_r\}\right]\mu \tag{4.4}$$

Taking the effects of gravity into account for vertical positioning stage design, the equation becomes

$$F = \left[\frac{K_{fa}}{K_p+K_f+K_{fa}} \{K_p L_0 - (K_p + K_f)C_r\}\right]\mu - mg \tag{4.5}$$

where K_{fa},K_f, K_p are the frictional plate stiffness, clamping frame stiffness, piezoelectric stack respectively and m represents the mass of the positioning stage platform.

The deflections obtained from previous analysis are considered here. The clamping forces of both the NU and NC clamps with respect to different side plate thickness are shown in Fig. 8 and Fig. 9. For the NC clamp, the value of $K_f = 28.88\ N/\mu m, K_p = 100\ N/\mu m$, μ=0.2, and $C_r = 2.5\ \mu m$. For the NU clamp, the value of $K_f = 4.05\ N/\mu m, K_p = 50\ N/\mu m$, μ=0.2, and $C_r = 2.5\ \mu m$.

It is noted that the platforms made of stainless steel exploit the piezoelectric displacements better. Both piezoelectric stacks are sufficient to provide clamping forces to lift a mass of 5 kg which is one of our design requirements.

The optimized platform design based on the analysis is made of stainless steel with top plate thickness of 12.7 mm, frictional plate thickness of 25.4 mm and side thickness of 9.53 mm. The stress distribution for this design is shown in Fig. 4.15 and shows that stress level is minimal and that the stiffness requirement governs the design. A platform model based on the previous analysis has been presented in Fig. 4.16.

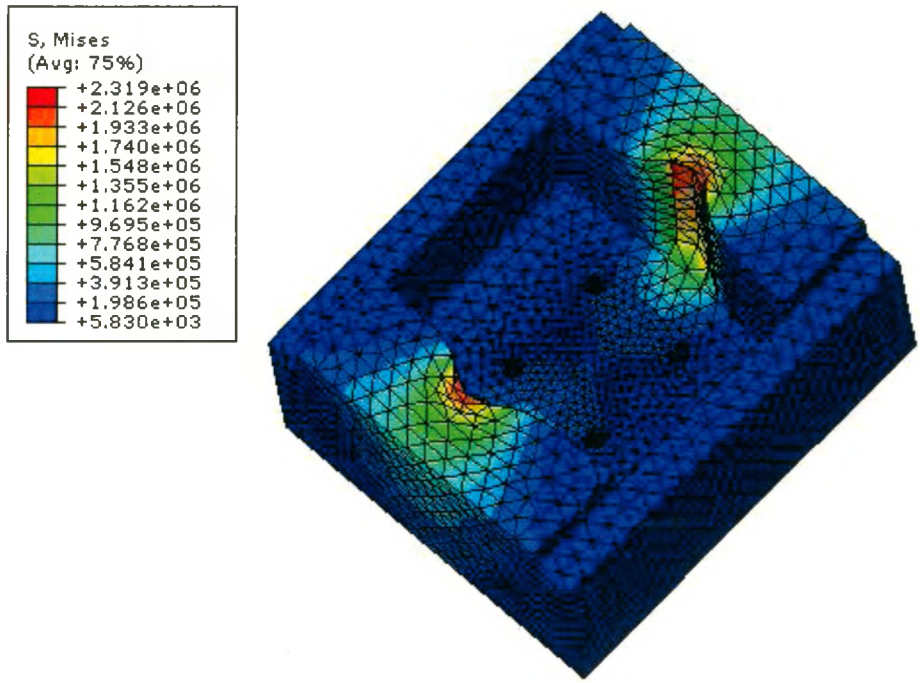

Fig. 4. 15. FEA stress distribution (Pa) of the vertical positioning stage platform mechanism.

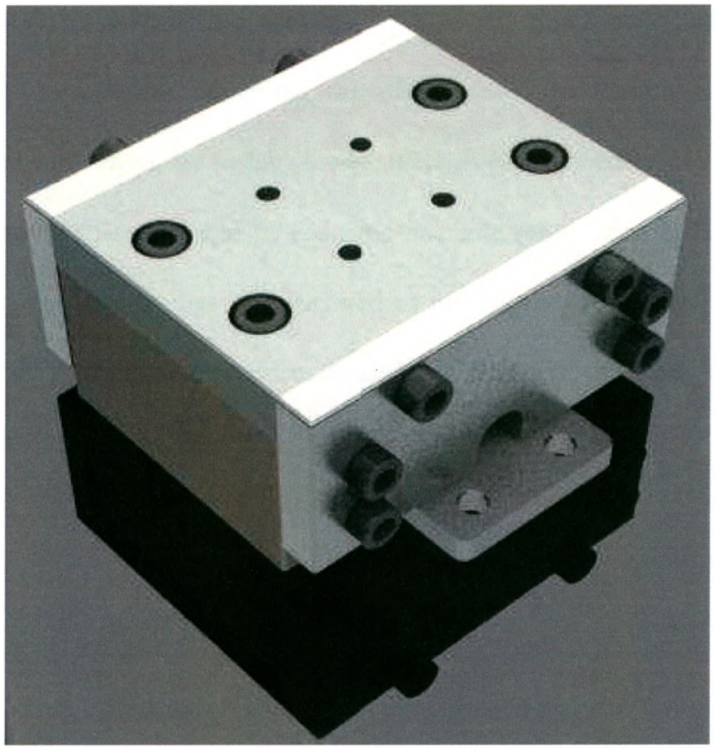

Fig. 4. 16. CAD model of the vertical positioning stage platform mechanism.

4.7 Conclusions

Most of the previous designs in nanopositioning are focus on actuators alone and they are too heavy to be effective as a vertical stage. This design strategy is focused on the light piezoworm actuator as well as compact positioning stage that can be readily configured into multi-coordinate systems to form unique precision manipulators with high speed. A complementary piezoworm configuration based on three piezoelectric stacks and two amplified piezoelectric actuators for Z-axis motion has been described. The identical NC type clamps are fixed to the base through chassis and all the motion was performed by the NU type clamp and the APAs. The APAs not only provide the motion but also the guidance to the NU type clamp during vertical movement. This

configuration allows the piezoworm actuator to hold the positioning platform at any state when unpowered. While designing, the efforts have been given to reduce the production costs and times by using fewer mechanical elements in assembly, by minimizing volume of materials, and by reducing machine setup times in fabricating the device. Finite element analysis has been utilized to investigate the maximum stress and deformations of the clamps and platform in order to improve the static and dynamic performance of the positioning stage.

Chapter 5

5 Prototype and Open Loop Experimental Assessment

5.1 Introduction

The prototype of the vertical positioner included consideration of the properties of the materials used, their method of fabrication into basic components, and the assembly of those components into the finished positioning stage. The positioning platform was made of stainless steel by machining the top plate, guide slides and side plates from rectangular metal bars. The clamp flexures were manufactured in harden stainless steel using a wire EDM process.

This chapter describes prototypes of a complementary clamp piezoworm with a positioning platform and base and their assembly process. It also presents experimental assessment of the basic components as well as the whole system. Since the piezoworm actuator was to be integrated into the positioning stage, ease of assembly of the parts was crucial. Ceramic strips were incorporated into the prototype in order to reduce the wear

in the friction surfaces. A laser interferometer was used to measure the displacements of the individual clamps, extenders and assembled positioner under the application of input driving voltages with various waveforms.

5.2 Fabrication

Even though being time consuming and therefore expensive, maintaining tight tolerances (as low as 0.013 mm) of the parts was an important design consideration for fabrication of precision positioning stage. Other factors included size, weight and shape of the parts, manufacturing techniques, availability of the tools. The design for fabrication also considered additional spaces in the parts for further machining in order to bring modifications if necessary. To achieve the proper alignment between the clamping surfaces of the platform and piezoworm actuator, the holes were made bigger so that necessary adjustments could be possible (see Fig. 5.1). On the other hand, to ensure the machining precision and to simplify the assembly process within compact size, the flexure based mechanisms of the clamps were machined using an electro-discharge machining (EDM). This tolerance was decided to be sufficient for the NU and NC clamp displacements capability of 7.5 μm and 6.5 μm respectively on each side. The base and the two chassis were also important because they determined the flatness of the system and the adjustment of the NC clamps respectively.

The top plate was, made of stainless steel, bolted to the top of the two guide slides in order to provide the ability to maintain parallelism of the guide slides with respect to the clamping surfaces. The platform before attaching the side plates provided the ability to observe the actuator alignment inside the channel. The two side plates were machined of stainless steel to produce the desired stiffness at the joints as optimized in

Chapter 4. The holes were deliberately made bigger so that the plates can be bolted to the guide slides and the top plate after making correct adjustment.

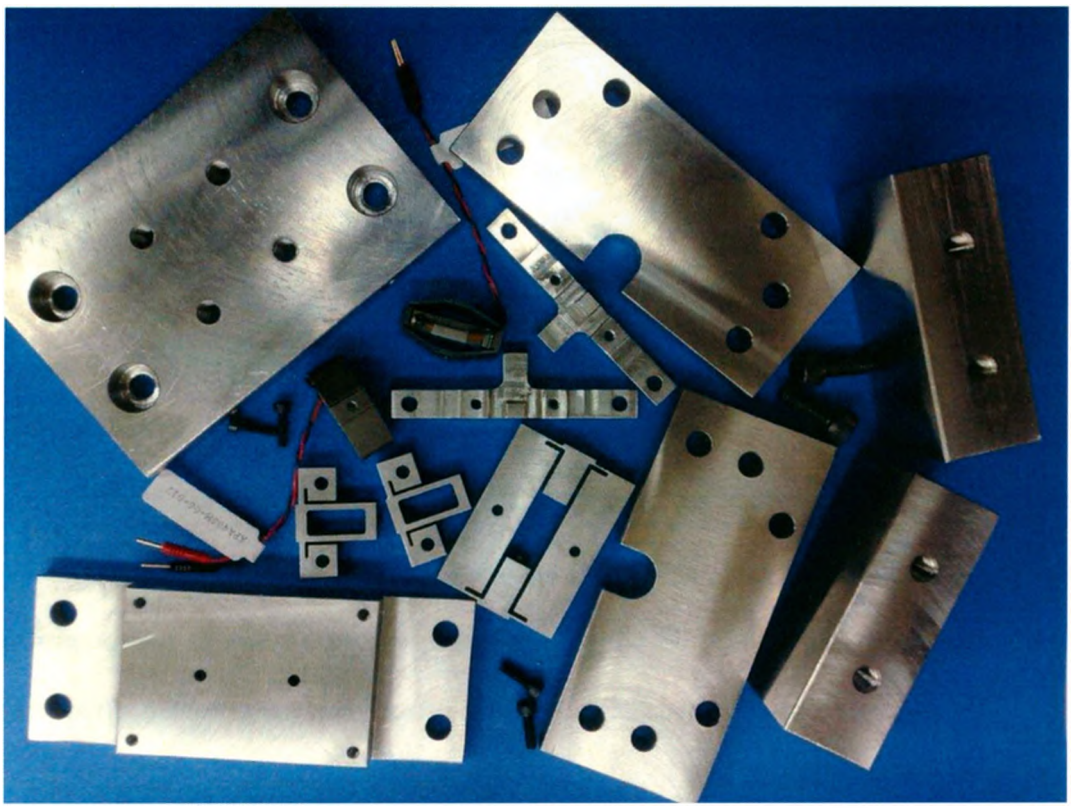

Fig. 5. 1. Photograph of the fabricated parts of vertical nanopositioner.

5.3 Test Results of Extending Mechanism

The extending actuators (see Fig. 5.2) used in the piezoworm had the capability to produce the performance needed to raise the positioning stage with the help of the clamps. The direct attachment of the NU clamp to the extending actuators enabled the compact design and also increased the stiffness of the piezoworm. Increasing the actuator's stiffness also allowed for higher drive frequencies to be achieved. This increase in drive frequency increased the velocity in which the motor is able to obtain. However, the most important advantage was to achieve longer ranges of the actuators in Z axis.

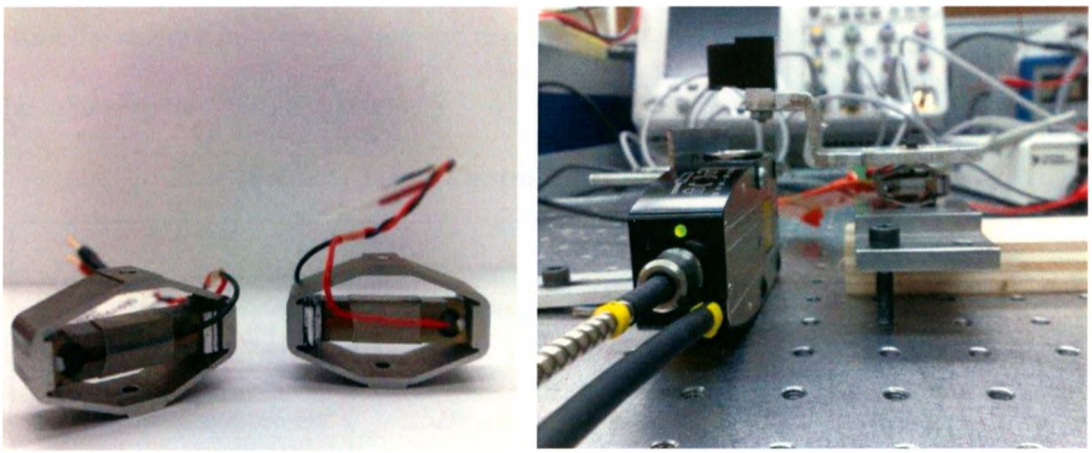

Fig. 5. 2. Cedrat 40SM Amplified Piezoelectric Actuators and their test set-up.

5.4 Assembly and Test Results of Clamps

Fig. 5.3 shows the assembled NC and NU type clamps. The lengths of the piezostacks for NU and NC clamps determined the width of the positioning stage. It was also important to select a proper piezostack for the NU clamp that demonstrated the same performance as the two piezostacks for the NC clamps together.

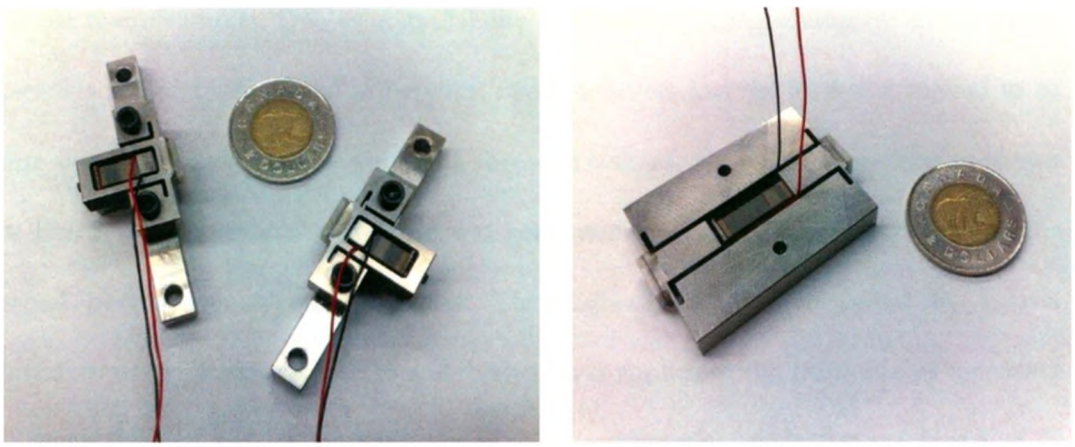

(a) **(b)**

Fig. 5. 3. Photographs of fabricated and assembled clamps: (a) NC clamps, (b) NU clamp.

From the analysis presented earlier and experiments conducted here, the piezoworm has the following characteristics at 100 V:

Table 5. 1. Piezoworm Prototype Properties

Property	Results		
	Analytical	FEA	Experimental
NC clamps displacement	5.08 μm	5.23 μm	5.18 μm
NU clamp displacement	13.94 μm	13.77 μm	14.30 μm
Extension displacement	52 μm	49.55 μm	47.50 μm

Before preloading the piezostacks inside the clamps, separate tests were performed to ascertain if the design parameters would be met. The first tests were of the displacements of the piezostacks to check whether they met the performances specified by the manufacturers. Due to unavailability of standard testing equipment or setup, the piezostack alone was placed in between two L-brackets and the load was applied to its one side by rotating a screw through a threaded hole of one of the L-brackets as shown in Fig. 5.4. A trapezoidal waveform was generated by NI Labview RT system and the signal passed through the amplifier. The displacement was measured by a laser interferometer, Renishaw RLE10 and the load was applied to the front side of the clamp through the load cell by rotating a screw. The laser interferometer has resolution of 20 nm and wavelength of 19.780938 nm. The results shown in Fig. 5.5 provide good agreements between the actual and the desired displacements.

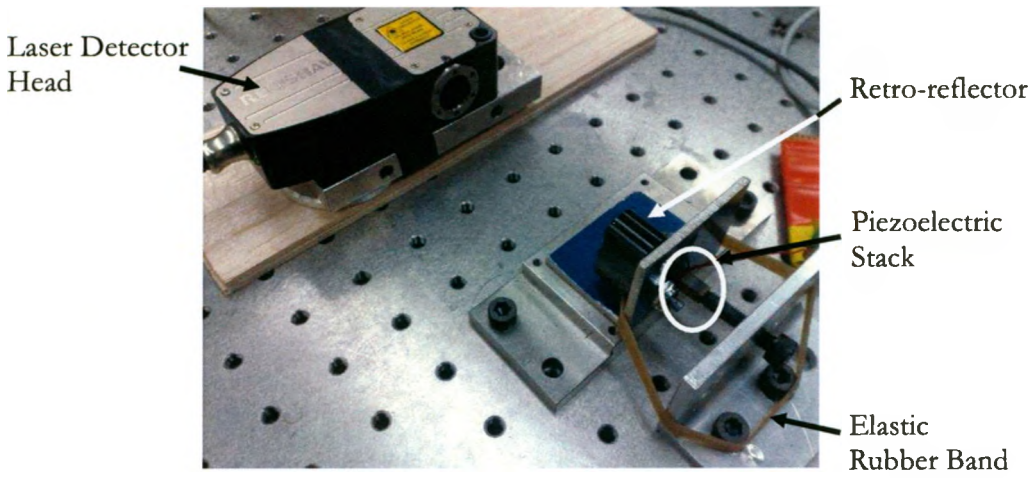

Fig. 5. 4. Experimental set-up for displacement measurement.

The second tests were of the stiffness of the NC clamp frames. The experimental set-up is shown in Fig. 5.6. The clamp was attached to the chassis such that there was gap between the tab and the inner surface of the clamp. Then the chassis is further attached to the base. The displacement was measured by the laser interferometer, RLE10 and the force was measured by a compression load cell, Measurement Specialties FC22. The load cell was attached to an wooden part which was placed between an L bracket and the clamp as shown in Fig. 5.6. The load was applied to the front side of the clamp through the load cell by rotating a screw.

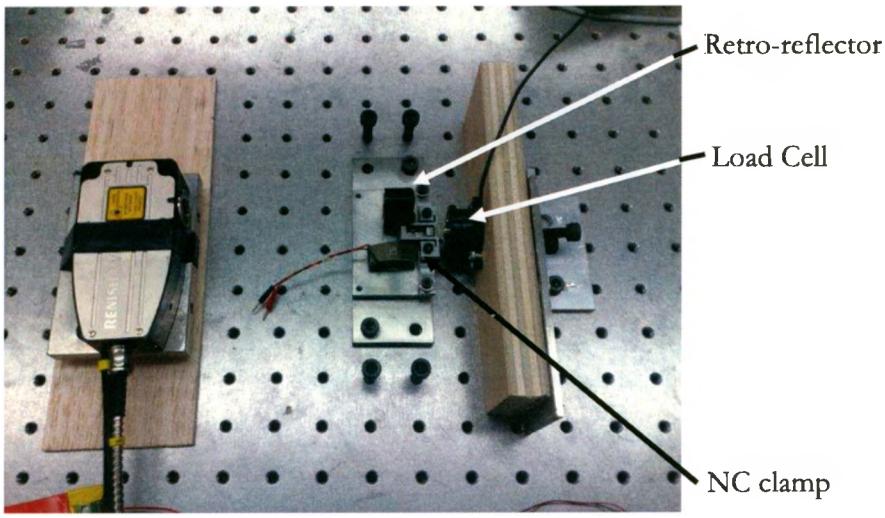

Fig. 5. 5. Experimental set-up for stiffness measurement.

One of the clamps flexure stiffness was found to be 5.01 N/μm while the other one was found to be 4.18 N/μm. Both values are considerably lower to the analytical and FEA results. Therefore, further investigations were required to identify the causes. The retro-reflector was attached to one of the fixed wings of the NC clamp to check whether there was any deflection. The laser sensor detected some deflections ranging from 1.5 μm to 2 μm at the fixed parts of the clamps which was unexpected. As a result, the NC clamps were not capable of generating the required forces and displacements. This was believed to be detrimental to the performance of the positioner with high force capacity. Therefore, the problem was identified as the fixed end condition was not met. A relative comparison of the FEA and real fixed end condition has been demonstrated in Fig. 5.6. In order to reach the identical fixed end conditions, four holes instead of two holes can be proposed.

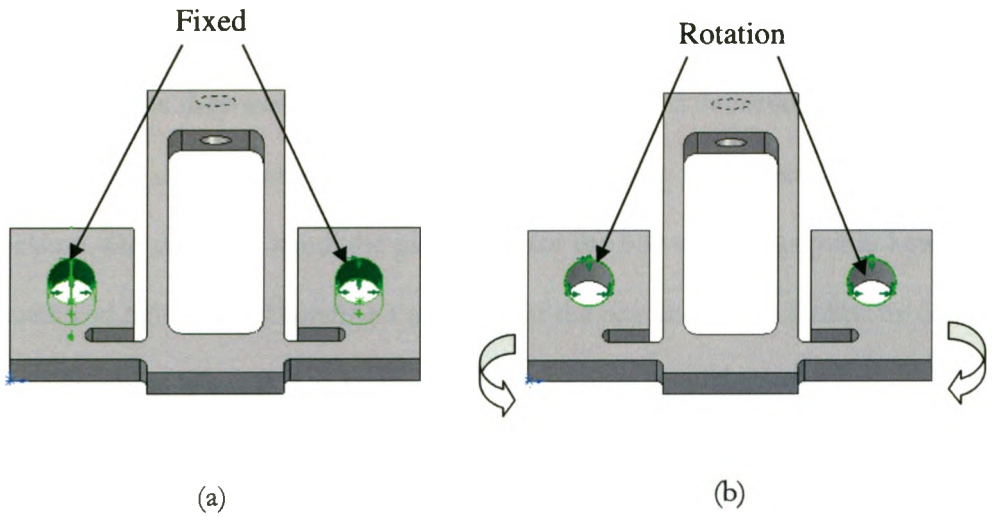

Fig. 5. 6. Fixed end conditions of the NC clamps (a) FEA state, (b) actual state.

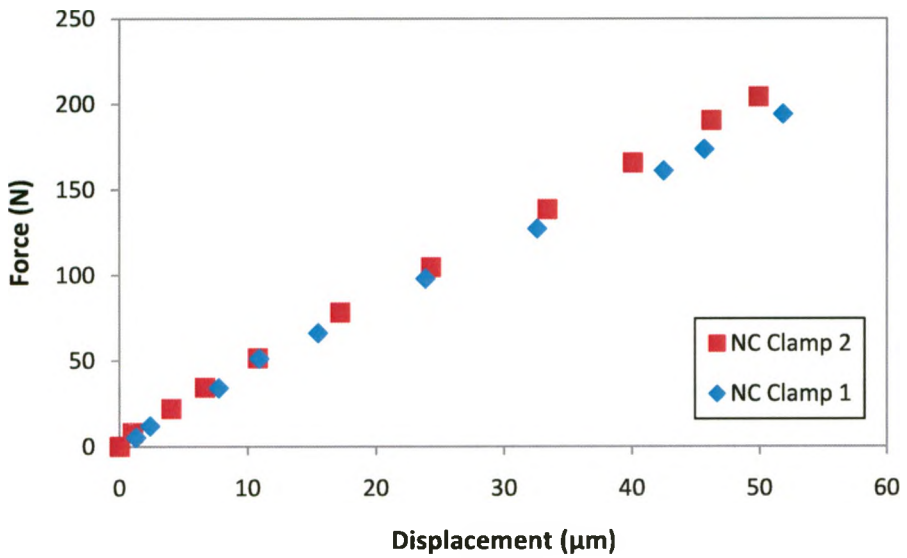

Fig. 5. 7. NC clamp stiffness measurement results.

By using flexure structure the overall size and weight of the clamping mechanisms were greatly reduced, while maintaining a preload on the piezostack actuators and preventing shear stress from being transferred to the actuators. Fig. 5.7 shows the preloading process of the piezoelectric actuators in both types of clamps used

in the piezoworm actuator. In case of the NC clamp, an initial load was applied to their front ends while they were fixed. This caused the required deflection of the flexure and the piezostack was tightened inside the frame by rotating a set screw at the rear end of the clamp. On the other hand, the piezostack for the NU clamp was put in between two flexures and tightened by rotating a set screw at the one end of the clamp. By doing this, the displacement losses due to interface clearances were also eliminated.

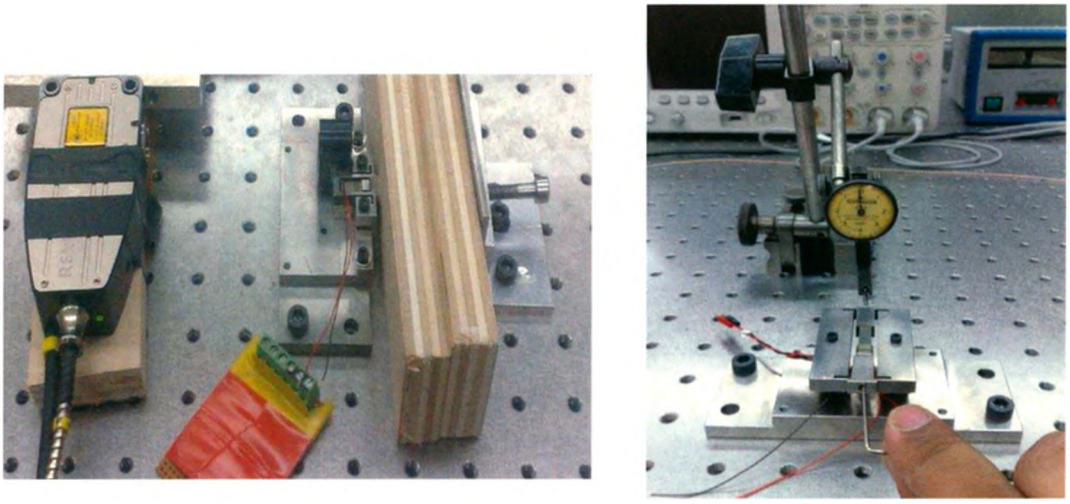

(a) (b)

Fig. 5. 8. Preloading of piezostacks inside frames (a) NC clamp, (b) NU clamp.

Since all loads are ultimately supported by the frictional forces between the guideway and clamps, the guideway-clamp interfaces to have high friction coefficient and a low wear rate. If wear occurs, the clamping actuators cannot compensate for such a small displacement provided. Lubrication can be an option to reduce wear but such option is not suitable for the piezoworm since its working principle is based on high friction force. Therefore, each friction surfaces was precisely ground and ceramic strips were used for each of the surfaces. Once the clamps were fully assembled, the final tests

on the individual clamps were performed. The displacement was measured by the laser sensor while the piezostack was excited to 100 V in trapezoidal waveform. Both NC clamps had displacements of 5.5 μm and the NU clamp had a displacement of 7.5 μm on its each side. While the NU clamp results are consistent with the original design, the NC clamps results are lower than the expected results due to the actual stiffness considerably lower than the predicted analytical and FEA results.

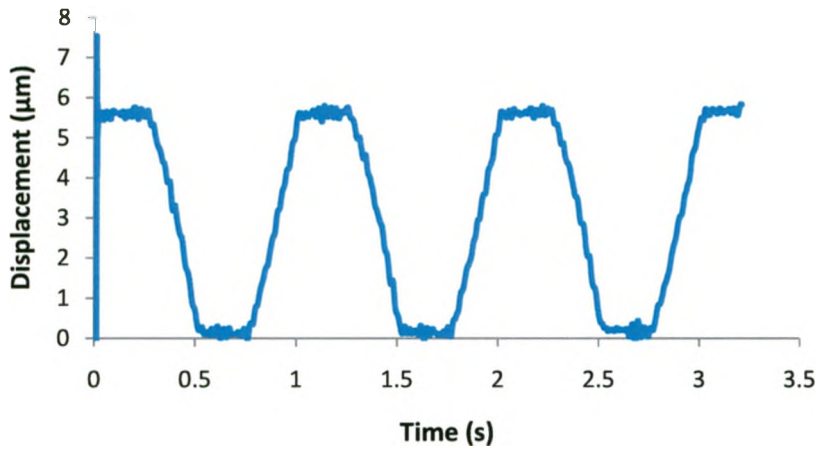

Fig. 5. 9. Displacement result of one of the NC clamps.

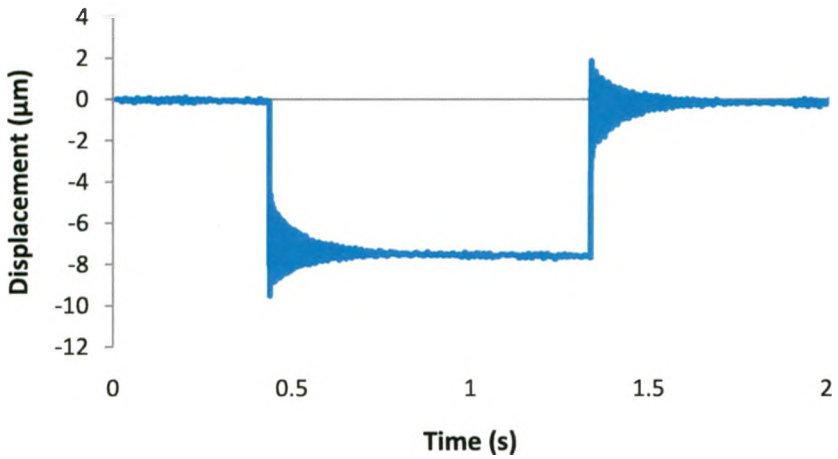

Fig. 5. 10. Displacement result of the NU clamp on each side.

5.5 Assembly of Positioning Stage

One of the objectives of the positioner design was easy of assembly of the basic components. Each of the components was made separate and could be replaced if necessary. The entire assembly process can be divided into two phases as shown in Fig. 5.11. The first phase in assembling was building the piezoworm actuator on the base plate that already attached to the smart table. Hence the NC clamps with their chassis were bolted to each side of the base. The screws that attached the chassis to the base were kept loosen deliberately so that the clamps could be adjusted. Then the amplified piezoelectric actuators were bolted to the base in between the NC clamps. Then the NU clamp was bolted to the extending actuators directly. To make necessary clearance between both types of clamps, some washers were used between the NU clamp and the extending actuators.

Next, the two guide slides were brought in touch of the clamps on each side and the top plate was placed on the top sides of them to implement the second phase of the assembly process. The platform consisted of a five plates producing an enclosed rectangular channel inside which the piezoworm actuator could operate. An alternative way could be attaching the side plates first instead of the top plate. However, the former method was found more effective. Therefore, the design of the top plate was made rather bulky in an effort to eliminate any angular deviation during alignments. To achieve the proper functionality of the NU clamp, 100 V is applied to its piezostack before tightening the top plates on the guide slides. This enabled to verify whether the NU clamp were able to hold the platform when it was energized. Then the NC clamps were squeezed towards the guide slides to eliminate any gap in between them. When the

voltage was applied to the NC clamp piezostacks, the gap increased that enabled the guide slides to move. The assembled positioner is shown in Figure 5.11.

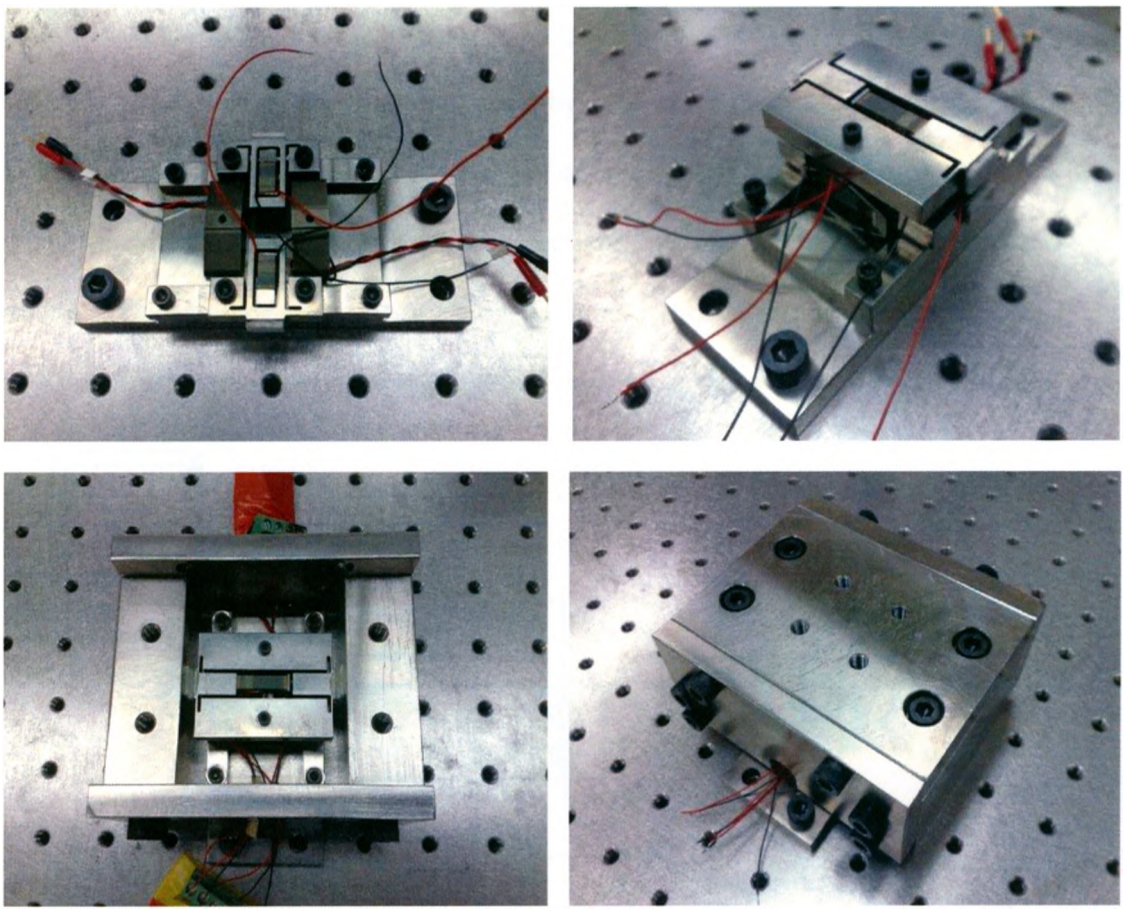

Fig. 5. 11. Photographs of vertical positioner prototype assembly.

5.6 Open Loop Experimental Results

Having completed the machining and assembly of the nanopositioning device, a series of investigations were performed using the experimental setup as presented in Fig. 5.12 to assess its positioning performance. A PC was used to generate various waveforms, i.e. sine waves, trapezoidal wave, and hybrid wave by using LabVIEW software. These waveforms were output by a PCI-6733 DAQ interface card (National

Instrument) to a PI (Physik Instrumente) E-505.00 power amplifier, where they were amplified and then supplied as drive signals to the piezoelectric actuator. The corresponding displacement of the positioning stage was measured by means of retro-reflector on the top of the stage connected by Z bracket. The measured displacement values were acquired by the PC through another DAQ interface card PCI-6259 (National Instrument). To improve the precision and reliability of the experimental results, the positioning stage was isolated from interference caused by external vibrations by fixing it to laminar flow isolator supported smart table with IQ Damping technology.

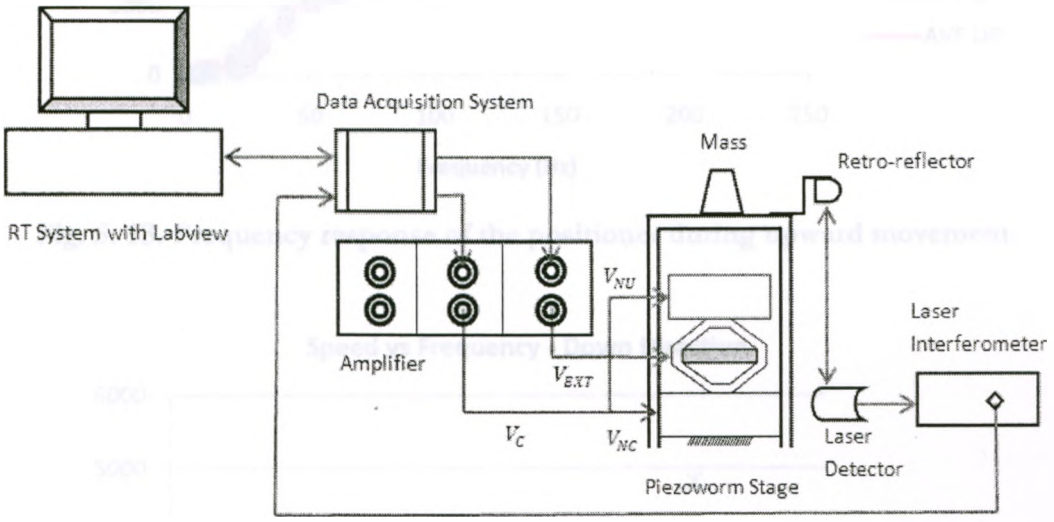

Fig. 5. 12. Experimental Setup.

Altering the waveform and phasing between input signal would lead to a optimal set of input signals that produced the better positioner performance. In this test, a trapezoidal waveform was used with duration of the rising and falling portions of the waveform limited to 25% of the signal period. The maximum speeds of the piezoworm were found as 5.4 mm/s during upward positioning and 4.8 mm/s during downward

positioning at 200 Hz and 100 V. The results are shown in Fig. 5.13, Fig. 5.14 and Fig. 5.15.

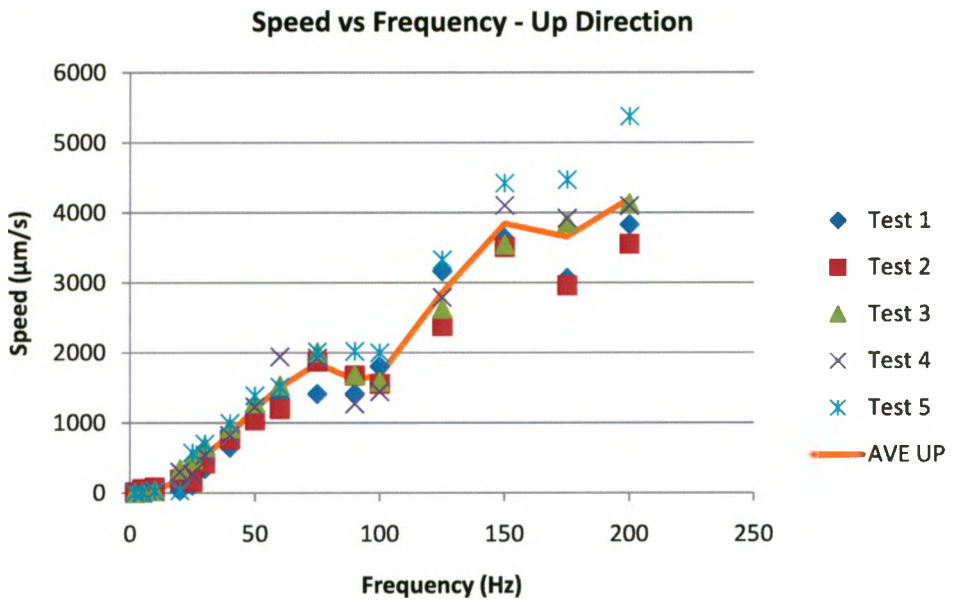

Fig. 5. 13. Frequency response of the positioner during upward movement.

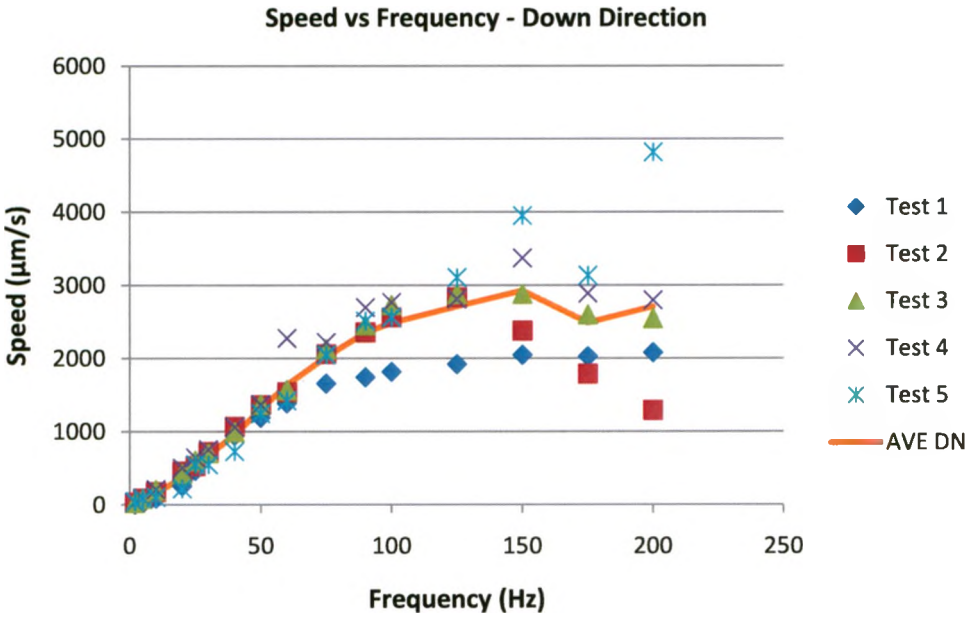

Fig. 5. 14. Frequency response of the positioner during downward movement.

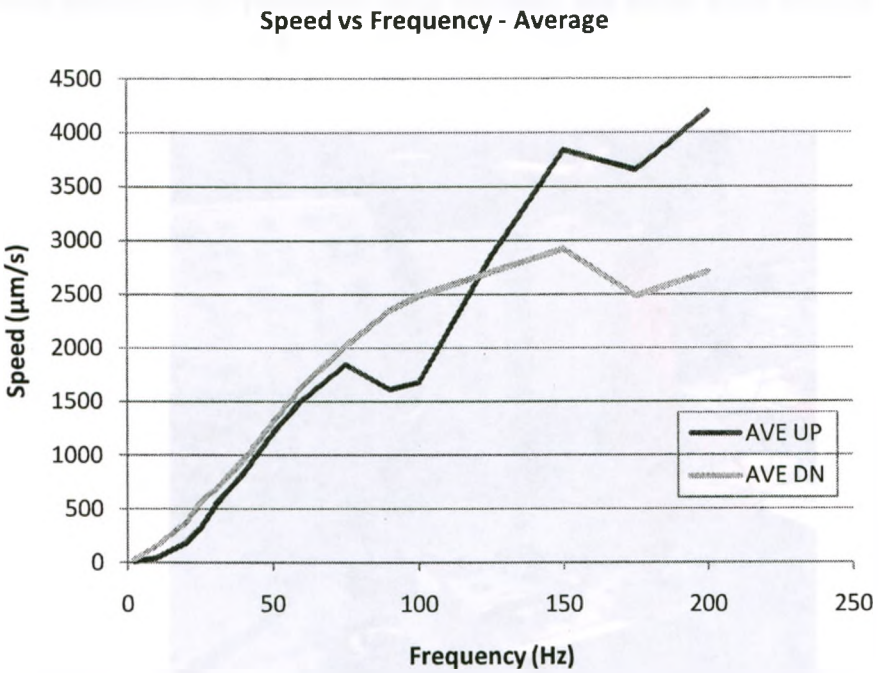

Fig. 5. 15. Comparison of average frequency responses in both directions.

Additional testing of the positioner to higher frequencies was performed to observe the affects of resonance on the piezoworm's performance and to find the resonant frequency for the piezoworm. It was found that maximum variation in the speed occurred at 200 Hz. In static evaluation, the positioner could carry a maximum mass of 2.9 kg while no voltage was applied to both types of clamps. When voltage was applied to both types of clamps, the positioner was found to carry a maximum mass of 4 kg. However, the piezoworm actuator could not lift the platform in dynamic evaluation. One of the possible reasons may be the NU type clamp drag was larger than the total restraining forces provided by the NC type clamps. Another explanation may be the amplified piezoelectric actuators which worked as extenders could not provide enough stiffness. Therefore, the effect of the applied load was studied using counterweights

which were applied to the positioner using the cable and pulley from the top (see Fig. 5.16).

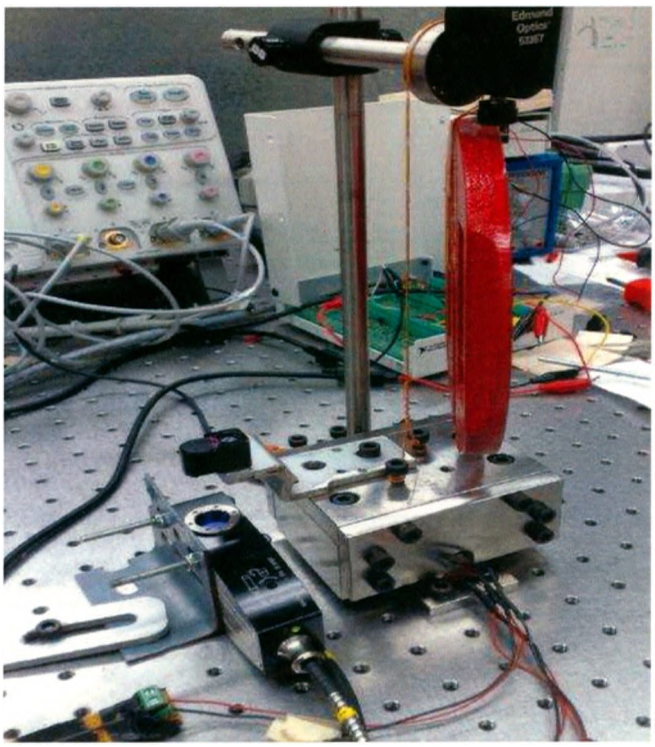

Fig. 5. 16. Experimental set-up for the vertical positioner using counterweights.

The same waveform at 50 Hz was used this time. The results in Fig. 5.17 show that the downward speed decreases quite sharply to a maximum load of about 3.4 kg. Since the positioning platform has its own weight of 2.4 kg, the positioner has the capacity to carry the load of 8 N. With proper counterweights, the positioner moved up to 20 mm in both upward and downward directions. Some of the positioning results in scanning modes are shown in Fig. 5.18 and Fig. 5.19.

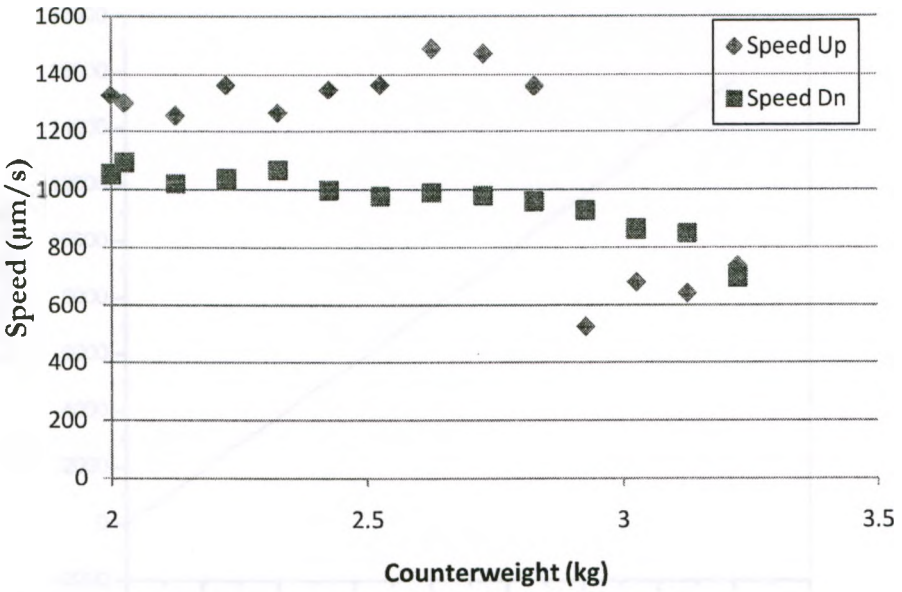

Fig. 5. 17. Positioner velocity as a function of applied load.

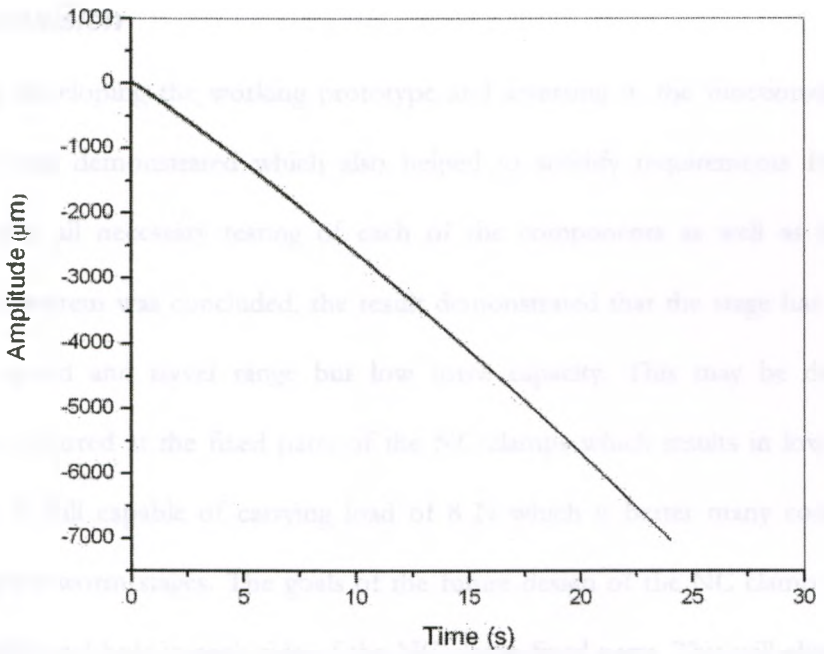

Fig. 5. 18. Experimental results for a downward scanning mode positioning test.

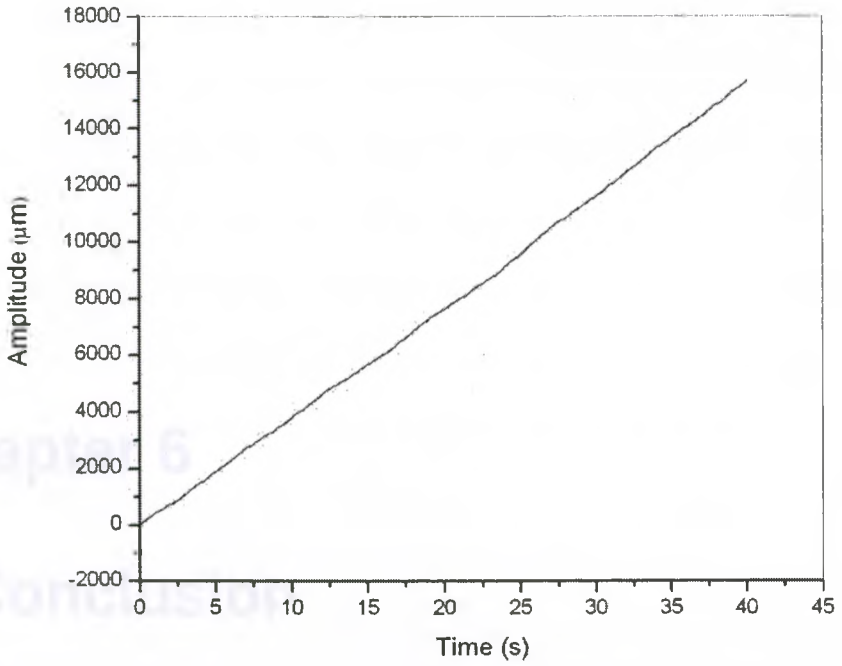

Fig. 5. 19. Experimental results for an upward scanning mode positioning test.

5.7 Conclusion

By developing the working prototype and assessing it, the functionality of the positioner was demonstrated which also helped to solidify requirements for the re-design. After all necessary testing of each of the components as well as the whole positioning system was concluded, the result demonstrated that the stage has sufficient accuracy, speed and travel range but low force capacity. This may be due to the deflection occurred at the fixed parts of the NC clamps which results in low stiffness. The stage is still capable of carrying load of 8 N which is better many commercially available piezoworm stages. The goals of the future design of the NC clamp will be to include additional hole in each side of the NC clamp fixed parts. This will eliminate any rotation or deflection of the fixed parts of the NC clamps, while improving its static and dynamic performance.

Chapter 6

6 Conclusion

6.1 Background

Nanopositioning technology proposes numerous applications in the fields of semiconductor technology, biomedical research, micro/nanofabrication process, optics, and metrology instrument. This wide range of applications requires the design and development of large load capacity, long stroke and compact positioning stages without compromising high speed and precision. This thesis deals with design-related research in vertical nanopositioning based on piezoelectric actuators. A prototype of the Z-axis positioning stage driven by flexure mechanism based complementary clamp piezoworm actuator has been developed. The compact design of the Z-axis positioning stage described herein makes it preferable for different applications. Traditionally, the motion in Z axis is being achieved by mounting a stage on an L-bracket which often has low force capacity and lacks compactness. Such arrangement also does not allow an object to

mount directly on the positioning stage. Some vertical positioners mounted on coarser micropositioners, for the extended travel ranges, are now commercially available and they can provide several mm range of travels and high load capacity. However, such systems suffer from non-linearities which are detrimental to the positioning accuracy and require compensations for backlash and stick-slip. In this thesis, these limitations have been addressed by developing a piezoworm actuator specifically for generating vertical motions which utilized to drive a newly designed compact vertical stage with long travel range and high speed capabilities. The actuator has long travel range and resolution to move the sample placed on the top of the platform precisely to the desired location. The stage does not require continuous electrical power to hold the sample in position.

6.2 Summary

Several researchers have previously developed piezoworm actuators for planner motion, however this work focuses on designing the actuator for vertical positioning with high precision. In addition, this work concentrates on designing an Z-axis stage and integrating the actuator into the stage while most of the previous related research works were concentrated on the actuators only. The benefit the structure becomes compact and the friction surfaces are not exposed to dust or any other contamination. Therefore, two major challenges have been faced and solved: proper installation of the actuator within the stage and perfect alignment of the actuator to the stage. The research activities on the development of vertical positioning stage have been divided into following phases:

- *Development of analytical model* - In this phase of the research, an improved stiffness model for the clamp which normally holds the slide was developed

and presented. The common stiffness model used in the literature is not feasible for the two different types of clamps used in complementary clamp piezoworm actuator. The effect of preload on the flexure mechanism was considered in the stiffness model which is significant in short flexures as it induces additional internal stress to the mechanism. This model was useful to prevent permanent deformation or even fracture of the flexure mechanism and validated by estimating the maximum stress during operations which is below the yield stress of the material.

- *Development of complementary piezoworm actuator* - Five piezoelectric actuators were used in this piezoworm configuration to achieve motion in vertical direction. The designs of the stationary and moving clamps were aimed to be symmetric in order to provide clamping forces to both directions. Each of the components of the piezoworm actuator was separate and can be adjusted or replaced if needed. FEA was used to select accurate flexure geometry of the clamps and to optimize their performances. Two amplified piezoelectric actuators were used in parallel for the extender sections. Such compact configuration reduced the height and size of the actuator by eliminating guide rods or flexure guides, allowing space for the stationary clamps and direct expansion or contraction of the moving clamps in vertical direction.
- *Development of vertical positioning stage* - An improved stiffness model for the positioning platform was described as part of vertical positioning stage design. The tradeoff between stiffness and mass was solved by estimating appropriate platform geometry where the deformations induced by the clamping forces

were restricted to minimum level. FEA was utilized to investigate the maximum stress and deformation of the platform and thus to improve its static and dynamic performance. For the given platform geometry, the clamping forces provided by two different clamping sections are also analyzed. Such platform design is useful to provide long travel range and support large load without using the highly accurate guide sliding mechanism.

- *Prototype fabrication, assembly and testing* – In order to achieve high machining accuracy, EDM technique was used to manufacture the flexure mechanisms for the clamps. The friction surfaces were precisely ground to avoid misalignment during rectilinear motion. Ceramic strips were attached to reduce wear of the friction surfaces. During assembly, the piezoworm actuator was well-suited inside the vertical stage and the stationary clamps were properly aligned by adjusting the chassis. With the assistance of proper counterweights, the platform of the stage developed could climb upto 20 mm with repeatability of less than 20 nm. The actuator had load capacity of 8 N. The overall dimensions of the finished stage were 115 mm (length) × 100 mm (width) × 57.25 mm (height).

6.3 Future Work

The future research efforts will be directed towards the development of a close-loop controller for the positioning stage to track a wide class of signals. In order to realize accurate positioning and tracking by addressing the non-linearities such as friction induced between the surfaces, hysteresis in piezoelectric actuators between the voltage-

displacement relationship, glitching during clamp switching, and misalignment between surfaces during assembly, closed loop control of the piezoworm is required. The clamping surfaces of the piezoworm clamps are coupled to the positioning platform through ceramic strips which reduce wear of the clamping surfaces without compromising the friction that is required to achieve high output force. This friction is non-linear in nature since it varies along the length of the travel of the slide. All the non-linearities can be addressed by closed loop control and highly precise positioning of the platform can be achieved. The laser interferometry-based closed-loop control for the vertical positioner will go under extensive testing. The vibration induced due to the impact between the clamp and friction surface during each clamping step can be addressed by proper control techniques.

There are several applications in which this vertical positioner can be found useful such as cell manipulation, surface metrology, lithography, deep space optical communication, molecular assembly and nano fabrication. The vertical positioner can provide precise high velocity in the Z direction which is needed in the typical cell manipulation such as clean penetration without dimpling, especially for tough cell membrane. In 3-D particle tracking, this vertical positioner will enhance the range capacity of the stand that uses standard epifluorescence video imaging in off-focus mode and allows the tracking of particles with 100-ms temporal resolution. This long range vertical positioner is expected to contribute to the emerging fields in high-speed fluorescence and confocal microscopy applications.

This vertical stage can be integrated to planner stages in order to make XYZ-axis positioning system that can provide centimeter of travel range in each direction.

Furthermore, piezoelectric rotary motors (PRM) can be utilized into the positioning system to achieve high resolution angular positioners. Thus manipulator that provides six degree of freedom motions with high precision and extended ranges can be acheived. Such system can provide great flexibility to the traditional stereotaxic devices used in neurosurgery by allowing the probe/tool to be precisely positioned at variable angles with respect to the target sample. High precision linear and rotary motion in extended ranges will bring new opportunities in nanorobotics research. Since the piezoworm actuator is integrated inside the positioning stage, the friction surfaces for this vertical stage are not exposed and become free of contamination in biochemical applications. The materials of the positioning stages can be made compatible with extreme environmental conditions such as ultra-high-vacuum, cryo-temperature, high-magnetic field etc.

References

[1] B. Awabdy, W. Shin and D. Auslander, "Nanometer positioning of a linear motion stage under static loads," *IEEE Transactions on Mechatronics*, vol. 3, June 1998, pp. 113–119.

[2] B. Zhang and Z. Zhu, "Developing a linear piezomotor with nanometer resolution and high stiffness," *IEEE Transactions on Mechatronics.*, vol. 2, June 1997, pp. 22–29.

[3] P. Tenzer and R. Ben Mrad, "A systematic procedure for the design of piezoelectric piezoworm precision positioners," *IEEE/ASME Transactions on Mechatronics*, vol. 9, no. 2, June 2004, pp. 427-435.

[4] J. J. Gorman and N. G. Dagalakis, "Modelling and disturbance rejection control of a nanopositioner with application to beam steering," ASME International Mechanical Engineering Congress, Washington, D.C., November 15-21, 2003, IMECE2003-41603.

[5] R. Ben Mrad and H. Hu, "Dynamic Modeling of Hystersis in Piezoceramics," Proc. Of IEEE/ASME International Conference on Advanced Intelligent Mechatronics, vol. 1, Jul. 2001, pp. 510-515.

[6] H. Zhang, K. Liu and A. El Haj, "Optical Manipulation of Stem Cells," European Cells and Materials, vol. 16, suppl. 3, 2008, pp. 98.

[7] A. Putra, S. Huang, K. Tan, S. Panda and T. Lee, "Design, Modeling, and Control of Piezoelectric Actuators for Intracytoplasmic Sperm Injection," IEEE Transactions on Control Systems Technology, vol. 15, no. 5, Sept. 2007, pp. 879 – 890.

[8] S. Jordan and P. Anthony, "Design Considerations for Micro- and Nanopositioning: Leveraging the Latest for Biophysical Applications," Current Pharmaceutical Biotechnology, vol. 10, 2009, pp. 515-521.

[9] S. Linden and D. Sullivan, "Breast Skin Calcifications: Localization with a stereotactic device," Radiology, vol. 171, 1989, pp. 570-571.

[10] P. Kelly, "Introduction and historical aspects," in *Tumor Stereotaxis*, Philadelphia, PA: Saunders, 1991.

[11] P. Gildenberg, "Stereotactic surgery: Present and past," in *Stereotactic Neurosurgery*, M. Peter Heilbrun, Ed. Baltimore, MD: Williams & Wilkins, 1988.

[12] V. Zhelyaskov, M. Broderick, A. Raphalovitz, and B. Davies, "*Long* Travel Ranges and Accurate Angular Movement Create New Opportunities in Biomedical Manipulation Systems," IEEE Circuits & Devices Magazine, Nov./Dec. 2006, pp-75-78.

[13] G. Binnig and H. Rohrer, "Scanning tunneling microscopy," *Helvetica Phys. Acta*, 1982, vol. 55, pp. 726–735.

[14] G. Binnig, C. F. Quate, and C. Gerber, "Atomic force microscope," *Phys. Rev. Lett.*, vol. 56, no. 9, , Mar. 1986, pp. 930–933.

[15] R. Wiesendanger, "Contributions of scanning probe microscopy and spectroscopy to the investigation and fabrication of nanometer-scale structures," Journal of Vacuum Science Technology B vol. 12, issue 2, March 1994, pp. 515-529.

[16] D. Kolb and M. Schneeweiss, "Scanning Tunneling Microscopy for Metal Deposition Studies," The Electrochemical Society Interface, Spring 1999, pp-26-30.

[17] N. Jalili, "Piezoelectric based vibration control: from marco to micro/nano scale systems," Springer Science, 2010.

[18] N. Shimizu, T. Kimura, T. Nakamura, and I. Umebu, "An ultrahigh vacuum scanning tunneling microscope with a new inchworm mechanism," Journal of Vac. Sci. Technol. A, vol. 8, Issue 1, , January 1990, pp. 333-335.

[19] Q. Zou, K. K. Leang, E. Sadoun, M. J. Reed, and S. Devasia, "Control issues in high-speed AFM for biological applications: Collagen imaging example," *Asian J. Control: Special Issue Adv. Nano-Technol. Control*, vol. 6, no. 2, Jun. 2004, pp. 164–178.

[20] C. Grimellec, E. Lesniewska, M. Giocondi, E. Finot, V. Vie, and J. Goudonnet, "Imaging of the Surface of Living Cells by Low-Force Contact-Mode Atomic Force Microscopy," *Biophys. J.*, Vol.75, 1998, pp. 695-703.

[21] M. Viani, T. Schaffer, A. Chand, M. Rief, H. Gaub, and P. Hansma, "Small Cantilever for Force Spectroscopy of Single Molecules," *J. Appl. Phys.*, Vol. 86, No. 4, 1999, pp. 2258-2262.

[22] M. Radmacher, M. Fritz, and P. Hansma, "Imaging Soft Samples with Atomic Force Microscope: Gelatin in Water and Propanol," *Biophys. J.*, Vol. 69, 1995, pp. 264-270.

[23] You, H. X., J. M. Lau, S. Zhang, and L. Yu, "Atomic force Microscopy Imaging of Living Cells: a Preliminary Study of the Disruptive Effect of Cantilever tip on Cell Morphology," *Ultramicroscopy*, vol. 82, 2000, pp. 297-305.

[24] "Nanopositioning Tools and Techniques for R&D Applications," nPoint, Inc., Madison, Wisconsin, [Online document], Available at http://www.npoint.com.

[25] V. Levi, Q. Ruan, K. Kis-Petikova and E. Gratton, "3-D Particle Tracking in a Two-Photon Microscope: Application to the Study of Molecular Dynamics in Cells," *Biophysical Journal*, vol. 88, April 2005, pp. 2919–2928.

[26] M. Speidel, A. Jona´s, and E. L. Florin, "Three-dimensional tracking of fluorescent nanoparticles with subnanometer precision by use of offfocus imaging," *Opt. Lett.*, vol. 69, 2003, pp.69–71.

[27] Canfield, S., Edinger, B., Frecker, M. and Koopmann, G., 1999, "Design of Piezoelectric Inchworm Actuator and Compliant End Effector for Minimally Invasive Surgery," *Proceeedings SPIE 6th International Symposium on Smart Materials and Structures.* Newport Beach, California, Paper 3668-78.

[28] M. Brequet, "Stick and slip actuators," Ph.D. dissertation, Ecole Polytechnique Federale De Lausanne, (EPFL), Switzerland, 1998.

[29] Meghana Honnatti, Gareth Hughes, and Rocky Draper, "Enabling Subcellular Nanotechnology: An Applications Overview of Piezoelectric-Based Micro- and Nano-Positioning Systems", Application Note 9719.

[30] Chabri et al., "Microfabricated Silicon Microneedles for Nonviral Cutaneous Gene Delivery," British Journal of Dermatolog., 2004, Vol. 150, pp. 869-877.

[31] Y. Haddab, N. Chaillet, A. Bourjault, "A microgripper using smart piezoelectric actuators," Proc. of the 2000 IEEE/RS International Conference on Intelligent Robots and Systems, pp. 659-664.

[32] D. Bruce and S. Hiller, "Micro Probing for Cell Turgor and Cell Wall Mechanical Properties," Postharvest Convention '98 Conference Proceedings, Cranfield University, Bedford, UK, March, 1998, pp. 869-877.

[33] S. Hiller, D. Bruce, and G. Jernoimidis, "A Micro Penetration Technique for Mechanical Testing of Plant Cell Walls," Journals of Texture Studies 27, 1996, pp. 559-587.

[34] Z. Rihong, X. Daocai, Y. Zhixing, and C. Jinbang, "Research on systems for measurements of CCD parameters," in *Proc. SPIE Detectors, Focal Plane Arrays, Imaging Devices II*, 1998, pp. 297–301.

[35] D. Krogmann *et al.*, "Image multiplexing system on the base of piezoelectrically driven silicon microlens arrays," in *Proc. 3rd Int. Conf. Micro Opto Electro Mechan. Syst. (MOEMS)*, 1999, pp. 178–185.

[36] J. Fasik, "An inchworm actuator for the next generation space telescope," Burleigh Instruments, Inc., Fishers, NY, 1998.

[37] B. Wallman and P. Crawley, "Nanolithography requirements— An equipment manufacturers view," in *Proc. NATO Adv. Workshop Nanolithography: A Borderland Between STM, EB, IB, X-Ray Lithographies*, 1993, pp. 95–101.

[38] L. Martiradonna, T. Stomeo, L. Carbone, G. Morello, A. Salhi, M. De Giorgi, R. Cingolani, M. Vittorio, "Nanopositioning of colloidal nanocrystal emitters by means of photolithography and e-beam lithography,"

[39] Y. Xu, Heavy-load nanopositioner with dual-parallel flexure design, US patent no.: 7348709 B2, Date: March 25, 2008

[40] S. Postnikov, S. Hector, C. Garza, R. Peters and V. Ivin, "Critical dimension control in optical lithography," Microelectronic Engineering 69 (2003) 452–458

[41] S. Verma, W. Kim and H. Shakir, "Multi-axis Maglev nanopositioner for precision manufacturing and manipulation applications," *IEEE Trans. Ind. Appl.*, vol. 41, no. 5, , Sep./Oct. 2005, pp. 1159–1167.

[42] Products for piezo motors/ultrasonic motor driven stages, Product Catalog of Physik Instrumente.

[43] T. Ikeda, Fundamentals of Piezoelectricity. Oxford, U.K.: Oxford Univ. Press, 1996.

[44] W. P. Mason, "Piezoelectricity, its history an applications," J. Acoust. Soc. Amer., vol. 70, no. 6, 1981, pp. 1561–1566.

[45] E. Fukada, "History and recent progress in piezoelectric polymers," IEEE Trans. Ultrason., Ferroelectr. Freq. Control, vol. 47, no. 6, pp. 1277–1290, Nov. 2000.

[46] IEEE Standard on Piezoelectricity, ANSI/IEEE Std. 976–987, 1988.

[47] I. J. Busch-Vishniac, "Electromechanical Sensors and Actuators," Berlin, Germany: Springer–Verlag, 1999.

[48] T. Ueno, J. Qiu, and J. Tani, "Magnetic force control with composite of giant magnetostrictive and piezoelectric materials," IEEE Trans. Magn., vol. 39, no. 6, Nov. 2003, pp. 3534–3540.

[49] S. Verma, W. J. Kim, and J. Gu, "Six-axis nanopositioning device with precision magnetic levitation technology," IEEE-ASME Trans. Mechatron., vol. 9, no. 2, Jun. 2004, pp. 384–391.

[50] M. Despont, U. Drechsler, W. Häberle, M. A. Lantz, and H. E. Rothuizen, "A vibration resistant nanopositioner for mobile parallel-probe storage applications," J. Microelectromechan. Syst., vol.16, no. 1, Feb. 2007, pp. 130–139.

[51] J. Grade, H. Jerman and T. Kenny, "Design of large deflection electrostatic actuators," Journal of Microelectromechanical Systems, vol. 12, no. 3, June 2003, pp. 335-343.

[52] R. Horowitz *et al.*, "Microactuators for dual-stage servo systems in magnetic disk files," in *Springer Handbook of Nanotechnology*, B. Bhushan, Ed. Berlin, Germany: Springer–Verlag, 2004, ch. 31, pp. 921–950.

[53] C. Kim, et al., "Polysilicon Microgripper," Tech. Dig. IEEE Solid-State Sensor and Actuator Workshop, Hilton head, SC, 1990, p. 48-51.

[54] D. Hah, et al., "A low voltage, large scan angle MEMS micromirror arrays with hidden vertical comb-drive actuators for WDM routers," Proc. 2002 Optical Fiber Communication Conference, Mar. 2002.

[55] L. R. Carley, J. A. Bain, G. K. Fedder,D.W. Greve, D. F.Guillou, M. S. C. Lu, T. Mukherjee, S. Santhanam, L. Abelmann, and S. Min, "Singlechip computers with microelectromechanical systems-based magnetic memory," *J. Appl. Phys.*, vol. 87, no. 9, 2000, pp. 6680–6685.

[56] S. Devasia, E. Eleftheriou and S. Moheimani, "A Survey of Control Issues in Nanopositioning," IEEE Transactions on Control Systems Technology, vol. 15, no. 5, Sept. 2007.

[57] S. Hoen, P. Merchant, G. Koke, and J.Williams, "Electrostatic surface drives: Theoretical considerations and fabrication," in *Proc. 9th Int. Conf. Solid-State Sensors Actuators (Transducers)*, 1997, pp. 41–44.

[58] D. Yan, A. Khajepour, and R. Mansour, "Design and modeling of a MEMS bidirectional vertical thermal actuator," *J. Micromech. Microeng.*, vol. 14, no. 7, Jul. 2004, pp. 841–850.

[59] T. Yih and I. Talpasanu, "Mirco and Nano Manipulations for Biomedical Applications," Artech House Inc., Norwood, MA, 2008.

[60] W. Cowan and V. Bright, "Vertical Thermal Actuators for Micro-Opto-Electro-Mechanical Systems," Proc. Of SPIE, vol. 3226, 1997, pp. 137-146.

[61] L. Que, J. Park and Y. Gianchandani, "Bent-beam electro-thermal actuators for high force applications," IEEE International Conference on Microelect. Systems, 1999, pp. 31-36.

[62] T. Dureig, et al., "Engineering Aspects of Shape Memory Alloys," London: Butterworth Heinemann, 1990.

[63] Borden, Tom. "Shape-Memory Alloys: Forming a Tight Fit." *Mechanical Engineering* Oct. 1991: 67-72

[64] Rogers, Craig. "Intelligent Materials." *Scientific American* Sept. 1995: 154-157.

[65] S. Salisbury, D. Waechter, R. Ben Mrad, S. Prasad, R. Blacow, and B. Yan, "Design Considerations for Complementary Inchworm Actuators," IEEE/ASME Transactions on Mechatronics, vol. 11, no. 3, 2006, pp. 265-272.

[66] B. Yang, M. Bonis, H. Tao, C. Prelle and F. Lamarque, "A magnetostrictive mini actuator for long-stroke positioning with nanometer resolution," Journal of Micromechanics and Microengineering, 16 (2006), pp. 1227–1232.

[67] R. Yeh, S. Hollar and K.S.J. Pister, "Single mask, large force, and large displacement electrostatic linear inchworm motors," J. of Microelectromechanical Systems, vol. 11, pp.330-336, 2002.

[68] J. Kim; J. D. Kim and S. B. Choi, "A Hybrid Inchworm Linear Motor," Mechatronics, vol. 12, pp. 525-42, 2002.

[69] S. Hsu and A. Blatter, "Transducer," US Patent 3 292 019, December 13, 1966.

[70] G. Galutva, A. Ryazantsev, G. Stepanovich and J. Modestov, "Device for Precision Displacment of a Solid Body," US Patent 3 684 904, August 15, 1972.

[71] W. May Jr., "Piezoelectric Electromechanical Translation Apparatus," US Patent 3 902 084, August 26, 1975.

[72] E. Shamoto, H. Shin and T. Moriwaki, " Development of precision feed mechanism by applying Principle and basic performance of walking drive (1st report) - Principle and basic performance of walking drive," J. Jpn. Soc. Prec. Eng., vol. 59, no. 2, pp. 317-322, Feb. 1993.

[73] M. Vaughan, "The Design, Fabrication, and Modeling of a Piezoelectric Linear Motor," *M.S. Thesis*, Virginia Polytechnic Institute and State University, 2001.

[74] T. Galante, J. Frank, J. Bernard, W. Chen, G. Lesieutre, "Design, modeling, and performance of a high force piezoelectric inchworm motor," *Journal of Intelligent Materials System Structure*, vol. 10, 1999, pp. 962–972.

[75] C. Moon, S. Lee, and J. Chung, "A new fast inchworm type actuator with the robust I/Q heterodyne interferometer feedback," *Mechantronics*, vol. 16, 2006, pp. 105-110.

[76] D. Pohl, "Dynamic piezoelectric translation devices," *Rev Sci Instrum,* 1987; vol. 58(1), pp. 55–57.

[77] P. Niedermann, R. Emch and P. Descouts, "Simple piezoelectric translation device," *Rev Sci Instrum* 1998; vol. 59(2), pp. 368–369.

[78] C. Renner, P. Niedermann, A. Kent, O. Fischer, "A vertical piezoelectric inertial slider," *Rev Sci Instrum* 1990, vol. 61, no. 3, pp. 965–967.

[79] A. Smith, S. Gwo and C. Shih, "A new high-resolution two-dimensional micropositioning device for scanning probe microscopy applications," *Rev Sci Instrum* 1994, vol. 65, no.10, pp. 3216–3219.

[80] S. Chang and S. Li, "A high resolution long travel friction drive micropositioner with programmable step size," *Rev Sci Instrum* 1999, vol. 70, no. 6, pp. 2776–2782.

[81] F. Scire and E. Teague, "Piezo-driven 50 μ m range stage with subnanometer resolution," *Rev Sci Instrum* 1978, vol. 42, no. 12, pp.1735–1740.

[82] Y. Wu and Z. Zhou, "An XYθ mechanism actuated by one actuator," Mechanism and Machine Theory, vol. 39, Issue 10, Oct. 2004, pp. 1101-1110.

[83] S. Chang and B. Du, "A precision piezodriven micropositioner mechanism with large travel range," *Rev Sci Instrum* 1998; vol. 69, no. 4, pp.1785–1791.

[84] C. L. Chu and S. H. Fan, "A novel long-travel piezoelectric-driven linear nanopositioning stage," *Precision Engineering*, vol. 30, 2006, pp. 85-95.
[85] K. Kihwan, C. Nahmgyoo, and J. Woojin, "The design and characterization of a piezo-driven inchworm linear motor with a reduction-lever mechanism," JSME International Journal, vol. 47, no. 3, 2004, pp. 803-810.
[86] P.E. Tenzer, R. Ben Mrad, "On amplification in inchworme precision positioners," Mechatronics 14 (2004) 515–531.
[87] E. Shamoto and T. Moriwaki, "Development of a 'walking drive' ultra-precision positioner, Prc Eng 1997; 20(2):85-92.
[88] Q. Chen, D. Yao, CJ. Kim and G. Carman, "Mesoscale actuator device: micro interlocking mechanism to transfer macro load," Sensors and Actuators A: Physical, vol. 73, issues 1-2, 9 March 1999, pp. 30-36.
[89] T. Murata, "Drive apparatus and motor unit using the same," US Patent: 4,974,077, 1990
[90] S.K. Lee, M. Esashi, Design of the electrostatic linear microactuator based on the inchworm motion, Mechatronics, vol. 5, issue 8,1995, pp. 963–972.
[91] S. Smith and D. Chetwynd, Foundations of Ultraprecision Mechanism Design, Canada: Gordon and Breach Science, 1992.
[92] B. Zhang and Z. Zhu, "Developing a Linear Piezomotor with Nanometer Resolution and High Stiffness," IEEE/ASME Transactions on Mechatronics, vol. 2, no. 1, Mar. 1997, pp. 22-29.
[93] S. Salisbury and R. Ben Mrad, "Analytical stiffness estimation for short flexures," *Mechatronics*, vol. 16, 2006, pp. 399–403.
[94] S. Choi and J. Salem, "Preloading technique in dynamic fatigue testing of ceramics: Effect of preloading on strength variation", Journal of Materials Science, vol. 15, 1996, pp. 1963-1965.
[95] S. Park and T. Shrout, "Ultrahigh strain and piezoelectric behavior in relaxor based ferroelectric single crystals", Journal of Applied Physics, 82(4), 1804, 1997.
[96] M. Takahashi, H. Yoshioka and H. Shinno, "A newly developed long-stroke vertical nano-motion platform with gravity compensator," Journal of Advanced Mechanical Design, Systems, and Manufacturing, vol. 2, no. 3, Mar. 2008, pp. 356-365.
[97] S. Dong, L. Li, Z. Gui, T. Zhou and X. Zhang, "A New Type of Linear Piezoelectric Stepper Motor," IEEE Trans. Comp., Pack. and Manf. Part A, vol. 18, no. 2, June 1995, pp. 4308-4313.
[98] R. Ben Mrad, A. Abhari, and J. Zu, "A Control Methodology for an Piezoworm Piezomotor," Journal of Mechanical Systems and Signal Processing, vol. 17, no. 2, 2003, pp. 457–471.
[99] F. Claeyssen, R. Le Lettey, F. Barillot, and O. Sosnicki, "Amplified Piezoelectric Actuators: Static & Dynamic Applications," Ferroelectrics, vol. 3, 2007, pp. 3-14.
[100] IEEE Standard on Piezoelectricity, ANSI/IEEE Standard 176-1987.
[101] ABAQUS, Version 6.9, HKS Inc of Rhode Island, USA.

Appendix A

Drawings of Piezoworm Stage

REVISIONS				
ZONE	REV.	DESCRIPTION	DATE	APPROVED
	A	INITIAL RELEASE		
	B	CHANGES DOC	2010/05/03	
	C	CHANGES DOC	2010/05/18	

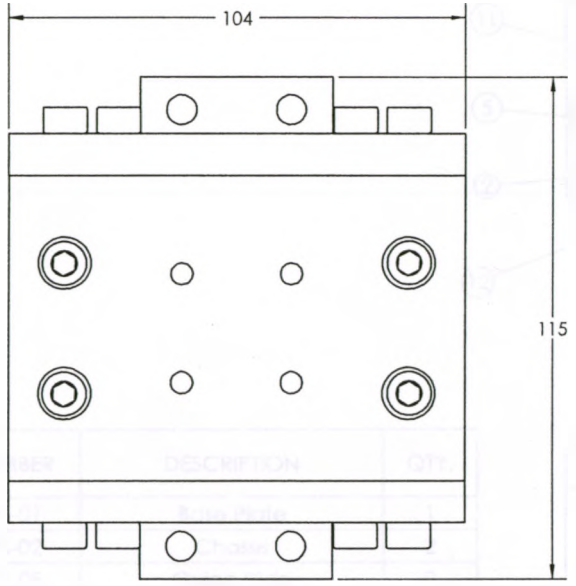

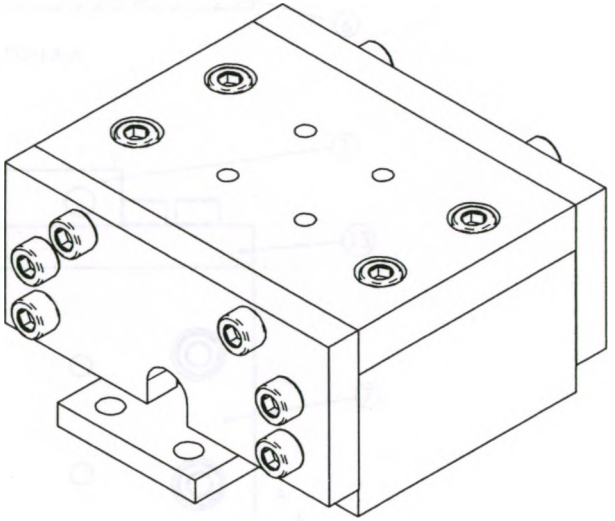

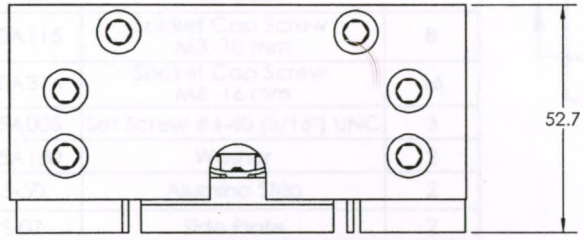

	NAME	DATE
DRAWN	T. MOHAMMAD	2010/03/08

UNLESS OTHERWISE SPECIFIED:
DIMENSIONS ARE IN INCHES
TOLERANCES:
LINEAR: ±0.1

INTERPRET GEOMETRIC TOLERANCING PER: ASME Y14.5M-1994

MATERIAL: NONE

FINISH: NONE

Department of Mechanical & Materials Engineering
UNIVERSITY of WESTERN ONTARIO

TITLE:
ASSEMBLY
Z AXIS

SIZE	DWG. NO.	REV
B	UWOZPS-00	C

SCALE: 1:1 | WEIGHT: | SHEET 1 OF 3

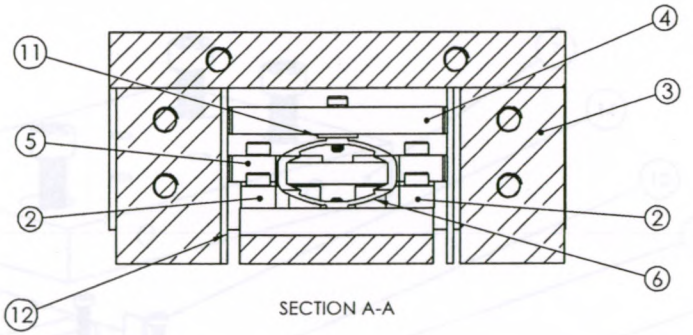

SECTION A-A

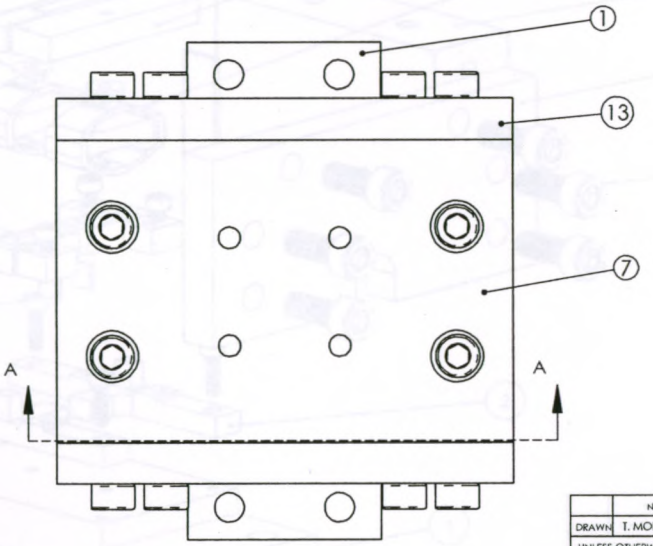

ITEM NO.	PART NUMBER	DESCRIPTION	QTY.
1	UWOZPS-01	Base Plate	1
2	UWOZPS-02	Chassis	2
3	UWOZPS-05	Guide Slide	2
4	UWOZPS-03	NU Clamp	1
5	UWOZPS-04	NC Clamp	2
6	APA40SM	Amplified Piezo Actuator	2
7	UWOZPS-06	Top Plate	1
8	MC 91290A115	Socket Cap Screw M3 -10 mm	8
9	MC 91290A316	Socket Cap Screw M6 -16 mm	16
10	MC 92765A005	Set Screw #4-40 (3/16") UNC	3
11	MC 91635A180	Washer	2
12	CS10-1.5-50	Alumina Strip	2
13	UWOZPS-07	Side Plate	2
14	MC 91290A103	Socket Cap Screw M2.5 - 10mm	4
15	UWOZPS-08	Preload Part	3

	NAME	DATE
DRAWN	T. MOHAMMAD	2010/03/08

UNLESS OTHERWISE SPECIFIED:
DIMENSIONS ARE IN INCHES
TOLERANCES:
LINEAR ±0.1

INTERPRET GEOMETRIC TOLERANCING PER: ASME Y14.5M-1994

MATERIAL: NONE

FINISH: NONE

Department of Mechanical & Materials Engineering
UNIVERSITY of WESTERN ONTARIO

TITLE:
ASSEMBLY Z AXIS

SIZE	DWG. NO.	REV
B	UWOZPS-00	C

SCALE: 1:1 | WEIGHT: | SHEET 2 OF 3

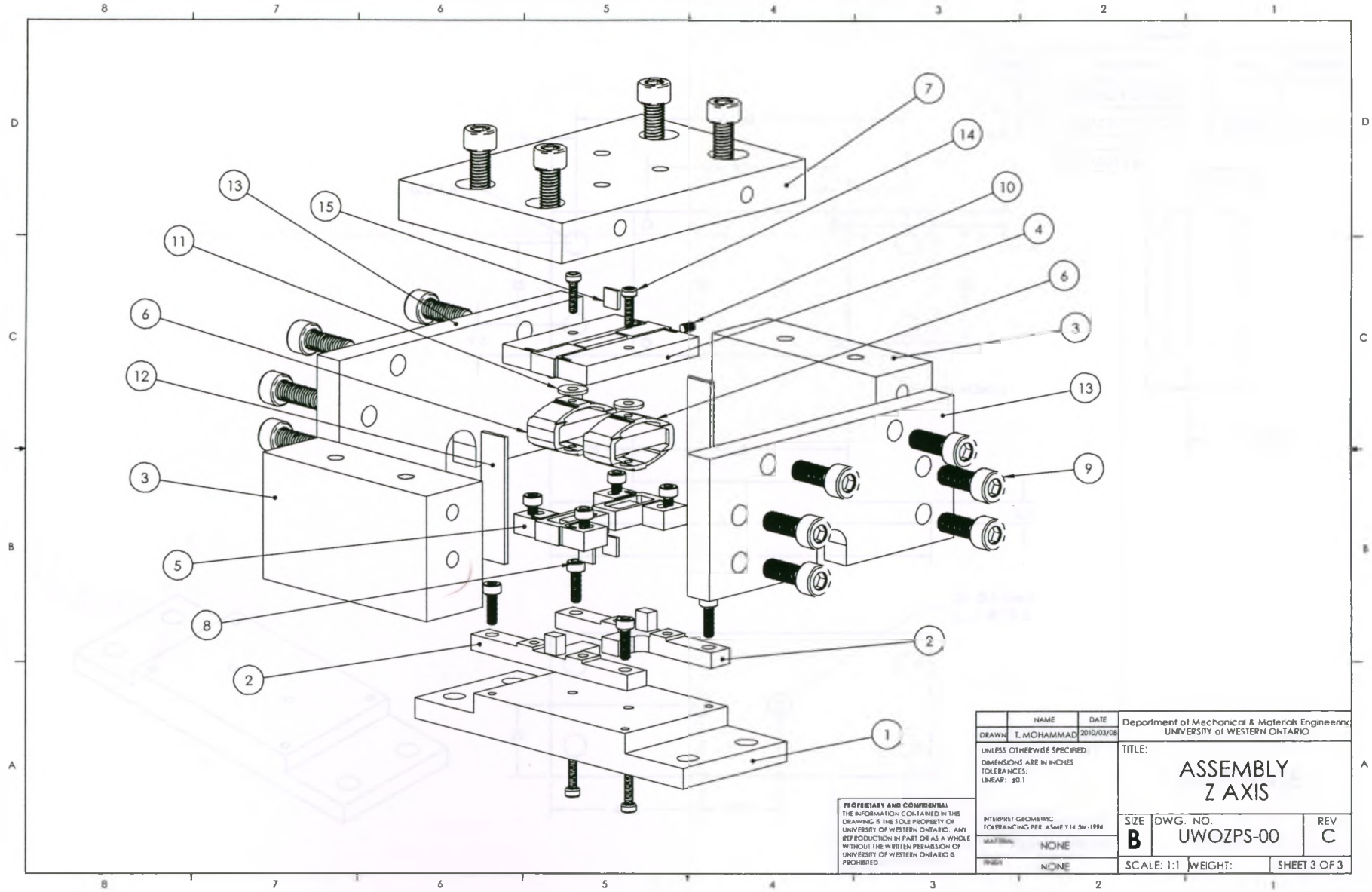

	NAME	DATE
DRAWN	T. MOHAMMAD	2010/03/08

UNLESS OTHERWISE SPECIFIED
DIMENSIONS ARE IN INCHES
TOLERANCES:
LINEAR: ±0.1

INTERPRET GEOMETRIC TOLERANCING PER: ASME Y14.5M-1994

MATERIAL: NONE

FINISH: NONE

Department of Mechanical & Materials Engineering
UNIVERSITY of WESTERN ONTARIO

TITLE:

ASSEMBLY Z AXIS

SIZE	DWG. NO.	REV
B	UWOZPS-00	C

SCALE: 1:1 | WEIGHT: | SHEET 3 OF 3

REVISIONS				
ZONE	REV.	DESCRIPTION	DATE	APPROVED
	A	INITIAL RELEASE		
	B	CHANGES DOC	2010/05/03	

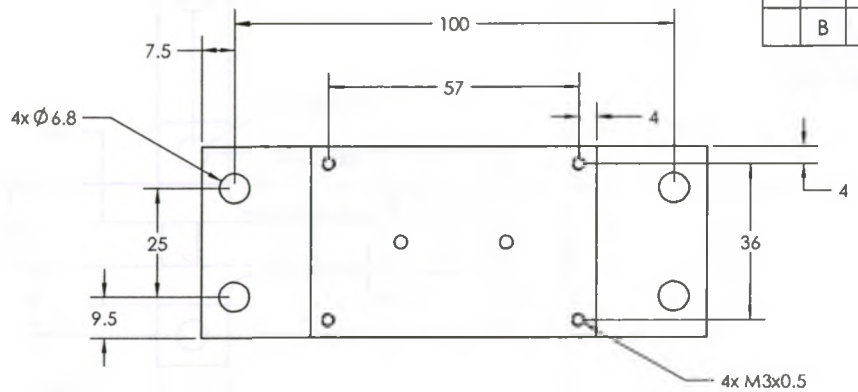

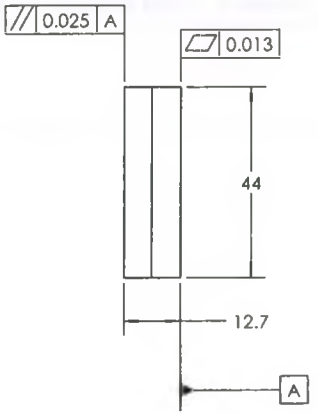

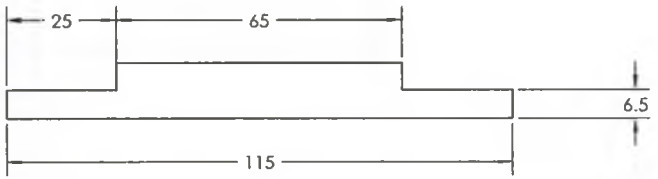

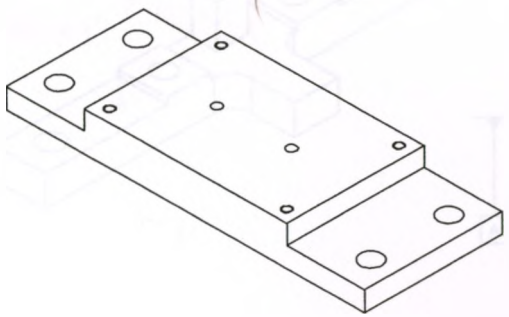

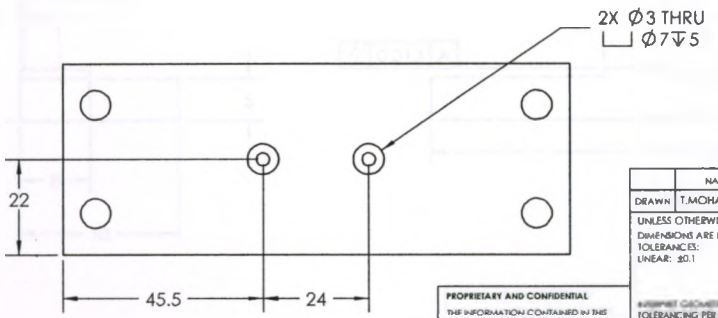

	NAME	DATE
DRAWN	T.MOHAMMAD	2010/03/10

UNLESS OTHERWISE SPECIFIED:
DIMENSIONS ARE IN MM
TOLERANCES:
LINEAR: ±0.1
ANGULAR: GEOMETRIC
TOLERANCING PER: ASME Y14.5M-1994
MATERIAL: STAINLESS STEEL 3XX
FINISH: NONE

Department of Mechanical & Materials Engineering
UNIVERSITY of WESTERN ONTARIO

TITLE:

BASE PLATE

SIZE	DWG. NO.	REV
B	UWOZPS-01	B

SCALE: 1:1 | WEIGHT: | SHEET 1 OF 1

REVISIONS				
ZONE	REV.	DESCRIPTION	DATE	APPROVED
	A	INITIAL RELEASE		
	B	CHANGES DOC	2010/05/03	
	C	CHANGES DOC	2010/05/18	

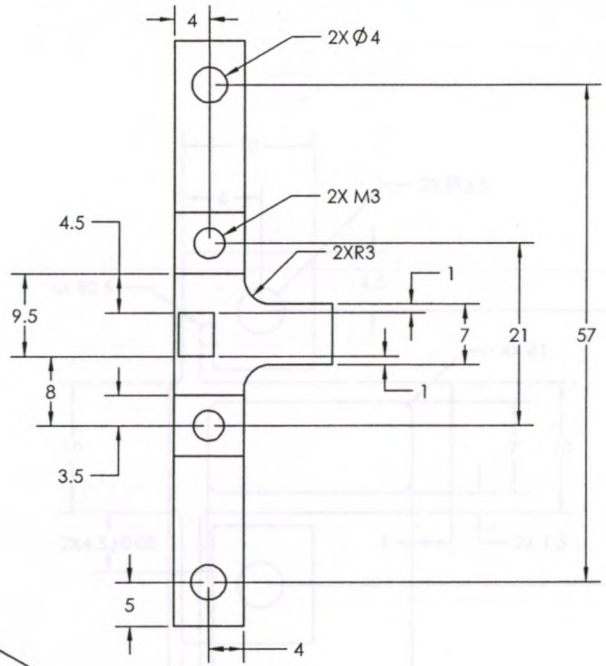

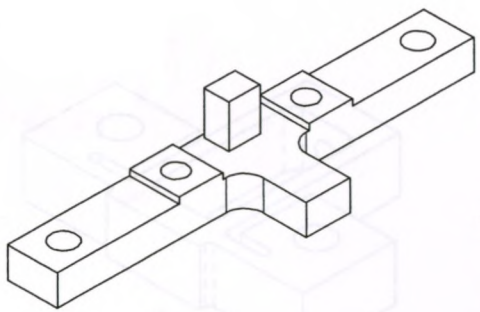

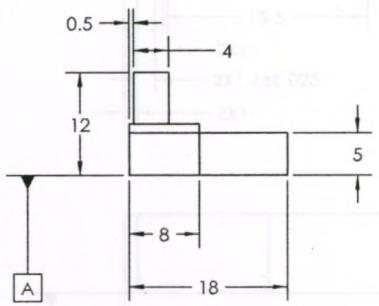

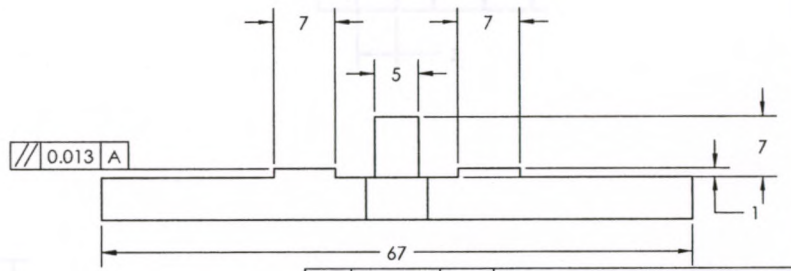

	NAME	DATE
DRAWN	T. MOHAMMAD	2010/03/08

Department of Mechanical & Materials Engineering
UNIVERSITY of WESTERN ONTARIO

UNLESS OTHERWISE SPECIFIED:
DIMENSIONS ARE IN MM
TOLERANCES:
LINEAR: 0.1

INTERPRET GEOMETRIC TOLERANCING PER: ASME Y14.5M-1994

MATERIAL: STAINLESS STEEL 3XX

FINISH: NONE

TITLE:

CHASSIS

SIZE	DWG. NO.	REV
B	UWOZPS-02	C

SCALE: 2:1 | WEIGHT: | SHEET 1 OF 1

REVISIONS				
ZONE	REV.	DESCRIPTION	DATE	APPROVED
	A	INITIAL RELEASE		
	B	CHANGES DOC	2010/05/03	
	C	CHANGES DOC	2010/05/18	

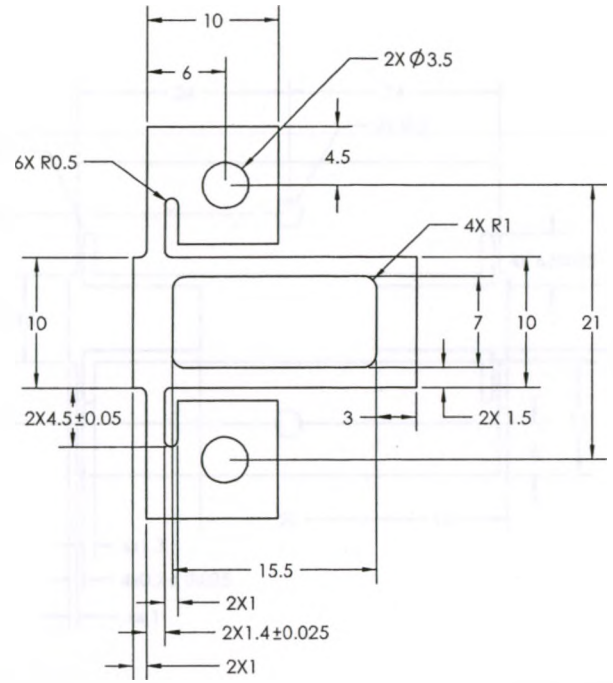

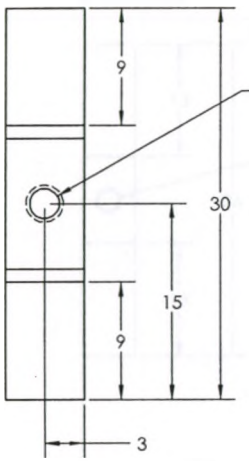

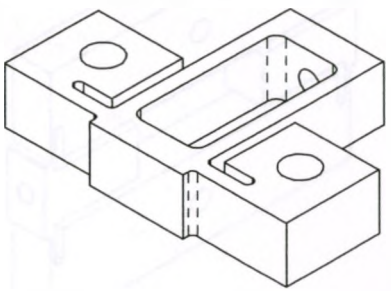

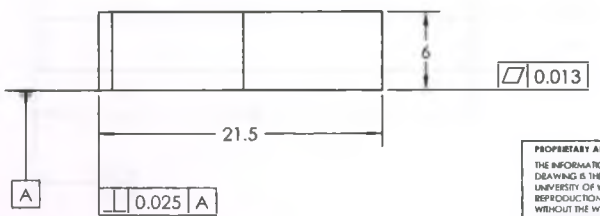

	NAME	DATE
DRAWN	T. MOHAMMAD	2010/03/08

UNLESS OTHERWISE SPECIFIED:
DIMENSIONS ARE IN MM
TOLERANCES:
LINEAR: ±0.1

INTERPRET GEOMETRIC TOLERANCING PER: ASME Y14.5M-1994

MATERIAL: SS 17-4 PH H1150

Finish: NONE

Department of Mechanical & Materials Engineering
UNIVERSITY of WESTERN ONTARIO

TITLE:

NC CLAMP

SIZE	DWG. NO.	REV
B	UWOZPS-03	C

SCALE: 3:1 | WEIGHT: | SHEET 1 OF 1

ZONE	REV.	DESCRIPTION	DATE	APPROVED
	A	INITIAL RELEASE		
	B	CHANGES DOC	2010/05/03	
	C	CHANGES DOC	2010/05/18	

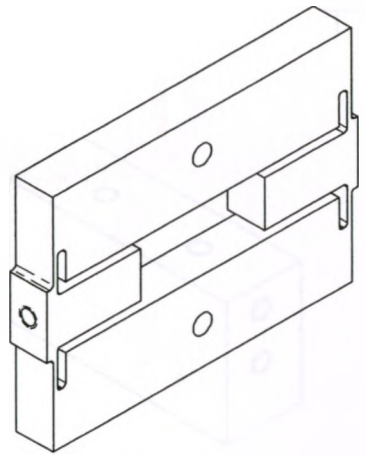

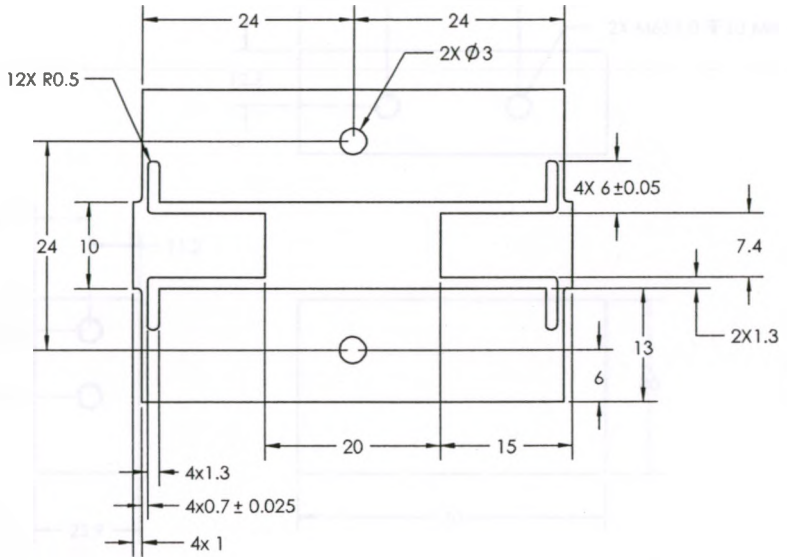

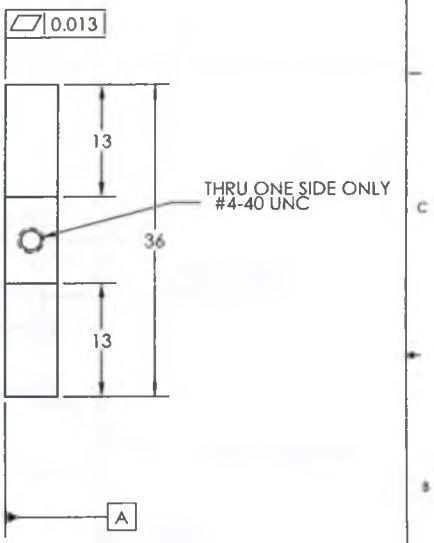

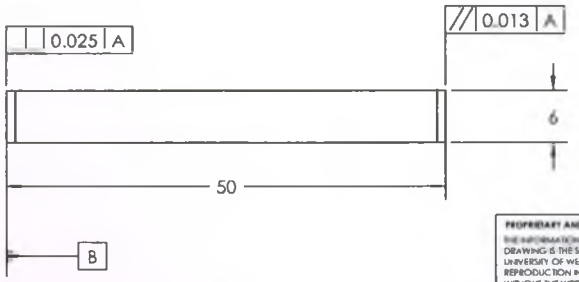

	NAME	DATE
DRAWN	T. MOHAMMAD	2010/03/08

UNLESS OTHERWISE SPECIFIED:
DIMENSIONS ARE IN MM
TOLERANCES:
LINEAR: ±0.1

INTERPRET GEOMETRIC TOLERANCING PER: ASME Y14.5M-1994

MATERIAL: SS 17-4 PH H1150

FINISH: NONE

Department of Mechanical & Materials Engineering
UNIVERSITY of WESTERN ONATRIO

TITLE:

NU CLAMP

SIZE	DWG. NO.	REV
B	UWOZPS-04	C

SCALE: 2:1 | WEIGHT: | SHEET 1 OF 1

REVISIONS				
ZONE	REV.	DESCRIPTION	DATE	APPROVED
	A	INITIAL RELEASE		
	B	CHANGES DOC	2010/05/03	
	C	CHANGES DOC	2010/06/18	

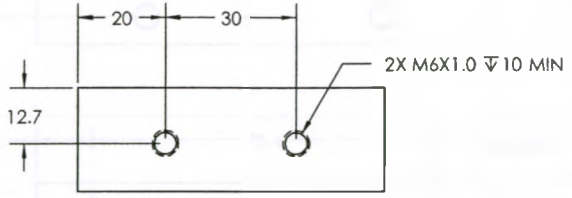

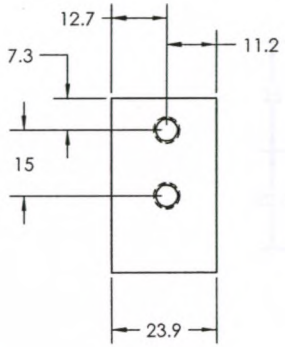

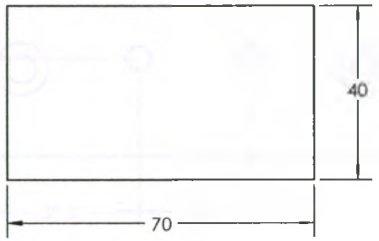

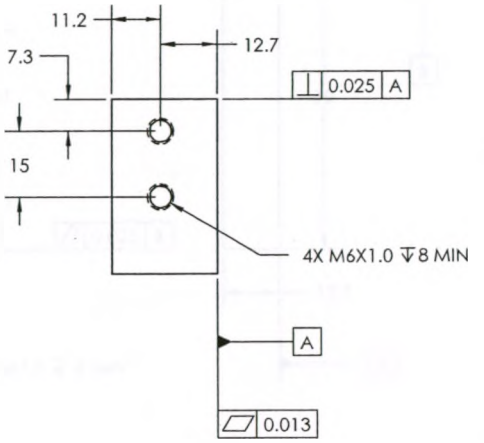

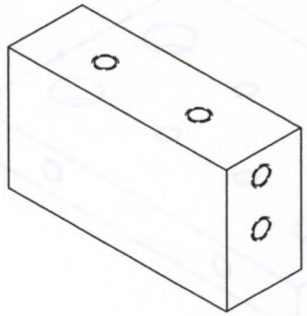

	NAME	DATE
DRAWN	T. MOHAMMAD	2010/03/08

UNLESS OTHERWISE SPECIFIED:
DIMENSIONS ARE IN MM
TOLERANCES:
LINEAR: ±0.1

INTERPRET GEOMETRIC TOLERANCING PER: ASME Y14.5M-1994

MATERIAL: STAINLESS STEEL 3XX

FINISH: NONE

Department of Mechanical & Materials Engineering
UNIVERSITY of WESTERN ONTARIO

TITLE:

GUIDE SLIDE

SIZE	DWG. NO.	REV
B	UWOZPS-05	C

SCALE: 1:1 | WEIGHT: | SHEET 1 OF 1

REVISIONS				
ZONE	REV.	DESCRIPTION	DATE	APPROVED
	A	INITIAL RELEASE		
	B	CHANGES DOC	2010/05/03	
	C	CHANGES DOC	2010/05/18	

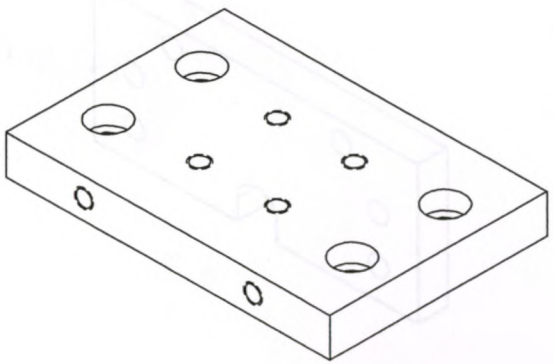

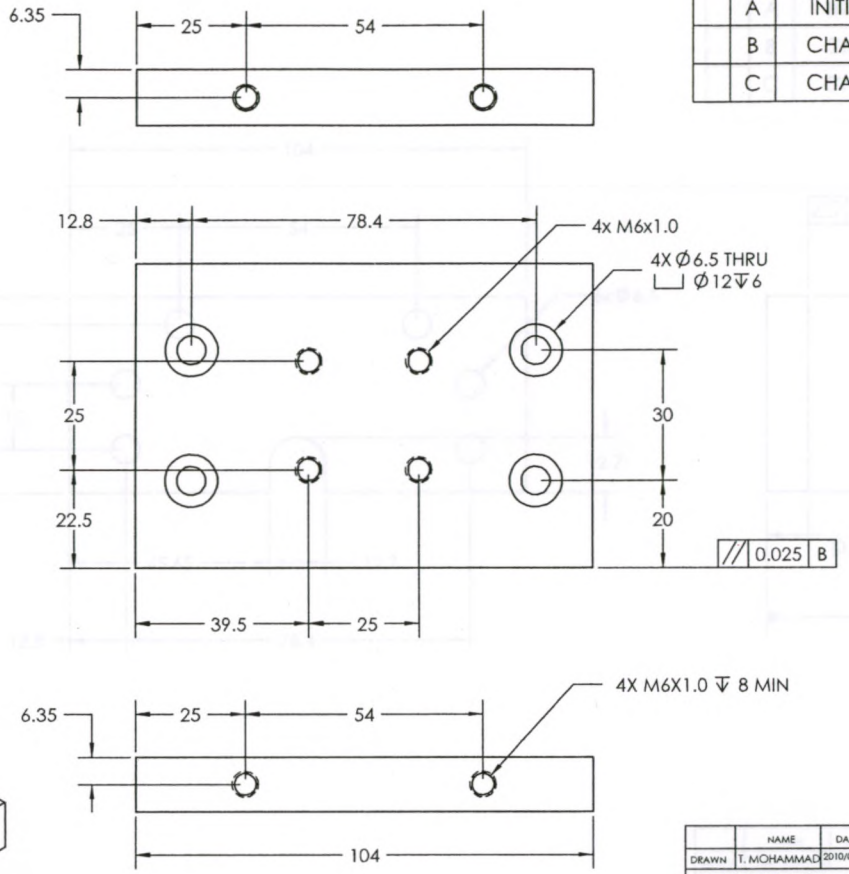

	NAME	DATE
DRAWN	T. MOHAMMAD	2010/03/08

UNLESS OTHERWISE SPECIFIED:
DIMENSIONS ARE IN MM
TOLERANCES:
LINEAR: ±0.1

INTERPRET GEOMETRIC TOLERANCING PER: ASME Y14.5M-1994

MATERIAL: STAINLESS STEEL 3XX

FINISH: NONE

Department of Mechanical & Materials Engineering
UNIVERSITY of WESTERN ONATRIO

TITLE:

TOP PLATE

SIZE	DWG. NO.	REV
B	UWOZPS-06	C

SCALE: 1:1 | WEIGHT: | SHEET 1 OF 1

REVISIONS				
ZONE	REV.	DESCRIPTION	DATE	APPROVED
	A	INITIAL RELEASE		
	B	CHANGES DOC	2010/05/03	
	C	CHANGES DOC	2010/05/18	

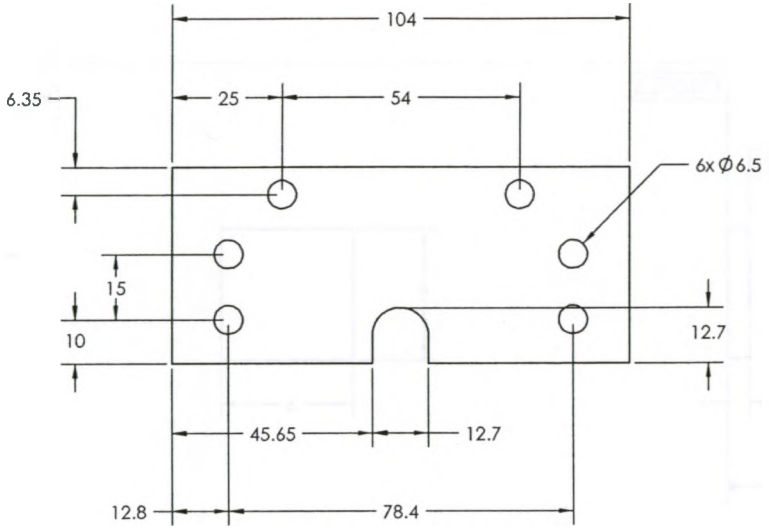

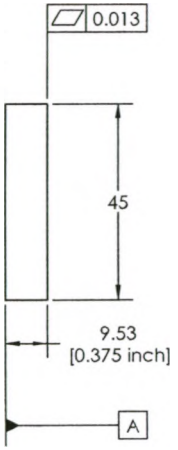

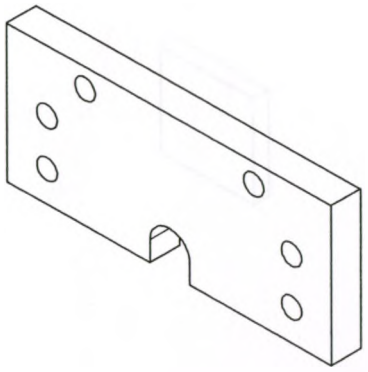

	NAME	DATE
DRAWN	T. MOHAMMAD	2010/03/08

UNLESS OTHERWISE SPECIFIED:
DIMENSIONS ARE IN MM
TOLERANCES
LINEAR: ±0.1

INTERPRET GEOMETRIC TOLERANCING PER: ASME Y14.5M-1994

MATERIAL: STAINLESS STEEL 3XX

FINISH: NONE

Department of Mechanical & Materials Engineering
UNIVERSITY of WESTERN ONATRIO

TITLE:

SIDE PLATE

SIZE	DWG. NO.	REV
B	UWOZPS-07	C

SCALE: 1:1 | WEIGHT: | SHEET 1 OF 1

REVISIONS				
ZONE	REV.	DESCRIPTION	DATE	APPROVED
	A	INITIAL RELEASE		

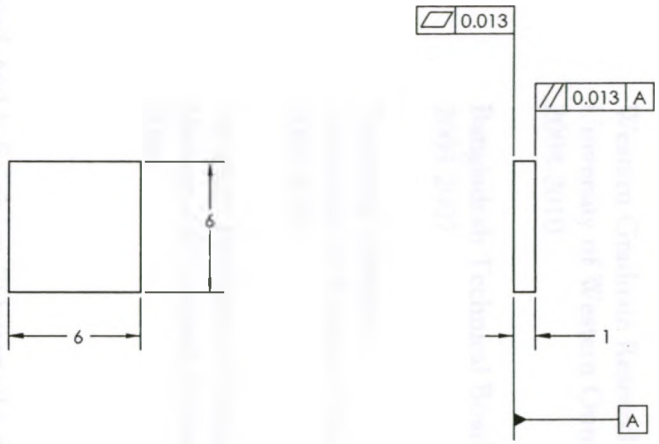

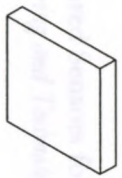

	NAME	DATE
DRAWN	T. MOHAMMAD	2010/05/03

UNLESS OTHERWISE SPECIFIED:
DIMENSIONS ARE IN INCHES
TOLERANCES
LINEAR: ±0.1

INTERPRET GEOMETRIC TOLERANCING PER: ASME Y14.5M-1994

MATERIAL: NONE

FINISH: NONE

Department of Mechanical & Materials Engineering
UNIVERSITY of WESTERN ONTARIO

TITLE:
PRELOAD PART

SIZE	DWG. NO.	REV
B	UWOZPS-08	A

SCALE: 5:1 | WEIGHT: | SHEET 1 OF 1